Quantum Correlations in Multipartite Quantum Systems

By

Muhammad Ibrahim

Department of Physics
Quaid-i-Azam University
Islamabad, Pakistan
2023

This work is submitted as a thesis for the partial
fulfillment of the requirements for the award of the degree
of

DOCTOR OF PHILOSOPHY
IN
PHYSICS

Muhammad Ibrahim

Department of Physics
Faculty of Natural Sciences
Quaid-i-Azam University
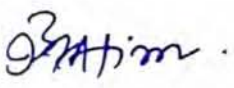Islamabad, Pakistan
2023

Declaration of Authorship

I, Muhammad Ibrahim declare that the work titled *"Quantum Correlations in Multipartite Quantum Systems"* presented in this thesis is my own and has been generated by me as the result of my own original research. Consulted the published work of others is clearly attributed and I have acknowledged all main source of help.

Muhammad Ibrahim
Department of Physics
Faculty of Natural Science
Quaid-i-Azam University
Islamabad, Pakistan.

Plagiarism Undertaking

I solemnly declare that research work presented in the thesis titled **"Quantum Correlations in Multipartite Quantum Systems"** is solely my research work with no significant contribution from any other person. Small contribution/help wherever taken has been dully acknowledged and that complete thesis has been written by me. I understand the zero-tolerance policy of the HEC and Quaid-i-Azam University Islamabad towards plagiarism. Therefore, I as an Author of the above titled thesis declare that no portion of my thesis has been plagiarized and any material used as reference is properly referred/cited. I undertake that if I am found guilty of any formal plagiarism in the above titled thesis even after award of Ph.D. degree, the university reserves the rights to withdraw/revoke my Ph.D. degree and that HEC and the University has the right to publish my name on the HEC/University Website on which names of students are placed who submitted plagiarized thesis.
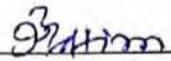
Student/Author Signature:

Name: Mr. Muhammad Ibrahim

Certificate of Approval

This is to certify that the research work presented in this thesis, entitled "**Quantum correlations in multipartite quantum systems**" was conducted by Mr. Muhammad Ibrahim under the supervision of Dr. M. Khalid Khan.

No part of this thesis has been submitted anywhere else for any other degree. This thesis is submitted to the Department of Physics, Quaid-i-Azam University Islamabad, Pakistan in partial fulfillment of the requirements for the degree of Doctor of Philosophy in Field of Quantum Information Theory, Department of Physics Quaid-i-Azam University Islamabad.
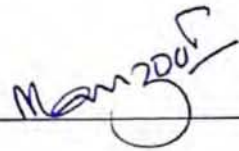
Student Name: **Mr. Muhammad Ibrahim**   Signature:_____

Examination Committee:

    a) Dr. Sajid Qamar,   Signature:_____
         Professor/Dean,
         Department of Physics
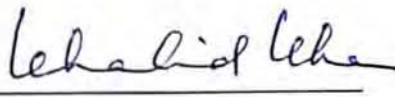   COMSATS University, Chak Shahzad,
         Islamabad.

    b) Dr. Manzoor Ikram   Signature:_____
         Chief Scientist,
         National Institute of Laser and Optronics
         Nilore, Islamabad.

    c) Prof. Dr. Kashif Sabeeh   Signature:_____
         Chairman,
         Department of Physics
         QAU, Islamabad

Prof. Dr. M. Khalid Khan   Signature:_____
Supervisor,

Chairman Signature:_____

Dedicated to my family and teachers

Acknowledgment

I am extremely thankful to Prof. Dr. M. Khalid Khan for his valuable guidance and constant encouragement throughout my research period. His timely advice and friendly supervision made the completion of my research work possible.

I must express my gratitude to Prof. Dr. Raheel Ali for providing me his kind support through the challenging time of my academic journey at Quaid-i-Azam University.

I am thankful to Prof. Dr. Jameel Aslam for encouraging me during my studies.

I am extremely thankful to Prof. Dr. Kashif Sabeeh, Chairman Department of Physics for providing a healthy academic atmosphere in the department.

I would like to thank Dr. M. Ramzan, Dr. M. Usman, and Dr. Syed Jamal Anwar for their time and continued support. Without their help, I can't carry out academic and research burdens.

MUHAMMAD IBRAHIM

List of Publications

Published:

M. Ibrahim, M. Usman, and M. K. Khan, "Global quantum discord and von Neuman entropy in multipartite two-level atomic systems" International Journal of Quantum Information **21**, 2350006 (2023).
(https://doi.org/10.1142/S0219749923500065)

M. Ibrahim, S. Jamal Anwar, and M. K. Khan, S. Almalki, Haifa S. Alqannas & S. Abdel-Khalek "Dynamics of N Two-level moving atoms under the influence of the Non-Linear Kerr Medium" Optical and Qauntum Electronics **55**, 1009 (2023).
(https://doi.org/10.1007/s11082-023-05215-8)

M. Ibrahim, S. Jamal Anwar, M. Ramzan, and M. K. Khan, "Entanglement dynamics of N two-level atoms interacting with the coherent field in the presence of the nonlinear Kerr Medium" European Physical Journal Plus **137**, 301 (2022).
(https://doi.org/10.1140/epjp/s13360-022-02415-1)

M. Ibrahim, S. Jamal Anwar, and M. K. Khan, S. Almalki, Haifa S. Alqannas & S. Abdel-Khalek, "Influence of the Stark shift and field nonclassicality on the dynamics of non-classical correlations of N two-level atomic system" accepted for publication, International Journal of Theoretical Physics (2023).
(https://doi.org/10.1007/s10773-023-05506-6)

S. Khan, **M. Ibrahim**, and M. K. Khan, "Environment assisted energy transfer in dimer system" Annals of Physics **341,** 1 (2014).
(https://dx.doi.org/10.1016/j.aop.2013.11.009)

Submitted for publication:

M. Ibrahim, S. Jamal Anwar, and M. K. Khan, S. Almalki, Haifa S. Alqannas & S. Abdel-Khalek, "The Effects of Kerr Medium on Quantum Correlations and Fisher Information in Multipartite two-level System" Submitted (2023).

List of Abbreviations

- Classical Correlations (CC)
- Global Quantum Discord (GQD)
- Intrinsic Decoherence (ID)
- Multipartite Quantum Correlations (MPQC)
- Mutual Information (MI)
- Non-linear Kerr Medium (NLKM)
- Quantum Discord (QD)
- Quantum Entanglement (QE)
- Quantum Information Processing (QIP)
- Quantum Information Theory (QIT)
- Relative Entropy (RE)
- Two-level Atomic System (TLS)
- von Neumann Entropy (VNE)

Abstract

This work is mainly based on the study of quantum entanglement (QE) and multipartite quantum correlation (MPQC) in many two-level atomic systems (TLS). QE and MPQC play a pivotal role in quantum computing and quantum information processing. We have computed the global quantum discord (GQD) and von Neumann entropy (VNE) of a multipartite system consisting of a TLS that interact with a field prepared in a single mode. We use the extended Tavis-Cumming model. The effects of intrinsic decoherence (ID) on the dynamics of the GQD and VNE are also investigated. We have extended the results for a large photon number n in the system. We have studied the effect of change in the size of the system on the maximum value of GQD and VNE and we have also estimated the scaling coefficients for this behavior. Moreover, the influence of the non-linear Kerr medium (NLKM) on the MPQC and entanglement in two, three and four TLS is also explored. The NLKM has a profound effect on both quantifiers, the GQD and VNE. For the higher values of the Kerr parameter, it is observed that the GQD and VNE show rather periodic behavior. We also consider the case of moving atoms. Both the quantifiers, the GQD and the VNE show periodic behavior, and the results are consistent with previous studies. The effect of the NLKM is also studied on the dynamics of the system in the presence of a single-mode coherent field. The collapses and revivals of the GQD and VNE are observed for various values of the Kerr parameter. Moreover, it is found that by increasing the values of Kerr medium parameter, the magnitude of the revivals of QE is suppressed. It is also noted that for mixed states the GQD shows comparatively damped oscillations as compared to the pure states. It is important to point out that by increasing the average number of photons in the multipartite quantum system, the GQD and VNE exhibit damping behavior. Furthermore, the revival time of both the GQD and VNE increases with the increase of NLKM parameter, for the systems with a relatively large number of atoms. Finally, we investigated the influence of Stark shift on the system consisting of two, three and four TLS interacting with a single-mode Fock and coherent field in the cavity. The dynamics of the GQD and VNE in the presence of Stark effect indicates that the MPQC decrease with the increase of the Stark parameter for both the Fock and coherent field. In a nutshell, our work gives a comparison between MPQC and

entanglement for a many TLS interacting with single mode field under the influence of different environments.

List of Figures

3

4

Contents

Chapter 1

Introduction

Quantum computing and quantum information processing (QIP) require quantum systems consisting of many two-level subsystems (TLS) [1]. The success of quantum computation and QIP depends on the controlled evolution and precise measurements of these quantum systems. Various phenomena in QIP and computation such as entanglement and the MPQC using a TLS and spin models are explored and understood [2–6]. However, quantifying entanglement and the MPQC for the multipartite systems remains a theoretical challenging task. Quantum correlations are more meaningful to study in many-body quantum systems as compared to bipartite entanglement [7].

The Jaynes-Cummings model [8] is a precisely solvable model that describes the interaction between a TLS and a single-mode quantized radiation field under the rotating-wave approximation. Much attention has been paid to generalizing the Jaynes-Cummings model [9–13]. Various attempts have been made to explore analytical solutions of multi-atoms interacting with the cavity field. The dynamical behavior of two TLS interacting with a single-mode field is a preliminary example [14–19]. Numerous investigations have been done on atom-atom and atoms-field QE in such systems [20, 21].

QE is a vital resource in the field of QIP and quantum computing [22]. Bipartite entanglement is well studied in various respects [23–30]. As for the multipartite systems, tripartite entanglement has triggered considerable interest in the study to increase the security in quantum cryptography [31] and in the efficiency of quantum cloning [32, 33]. Tripartite entanglement [34–37], processing of quantum information [38] and entropy [39, 40] have been studied extensively. Relative entropy of the system has been proposed as a measure of entanglement and effectively used for the mixed states [41, 42].

8

It has been identified that entanglement is not the only parameter to measure the quantumness of a system [43] by introducing a suitable tool to measure quantum correlations, known as quantum discord, presented by Ollivier and Zurek [44]. Quantum discord and its dynamics have been extensively explored in atomic systems, spin models and cavity quantum electrodynamics [45–55]. Quantum correlations have also been thought of as a useful measurement in quantum evolution under decoherence [56, 57] and a resource for quantum computation [58] have the property that almost all types of quantum states have non-vanishing quantum discord [59–61]. A multipartite version of quantum discord, called the global quantum discord (GQD) has been studied and derived by Rulli and Sarandy [7]. The non-classical states in multipartite systems are studied by Saguia et. al. [62] which provides a sufficient condition for the non-classicality of the system.

In practical scenarios, it cannot be assumed that the atom is static during its interaction: therefore, it is reasonable to take the effect of atomic motion into account. Besides the experimental drive, there also exists a theoretical motivation to include the atomic motion effect in the Jaynes-Cummings model because its dynamics become more interesting. Several authors have treated the Jaynes-Cummings model in the presence of atomic motion by the use of analytic approximations [63–65] and numerical calculations [66].

In a more realistic situation, in atom-field interaction, the cavity is filled with a nonlinear Kerr medium (NLKM). In the field of quantum optics, the Kerr effect is a non-linear phenomenon, consisting of a change in the refractive index of the material which is directly proportional to the square of the electric field [67–70]. Under this process, the intensity-dependent phase shift appears in the field. Thus, the intensity of the field is proportional to the refractive index of the Kerr medium. The entropy of a TLS, non-linear atomic system has been studied in the atomic motion case in the presence of the NLKM [44]. A moving rubidium atom, in the presence of the NLKM, interacting with a single-mode cavity field is studied in Ref. [71]. The quantum Fisher information of the atomic system interacting with a single cavity mode in the presence of NLKM has been investigated in Ref. [72]. The effect of the detuning parameter and the NLKM on the dynamics of a moving four-level N-type atom interacting with the coherent field has been discussed in Ref. [45]. The influence of atomic motion on the atomic population inversion has been described in Ref. [73] by considering the field-mode structure parameter. Moreover, a moving atomic system that interacts with a two-mode coherent field undergoing a two-

photon transition has been studied in Ref. [74].

The Stark shift effect is another well-studied aspect in the field of light-matter interaction[75]. In the field of quantum optics, the Stark effect is extensively studied [75]. In the field of cavity quantum electrodynamics, recent studies [75] have made it experimentally possible to witness the ultra-strong and strong light-matter-interaction effects. Schemes have been suggested for applying the perturbation and dynamical Stark shifts on quantum logic gates and algorithms [75, 76], and to improve the photon sources for the interferometer [77]. It may be interesting to investigate the influence of Stark shift on atom-atom, and atom-field MPQC and QE. It may be worth doing to explore, how Stark shift can be utilized to enhance atom-atom entanglement, as well. Quantum Fisher Information of a moving TLS under the influence of the thermal field, ID, Stark effect, and Kerr-like medium is studied in Ref. [78]. Recently, the Kerr effect and Stark effect on the dynamics of QE of a system consisting of two three-level moving atoms is studied [79]. In this context we explored the influence of Stark shift on the MPQC and QE for the case of two, three and four TLS.

We have used a scheme that allows us to compute how information is processed in the different number of a TLS via the analysis of the multipartite correlations, more specifically by measuring the GQD and VNE. A quantum system composed of various numbers of identical TLS which interacts with a single-mode field in the Fock state basis is the one case that we have investigated. The quantum system is prepared initially in a mixed state and different parameters are added to see how they affect the information processing in the system. The dynamical character of the GQD and VNE show an interplay between classical and non-classical correlations. Photons in this model play an important role to assist the GQD and VNE and we observed that the effects of the field on the GQD and VNE reside in the system dynamics that indicate that both atom and field states have become mixed. The GQD evolves in a non-linear fashion with the number of photons in the system. The GQD and VNE show linear behavior with each other in the dynamics of the system. The effects of ID on the dynamics of the GQD and VNE are also studied. We find the behavior of quantifiers for higher number N atomic systems and estimated the scaling coefficients.

Moreover, we study the dynamical character of the quantifiers for an N TLS (two, three, and four TLS) in the presence of Kerr Medium, and the system interacts with the single-

mode Fock field. The results are quite interesting and promising. We have observed that by increasing the Kerr parameter values, the GQD and VNE show periodic behavior, which indicates the collapses and revivals of the QE. It is observed that mixed states have comparatively suppressed oscillations of the GQD. The VNE has non-zero values throughout the dynamics of the system for initial mixed states. It is also observed that the multipartite systems show sustained response to QE during the evolution of time. The Kerr Medium has prominent effects on the GQD and VNE for all the Kerr parameter values. The effect of the increase in the number of photons in the cavity is also significant. Moreover, in the case of moving atoms, the periodic behavior of the GQD and VNE is rather similar for the initial pure and mixed atomic states.

Furthermore, we study the dynamical evolution of the GQD and VNE of the different number of a moving TLS. The system interacts with a single-mode coherent field. We also assume that the system is under the influence of the NLKM. We aim to make a comprehensive study of N TLS interacting with different types of fields and use various quantifiers to estimate the MPQC and QE.

The layout of this thesis is given as follows; in chapter two, we discuss some basic concepts of quantum optics that are required for this research work. In chapter three, we study the behavior of open quantum system and discuss some properties of the open quantum systems. In chapter four, we introduce some tools to investigate the MPQC and QE in a quantum system. In chapter five, we study the GQD and VNE in two, three, four, and five TLS coupled with the single-mode field in a Fock state. In chapter six, we investigate the entanglement dynamics in the presence of the NLKM of moving two, three, and four TLS which interact with a coherent field. In chapter seven, we focus on the influence of Non-Linear Kerr Medium, on the dynamics of moving two, three, and four TLS which interact with a single-mode Fock field. In chapter eight, we investigate the entanglement and quantum discord dynamics of two, three, and four TLS under the influence of the Stark effect. The system is interacting with the Fock and coherent field. Finally, in chapter nine, we summarize and conclude our work.

Chapter 2

Some Basic Concepts in Quantum Optics

2.1 Introduction

Some basic concepts of quantum mechanics and quantum optics related to this work are briefly described in this chapter. Quantum states, quantization of electromagnetic field, Jaynes-Cummings model, and Tavis-Cumming model are briefly presented. We present the quantum mechanical formalism of atom-field interaction where both atom and field are treated as quantized. In the quantum mechanical treatment, light is treated as photons to explain the interaction of the field with atoms.

2.2 Quantum States

We use a ket vector, denoted by $|\psi\rangle$, to represent the state of a quantum mechanical system. It has a unit length. It resides in an $\mathcal{N}$-dimensional Hilbert space $\mathcal{H}$. "Hilbert space" $\mathcal{H}$ is spanned by a complete set of orthonormal basis vectors $\{|a_n\rangle\}$ and in the basis vectors, ket vector $|\psi\rangle$ is given as

$$|\psi\rangle = \sum_n \alpha_n |a_n\rangle, \qquad (2.1)$$

where α_n are complex numbers, such that

$$\sum_n |\alpha_n|^2 = 1. \qquad (2.2)$$

2.3 Two-level atomic system

A TLS is a simple quantum system. A typical type of atomic system generally has many different energy levels. In many experiments, however, only two energy levels usually a ground state and one excited state are considered.
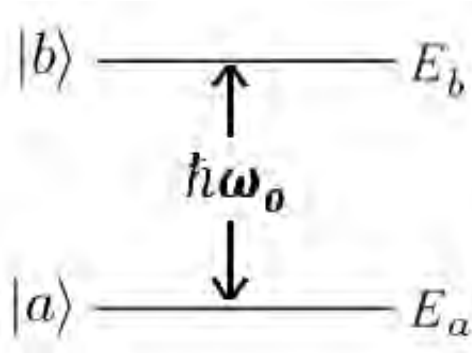
Figure 2.1: Figure shows a simple TLS with an energy difference of $\hbar\omega_o$.

Let E_a and E_b describe the ground and an excited state of a quantum system composed of TLS, as shown in Fig. (2.1). The energy difference between the two levels is $\hbar\omega_o$. These states correspond to a quantum state of an atom, denoted by a ket $|a\rangle$ is the ground state and ket $|b\rangle$ is the excited state. Furthermore, the energy level states are orthonormal, i.e.

$$\langle a|a\rangle = \langle b|b\rangle = 1$$

$$\langle a|b\rangle = \langle b|a\rangle = 0$$

The superposition principle allows us that there are other possible states of the system as well. These states are formed by the linear complex combination of the basis states $|a\rangle$ and $|b\rangle$. In general, the atom is in a superposition state

$$|\psi\rangle = \alpha\,|a\rangle + \beta\,|b\rangle \tag{2.3}$$

The probability amplitudes are $\alpha = \langle a|\psi\rangle$ and $\beta = \langle b|\psi\rangle$. For an atom in the given state $|\psi\rangle$ as shown in Eq. (2.3), its energy measurements E will provide E_a with the probability $|\alpha|^2$ and E_b with the probability $|\beta|^2$.

2.4 Qubit

A quantum system with two-level is called a quantum bit or a qubit in quantum information theory (QIT). In QIT and quantum computation, a qubit describes a basic unit in the field. It is a quantum analog of the classical bit. The state vectors $|a\rangle$ and $|b\rangle$ (also defined as $|0\rangle$ and $|1\rangle$) are the basis vectors in a two-dimensional Hilbert space $\mathcal{H}$. It can be described by the standard matrix notation as

$$|a\rangle = |0\rangle = \begin{pmatrix} 1 \\ 0 \end{pmatrix}, \quad |b\rangle = |1\rangle = \begin{pmatrix} 0 \\ 1 \end{pmatrix}. \tag{2.4}$$

We can write a qubit in standard basis as,

$$|\psi\rangle = \alpha |0\rangle + \beta |1\rangle, \tag{2.5}$$

where the complex numbers α and β satisfies

$$|\alpha|^2 + |\beta|^2 = 1. \tag{2.6}$$

2.5 Pauli Spin Matrices

The Pauli spin matrices are generally denoted by the symbol $\hat{S}$. Pauli spin matrices are angular momentum operators that correspond to the spin of a spin $\frac{1}{2}$ particle, in each of the three spatial dimensions. Pauli spin operators are three 2×2 Hermitian and unitary matrices satisfy the commutation relation

$$\left[\hat{S}_x, \hat{S}_y\right] = i\hbar \hat{S}_z, \tag{2.7}$$

$$\left[\hat{S}_y, \hat{S}_z\right] = i\hbar \hat{S}_x, \tag{2.8}$$

$$\left[\hat{S}_z, \hat{S}_x\right] = i\hbar \hat{S}_y. \tag{2.9}$$

$$\hat{S}^2 = \hat{S}_x^2 + \hat{S}_y^2 + \hat{S}_z^2 \tag{2.10}$$

We define the ladder operators for a spin,

$$\hat{S}_\pm = \hat{S}_x \pm i\hat{S}_y, \tag{2.11}$$

The eigenvalues of $\hat{S}^2$ and $\hat{S}_z$ are

$$\hat{S}^2 |\uparrow\rangle = \frac{3}{4}\hbar^2 |\uparrow\rangle \tag{2.12}$$

$$\hat{S}^2 \left| \downarrow \right\rangle = \frac{3}{4}\hbar^2 \left| \downarrow \right\rangle \tag{2.13}$$

$$\hat{S}_z \left| \uparrow \right\rangle = \frac{\hbar}{2} \left| \uparrow \right\rangle \tag{2.14}$$

$$\hat{S}_z \left| \downarrow \right\rangle = -\frac{\hbar}{2} \left| \downarrow \right\rangle \tag{2.15}$$

It follows that

$$\hat{S}_+ \left| \downarrow \right\rangle = \hbar \left| \uparrow \right\rangle, \ \hat{S}_+ \left| \uparrow \right\rangle = 0 \tag{2.16}$$

$$\hat{S}_- \left| \downarrow \right\rangle = 0, \ \hat{S}_- \left| \uparrow \right\rangle = \hbar \left| \downarrow \right\rangle \tag{2.17}$$

We can construct the matrix elements of $\hat{S}_x$, $\hat{S}_y$, and $\hat{S}_z$ for a two-level spin system in $\left| \uparrow \right\rangle$, $\left| \downarrow \right\rangle$ basis. Using the Eqs. (2.16) and (2.17) can be written as,

$$(\hat{S}_x + i\hat{S}_y) \left| \uparrow \right\rangle = \hbar \left| \downarrow \right\rangle \tag{2.18}$$

$$(\hat{S}_x - i\hat{S}_y) \left| \uparrow \right\rangle = 0 \tag{2.19}$$

Adding and subtracting these two equations, respectively, gives

$$\hat{S}_x \left| \uparrow \right\rangle = \frac{\hbar}{2} \left| \downarrow \right\rangle \tag{2.20}$$

$$\hat{S}_y \left| \uparrow \right\rangle = \frac{i}{2}\hbar \left| \downarrow \right\rangle \tag{2.21}$$

Similarly, we can show that

$$\hat{S}_x \left| \downarrow \right\rangle = \frac{\hbar}{2} \left| \uparrow \right\rangle, \tag{2.22}$$

$$\hat{S}_y \left| \downarrow \right\rangle = -\frac{i}{2}\hbar \left| \uparrow \right\rangle, \tag{2.23}$$

Eqs. (2.14) and (2.15) with Eqs. (2.20), (2.23) are used to calculate the matrix elements of $\hat{S}_x$, $\hat{S}_y$ and $\hat{S}_z$. We find that,

$$\hat{S}_x = \begin{pmatrix} \langle \uparrow \left| \hat{S}_x \right| \uparrow \rangle & \langle \uparrow \left| \hat{S}_x \right| \downarrow \rangle \\ \langle \downarrow \left| \hat{S}_x \right| \uparrow \rangle & \langle \downarrow \left| \hat{S}_x \right| \downarrow \rangle \end{pmatrix} = \frac{\hbar}{2} \begin{pmatrix} 0 & 1 \\ 1 & 0 \end{pmatrix}, \tag{2.24}$$

Similarly

$$\hat{S}_y = \frac{\hbar}{2} \begin{pmatrix} 0 & -i \\ i & 0 \end{pmatrix}, \tag{2.25}$$

and

$$\hat{S}_z = \frac{\hbar}{2} \begin{pmatrix} 1 & 0 \\ 0 & -1 \end{pmatrix}. \tag{2.26}$$

We define the Pauli spin operator as

$$\hat{\sigma} \equiv \frac{2}{\hbar}\hat{S}, \tag{2.27}$$

and thus Pauli spin operators in $\hat{\sigma}^2$, $\hat{\sigma}_z$ representation are

$$\hat{\sigma}_x = \begin{pmatrix} 0 & 1 \\ 1 & 0 \end{pmatrix}, \hat{\sigma}_y = \begin{pmatrix} 0 & -i \\ i & 0 \end{pmatrix}, \hat{\sigma}_z = \begin{pmatrix} 1 & 0 \\ 0 & -1 \end{pmatrix}. \tag{2.28}$$

2.6 Quantization of single-mode electromagnetic field

Let us assume a single-mode electromagnetic field in the one-dimensional cavity of length L along the z-axis. In free space, Maxwell's equations can be written as,

$$\nabla \cdot \mathbf{E} = 0 \tag{2.29}$$

$$\nabla \cdot \mathbf{B} = 0 \tag{2.30}$$

$$\nabla \times \mathbf{E} = \frac{\partial \mathbf{B}}{\partial t} \tag{2.31}$$

$$\nabla \times \mathbf{B} = \mu_o \epsilon_o \frac{\partial \mathbf{E}}{\partial t} \tag{2.32}$$

The permittivity and permeability of free space are given by ϵ_o and μ_o, respectively. These are coupled differential equations. In order to solve for the $\mathbf{E}$ and $\mathbf{B}$, we take $\nabla \times$ of Eqs. (2.31) and (2.32) and by using Eqs. (2.29) and (2.30), we get,

$$\nabla^2 \mathbf{E} = -\mu_o \epsilon_o \frac{\partial_2 \mathbf{E}}{\partial^2 t} \tag{2.33}$$

and

$$\nabla^2 \mathbf{B} = -\mu_o \epsilon_o \frac{\partial_2 \mathbf{B}}{\partial^2 t} \tag{2.34}$$

These equations can be easily solved by the separation of variables method. A solution for the single mode field that satisfy Maxwell's equations and the boundary conditions is

$$E_x(z,t) = \left(\frac{2\omega^2}{V\epsilon_o}\right)^{1/2} q(t)\sin(kz) \tag{2.35}$$

where ω denotes the frequency of the field, k being the wave number, so that $k = \omega/c$. V is the effective volume of the cavity. $q(t)$ is a time-dependent factor with the dimension of length. The expression of the magnetic field, from Eqs. (2.32) and (2.35) is given as

$$B_y(z,t) = \left(\frac{\mu_o \epsilon_o}{k}\right)\left(\frac{2\omega^2}{V\epsilon_o}\right)^{1/2} \dot{q}(t)\cos(kz) \tag{2.36}$$

The corresponding Hamiltonian H is

$$H = \frac{1}{2}\int dV\left[\epsilon_o E_x^2(z,t) + \frac{1}{\mu_o}B_y^2(z,t)\right] \tag{2.37}$$

By using Eqs. (2.35) and (2.36), Eq. (2.37) reduces to

$$H = \frac{1}{2}\left(p^2 + \omega^2 q^2\right) \tag{2.38}$$

where $p(t) = \dot{q}(t) = \frac{\partial q}{\partial t}$. Eq. (2.38) represents the field which is equivalent to a unit mass harmonic oscillator. With different scaling factors than the harmonic oscillator, electric and magnetic fields for the single mode field, in Eq. (2.38), indicate the role of canonical position and momentum. In quantum mechanics, electric and magnetic field (Eqs. (2.35) and (2.36)) can be expressed in terms of canonical operators of $\hat{p}$ and $\hat{q}$,

$$\hat{E}_x(z,t) = \left(\frac{2\omega^2}{V\epsilon_o}\right)^{1/2}\hat{q}(t)\sin(kz) \tag{2.39}$$

and

$$\hat{B}_y(z,t) = \left(\frac{\mu_o \epsilon_o}{k}\right)\left(\frac{2\omega^2}{V\epsilon_o}\right)^{1/2}\hat{p}(t)\cos(kz) \tag{2.40}$$

The Hamiltonian becomes,

$$\hat{H} = \frac{1}{2}\left(\hat{p}^2 + \omega^2\hat{q}^2\right) \tag{2.41}$$

where $\left[\hat{p},\hat{q}\right] = i\hbar$. In Eq. (2.41), the operators, $\hat{p}$ and $\hat{q}$ belong to the observable quantities. We define,

$$\hat{a} = \frac{1}{\sqrt{2\hbar\omega}}(\omega\hat{q} + i\hat{p}) \tag{2.42}$$

$$\hat{a}^\dagger = \frac{1}{\sqrt{2\hbar\omega}}(\omega\hat{q} - i\hat{p}) \tag{2.43}$$

where

$$\left[\hat{a},\hat{a}^\dagger\right] = 1 \tag{2.44}$$

By substituting Eqs. (2.42) and (2.43) in Eq. (2.41), we get

$$\hat{H} = \hbar\omega(\hat{a}^\dagger\hat{a} + \frac{1}{2}) \tag{2.45}$$

The field operators becomes,

$$\hat{E}_x(z,t) = \left(\frac{\hbar\omega}{V\epsilon_o}\right)^{1/2} (\hat{a} + \hat{a}^\dagger)\sin(kz) \tag{2.46}$$

$$\hat{B}_y(z,t) = \left(\frac{\mu_o}{k}\right)\left(\frac{\epsilon_o\hbar\omega^3}{V}\right)^{1/2}\frac{1}{i}(\hat{a} - \hat{a}^\dagger)\cos(kz) \tag{2.47}$$

Eqs. (2.46) and (2.47) describe the quantized form of the electric and magnetic field of a single mode cavity field, respectively.

2.7 Fock or Number States

Consider a single mode field having frequency ω. The Hamiltonian $\hat{H}$ given in Eq. (2.45) is the Hamiltonian of a simple quantum harmonic oscillator. The algebra of harmonic oscillator is, therefore, applicable. The state $|n\rangle$ of harmonic oscillator becomes a number state of the system of n photons, we write

$$\hat{H}|n\rangle = \hbar\omega\left(\hat{a}^\dagger\hat{a} + \frac{1}{2}\right)|n\rangle = E_n|n\rangle \tag{2.48}$$

where $E_n = (n + \frac{1}{2})$. By exploiting Eq. (2.44), it is easy to show that $\hat{a}^\dagger$ acts as a generator of producing a higher energy state (also called creation operator) and $\hat{a}$ acts as a generator of producing lower energy states (also called annihilation or destruction operator). The normalized equations correspond to field operators are

$$\hat{a}^\dagger|n\rangle = \sqrt{n+1}\,|n+1\rangle$$

$$\hat{a}|n\rangle = \sqrt{n}\,|n-1\rangle \tag{2.49}$$

where n is the eigenvalue of $\hat{N} = \hat{a}^\dagger\hat{a}$ such that $\hat{N}|n\rangle = n|n\rangle$ and is called photon or quanta number with energy $E_n = \hbar\omega$. The eigenstates $|n\rangle$ that satisfy the Eqs. (2.48) and (2.49) are called Fock states or photon number states. These states form a complete set of basis,

$$\sum_{n=0}^{\infty} |n\rangle\langle n| = 1 \tag{2.50}$$

18

We also put a lower bound on the Fock states such that there is no possible energy eigenvalue less than E_0. This argument concludes

$$\hat{a} \left|0\right\rangle = 0 \tag{2.51}$$

where $\left|0\right\rangle$ is called the vacuum state. From Eq. (2.48) we can easily check

$$E_0 = \frac{1}{2}\hbar\omega \tag{2.52}$$

is the ground energy of a harmonic oscillator. With a repeated operation of Eq. (2.49), we can obtain any Fock state from the vacuum state, and a general generating function is

$$(\hat{a}^\dagger)^n \left|0\right\rangle = \sqrt{n!} \left|n\right\rangle \tag{2.53}$$

2.8 Coherent States

When we deal with the quantized electromagnetic field, we have to notice the nature of the field. The term "nature" accounts for the amount of quantumness present in the electromagnetic states. Some states are pure quantum mechanical states, for example, the Fock states. While some other states have the least quantum mechanical feature, for example, the coherent field and the squeezed states. We use the uncertainty relation to measure the quantum behavior of a state under observation. The states which have maximum uncertainty in them have the maximum amount of quantumness while the states which show the least i.e. minimum uncertainty in the uncertainty relation are the least quantum mechanical states. Here, we briefly describe some properties of coherent field and analyze their behavior. These states exhibit many interesting properties when they are investigated with different quantum models and situations [80–88].

2.8.1 Coherent States in Fock State Representation

We define a normalized eigenstate of the annihilation operator $\hat{a}$ as the coherent field, denoted by $\left|\alpha\right\rangle$, such that

$$\hat{a}\,|\alpha\rangle = \alpha\,|\alpha\rangle \tag{2.54}$$

where α is the eigenvalue of the coherent field and can be expressed as $\alpha = |\alpha|\exp[i\phi]$ with ϕ as a general phase term. The coherent field can be expanded in the number state basis as

$$|\alpha\rangle = \sum_{n=0}^{\infty} c_n\,|n\rangle \tag{2.55}$$

the coherent field forms a complete basis, this means $\langle\alpha|\alpha\rangle = 1$. Since $|n\rangle$ basis are orthonormal, the product of number state $\langle n|$ with Eq. (2.55) produces $c_n = \langle n|\alpha\rangle$. Using this coefficient in Eq. (2.55) we have

$$|\alpha\rangle = \sum_{n=0}^{\infty} |n\rangle\,\langle n|\alpha\rangle \tag{2.56}$$

By exploiting the property of the creation operator Eq. (2.53), that is $\langle n| = \frac{1}{\sqrt{n!}}\langle 0|\,(\hat{a})^n$ we have

$$|\alpha\rangle = \sum_{n=0}^{\infty} \frac{1}{\sqrt{n!}}\,|n\rangle\,\langle 0|\,(\hat{a})^n\,|\alpha\rangle$$

or

$$|\alpha\rangle = C_o \sum_{n=0}^{\infty} \frac{\alpha^n}{\sqrt{n!}}\,|n\rangle \tag{2.57}$$

Where $C_o = \langle 0|\alpha\rangle$. By using the orthonormality condition, we can find the value of C_o,

$$C_o = \exp[-\frac{1}{2}|\alpha|^2]$$

By substituting the value of C_o into Eq. (2.57), we have

$$|\alpha\rangle = \exp[-\frac{1}{2}|\alpha|^2]\sum_{n=0}^{\infty} \frac{\alpha^n}{\sqrt{n!}}\,|n\rangle \tag{2.58}$$

This equation represents the normalized coherent field. Another way to write Eq. (2.58) is

$$|\alpha\rangle = \exp[-\frac{1}{2}|\alpha|^2]\sum_{n=0}^{\infty} \frac{\alpha^n}{\sqrt{n!}}\frac{1}{\sqrt{n!}}(\hat{a}^\dagger)^n\,|0\rangle \tag{2.59}$$

One can easily simplify the above equation by using the identity

$$\exp[\alpha(\hat{a})^\dagger]\,|0\rangle = \sum_n \frac{\alpha^n(\hat{a}^\dagger)^n}{n!}\,|0\rangle \tag{2.60}$$

This implies

$$|\alpha\rangle = \exp[-\frac{1}{2}|\alpha|^2]\exp[\alpha(\hat{a})^\dagger]|0\rangle = \exp[-\frac{1}{2}|\alpha|^2 + \alpha(\hat{a})^\dagger]|0\rangle \qquad (2.61)$$

The above representation of a coherent field can be simplified by using Baker-Campbell-Hausdorff (BCH) formula,

$$\exp[X + Y] = \exp[-\frac{1}{2}[X,Y]]\exp[X]\exp[Y] \qquad (2.62)$$

valid if $[X,Y] \neq 0$. With the help of BCH formula, for $X = \alpha(\hat{a})^\dagger$ and $Y = \alpha^*\hat{a}$ one can check

$$\exp[\alpha(\hat{a})^\dagger - \alpha^*\hat{a}] = \exp[\alpha(\hat{a})^\dagger]\exp[-\alpha^*\hat{a}]\exp[-\frac{1}{2}|\alpha|^2] \qquad (2.63)$$

Expanding $\exp[-\alpha^*a]$, one can check,

$$\exp[-\alpha^*\hat{a}]|0\rangle = 0 \qquad (2.64)$$

Furthermore,

$$\exp[\alpha(\hat{a})^\dagger]|0\rangle = \sum_{n=0}^{\infty} \frac{\alpha^n}{\sqrt{n!}}|n\rangle \qquad (2.65)$$

By using Eqs. (2.63) to (2.65), Eq. (2.61) will be simplified as

$$|\alpha\rangle = \hat{D}(\alpha)|0\rangle \qquad (2.66)$$

where,

$$\hat{D}(\alpha) = \exp[\alpha(\hat{a})^\dagger - \alpha^*\hat{a}] \qquad (2.67)$$

where $\hat{D}(\alpha)$ is called the displacement operator. Eq. (2.66) states that the coherent field are produced with the displacement operator $\hat{D}(\alpha)$ which is applied to the ground state of the harmonic oscillator.

Some Properties of Coherent States

(a) The average photons in the coherent field $|\alpha\rangle$ are given by

$$\langle\alpha|\hat{a}^\dagger\hat{a}|\alpha\rangle = <n> = |\alpha|^2 \qquad (2.68)$$

(b) The probability of finding number of photons n, defined by $p(n)$, is given by the Poisson distribution (see Eq. (2.58)),

$$p(n) = |<n|\alpha>|^2 = \exp[-|\alpha|^{2n}]\frac{|\alpha|^{2n}}{n!} \qquad (2.69)$$

21

2.9 Interaction of Atom With Quantized Electromagnetic Field

In general, the wavelength λ of a typical electromagnetic radiation inside the cavity is much bigger than the size of an atomic system. A single electron atom, which is considered as a dipole with magnitude of charge e and charge separation $\mathbf{r}$, has dipole moment $\mathbf{d} = e\mathbf{r}$. In the dipole approximation $\mathbf{k.r} << 1$, with $\mathbf{k} = \frac{2\pi}{\lambda}$. The Hamiltonian of a single electron atom with the radiation field $\mathbf{E}$, in dipole approximation can be described by the following equation [89],

$$\hat{H} = \hat{H}_A + \hat{H}_F - e\mathbf{r} \cdot \mathbf{E} \tag{2.70}$$

The atomic and field Hamiltonian are represented by $\hat{H}_A$ and $\hat{H}_F$, respectively. We have assumed the dipole approximation to obtain the interaction part in the Hamiltonian Eq. (2.70) and the field is supposed to be uniform over the entire submerged atom.

The field Hamiltonian $\hat{H}_F$ (Eq. (2.41)) is written as

$$\hat{H}_F = \hbar\omega\big(\hat{a}^\dagger\hat{a} + \frac{1}{2}\big) \tag{2.71}$$

We define atomic transition operators

$$\hat{\sigma}^{ij} = |i\rangle \langle j| \tag{2.72}$$

and $\{|i\rangle\}$ represents the set of atomic energy eigenstates, i.e. $\hat{H}_A |i\rangle = E_i |i\rangle$ and this set is complete i.e. $\sum_i |i\rangle \langle i| = 1$. In the terms of these basis $\{|i\rangle\}$, the atomic energy Hamiltonian $\hat{H}_A$ is given as

$$\hat{H}_A = \sum_i E_i |i\rangle \langle i| = E_i\hat{\sigma}^{ii} \tag{2.73}$$

The term $e\mathbf{r}$ can be expressed in terms of atomic transition operators

$$e\mathbf{r} = \sum_{i,j} e |i\rangle \langle i| \mathbf{r} |j\rangle \langle j| = \sum_{i,j} \wp^{ij}\hat{\sigma}^{ij} \tag{2.74}$$

where $\wp^{ij} = e \langle i| \mathbf{r} |j\rangle$ are the element of matrix corresponds to transition matrix. We suppose a single-mode electromagnetic field with polarization vector $\boldsymbol{\epsilon}$ in free space, the

electric field $\mathbf{E}$ can be represented as

$$\mathbf{E} = -\boldsymbol{\epsilon}\left(\frac{\hbar\omega}{2\epsilon_0 V}\right)^{1/2}(\hat{a} + \hat{a}^\dagger) \tag{2.75}$$

Now upon substituting Eqs. (2.71), (2.73), (2.74) into Eq. (2.70) we have

$$\hat{H} = \hbar\omega\hat{a}^\dagger\hat{a} + \sum_i E_i \sigma^{ii} + \hbar\sum_{i,j} g^{ij}\sigma^{ij}(\hat{a} + \hat{a}^\dagger) \tag{2.76}$$

where

$$g^{ij} = -\frac{\boldsymbol{\epsilon} \cdot \boldsymbol{\wp}^{ij}(\hbar\omega)^{1/2}}{(2\epsilon_0 V)^{1/2}\hbar} \tag{2.77}$$

We have omitted the zero point energy in the field in the first term in Eq. (2.76).

2.10 The Jaynes-Cummings Model

The Jaynes-Cummings model [8] is the quantum version of the Rabi model [90]. In this model, we treat the field quantum mechanically (Eq. (2.75)). Physically, an atom can interact with an infinite field modes, but it is assumed that it interacts only with a single-mode field. The energy associated with the atom and field is given by Eqs. (2.73) and (2.71) respectively. The interaction Hamiltonian is modified by using some approximations and a refined form of this Hamiltonian is obtained in this section. The resulting total Hamiltonian is called the Jaynes-Cummings Hamiltonian or Rabi Hamiltonian under some approximations.

We consider an atom, with two levels denoted by $|0\rangle$ and $|1\rangle$, which interacts with a single mode electromagnetic field

$$\mathbf{E} = \boldsymbol{\epsilon}\left(\frac{\hbar\omega}{2\epsilon_0 V}\right)^{1/2}(\hat{a} + \hat{a}^\dagger)\sin(k_z z) \tag{2.78}$$

$\boldsymbol{\epsilon}$ is a polarization vector with arbitrary orientation. The interaction Hamiltonian is

$$\hat{H}_1 = -e\mathbf{r} \cdot \mathbf{E} = g\mathbf{d} \cdot (\hat{a} + \hat{a}^\dagger) \tag{2.79}$$

where $g = -\boldsymbol{\epsilon}\left(\frac{\hbar\omega_k}{2\epsilon_0 V}\right)^{1/2}\sin(k_z z)$ and $\mathbf{d} = e\mathbf{r}$.
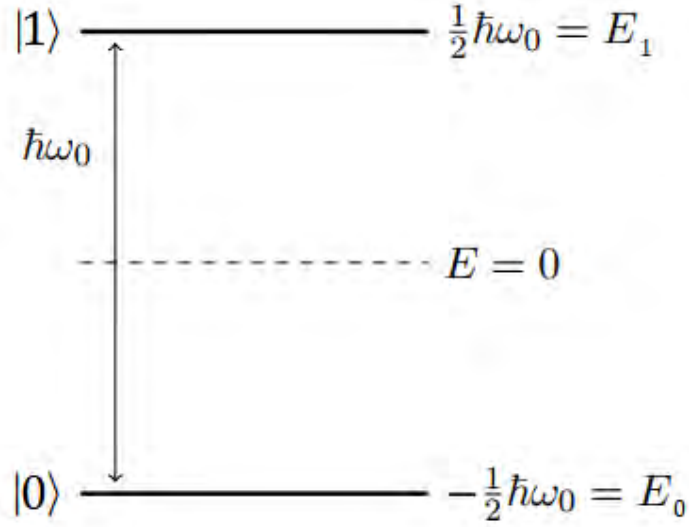
Figure 2.2: Energy level scheme of a TLS where $E = 0$ is taken at the center of the two energy states

We now define atomic transition operators. The operator $\hat{\sigma}_+$ raises the atom from its ground state $|0\rangle$ to an excited state $|1\rangle$ is called the atomic raising operator and the operator $\hat{\sigma}_-$ performs the opposite is called atomic lowering operator. These operators are defined as

$$\hat{\sigma}_+ = |1\rangle \langle 0|, \ \hat{\sigma}_- = |0\rangle \langle 1| \tag{2.80}$$

The atomic inversion operator can be defined as

$$\hat{\sigma}_z = |0\rangle \langle 0| - |1\rangle \langle 1| \tag{2.81}$$

The operators $\hat{\sigma}_\pm$ and $\hat{\sigma}_z$ obey the Pauli spin algebra

$$[\hat{\sigma}_+, \hat{\sigma}_-] = \hat{\sigma}_z, \ [\hat{\sigma}_z, \hat{\sigma}_\pm] = 2\hat{\sigma}_\pm \tag{2.82}$$

To find another useful form of the interaction Hamiltonian, we use Eq. (2.74) to find the elements of the dipole operator. For the sake of the parity conservation, the diagonal electric dipole transition matrix elements are zero $\wp^{ee} = e \langle e| \mathbf{r} |e\rangle = 0 = \wp^{gg}$ and the off-diagonal elements are given by (Eq. (2.74))

$$\mathbf{d} = e\mathbf{r} = \wp^{01} |0\rangle \langle 1| + \wp^{*10} |1\rangle \langle 0| \tag{2.83}$$

24

We assume that $\wp^{ge} = \wp^{*eg} = \wp$, therefore, Eq. (2.83) will become

$$\mathbf{d} = \wp(\hat{\sigma}_+ + \hat{\sigma}_-) \tag{2.84}$$

By using Eq. (2.84) into Eq. (2.79), the interaction Hamiltonian will become

$$\hat{H}_1 = \hbar\lambda(\hat{\sigma}_+ + \hat{\sigma}_-)(\hat{a} + \hat{a}^\dagger) \tag{2.85}$$

where we have defined $\lambda = \frac{g\wp}{\hbar}$

We use Fig. (2.2) to derive a convenient form of atomic Hamiltonian. We define a zero energy level in the middle of the atomic energy levels $|0\rangle$ and $|1\rangle$. In this configuration, atomic level $|1\rangle$ has energy $E_1 = \frac{1}{2}\hbar\omega_0$ and atomic level $|0\rangle$ has energy $E_0 = -\frac{1}{2}\hbar\omega_0$ with respect to the $E = 0$ energy level. The total energy (Eq. (2.73)) between the levels is, therefore

$$\hat{H}_A = E_1 |1\rangle \langle 1| + E_0 |0\rangle \langle 0| = \frac{1}{2}\hbar\omega_0\hat{\sigma}_z \tag{2.86}$$

Thus total Hamiltonian can be obtained by using Eqs. (2.85), (2.86) and (2.71) into Eq. (2.70) and dropping zero point energy term, we get

$$\hat{H} = \frac{1}{2}\hbar\omega_0\hat{\sigma}_z + \hbar\omega\hat{a}^\dagger\hat{a} + \hbar\lambda(\hat{\sigma}_+ + \hat{\sigma}_-)(\hat{a} + \hat{a}^\dagger) \tag{2.87}$$

This is the famous Rabi Hamiltonian or Jaynes-Cummings Hamiltonian without the rotating wave approximation (RWA). This Hamiltonian can be simplified by using the RWA. This approximation modifies the interaction part of the Rabi Hamiltonian. For this purpose, we use the unitary evolution of the field and atomic operators. In the free-field case, $\hat{a}^\dagger(t) = \hat{a}^\dagger(0)\exp[i\omega t]$ and $\hat{a}(t) = \hat{a}(0)\exp[-i\omega t]$ and free-atomic case $\hat{\sigma}_\pm(t) = \hat{\sigma}_\pm(0)\exp[\pm i\omega_0 t]$ we expand and analyze the time-dependent interaction parts of Eq. (2.87) as

$$\hat{\sigma}_+\hat{a} \sim \exp[i(-\omega + \omega_0)t]$$

$$\hat{\sigma}_-\hat{a}^\dagger \sim \exp[-i(-\omega + \omega_0)t]$$

$$\hat{\sigma}_+\hat{a}^\dagger \sim \exp[i(\omega + \omega_0)t]$$

$$\hat{\sigma}_-\hat{a} \sim \exp[-i(\omega + \omega_0)t] \tag{2.88}$$

In the case of $\omega_0 \approx \omega$ the last two terms of Eq. (2.88) vary more rapidly as compared to the other terms. These terms also violate energy conservation as compared to the first terms. $\hat{\sigma}_+ \hat{a}^\dagger$ represents the excitation of an atom with the creation of a photon, which is physically not possible, $\hat{\sigma}_- \hat{a}$ represents to de-excitation of an atom with the absorption of a photon, which is also physically not possible. So we drop these terms and we get

$$\hat{H} = \frac{1}{2}\hbar\omega_0\hat{\sigma}_z + \hbar\omega\hat{a}^\dagger\hat{a} + \hbar\lambda(\hat{\sigma}_+\hat{a} + \hat{\sigma}_-\hat{a}^\dagger) \tag{2.89}$$

The interaction of the field with the atom, represented by the above Hamiltonian, is used widely and is called the Jaynes-Cummings (JC) Hamiltonian.

2.11   The Tavis-Cummings Model

The JC model presents an atom coupled with a single mode quantized electromagnetic field. This model is a bipartite system [91]. Whereas in the Tavis-Cummings model, two identical TLS, let atom A and B, are coupled with a single mode quantized electromagnetic field. This model is referred to as a multipartite system. The atomic Hamiltonians of atom A and B can be calculated by using Eq. (2.86) and the total energy associated with the atom A and B is, therefore,

$$\hat{H}_{AB} = \hat{H}^A + \hat{H}^B = \frac{1}{2}\hbar\omega_0\hat{\sigma}_z^A + \frac{1}{2}\hbar\omega_0\hat{\sigma}_z^B \tag{2.90}$$

where ω_0 is the transition frequency of both atoms. These atoms are coupled with the single-mode quantized electromagnetic field of frequency ω. Again, by dropping the zero point energy term, the energy of this field is given by

$$\hat{H}_F = \omega\hat{a}^\dagger\hat{a} \tag{2.91}$$

This field interacts with both atoms with the same coupling strengths. By using the RWA, the interaction Hamiltonian of the TC model can be written as

$$\hat{H}_I = \hbar\lambda \sum_{i=A,B} (\hat{\sigma}_+^i\hat{a} + \hat{\sigma}_-^i\hat{a}^\dagger) \tag{2.92}$$

where λ denoted the coupling strength of the field with atoms. We also assume that the atoms resonantly interact with the single-mode field. This assumption is used to implement the RWA in the Tavis-Cummings model. The total Hamiltonian of this multipartite system is therefore

$$\hat{H} = \frac{1}{2}\hbar\omega_0(\hat{\sigma}_z^A + \hat{\sigma}_z^B) + \omega\hat{a}^\dagger\hat{a} + \hbar\lambda \sum_{i=A,B} (\hat{\sigma}_+^i\hat{a} + \hat{\sigma}_-^i\hat{a}^\dagger) \tag{2.93}$$

The above equation represents the Tavis-Cummings model Hamiltonian and this Hamiltonian is vastly used to study the dynamics of multipartite systems.

2.12   Summary

We have reviewed some basic concepts of quantum optics. We have studied quantum states, the quantum state of a qubit, and described Pauli spin matrices. Furthermore, we have discussed the quantization of electromagnetic field and the interaction of the quantized electromagnetic field with an atom. And finally, we reviewed the Jaynes-Cummings and the Tavis-Cummings model.

Chapter 3

Open Quantum System

3.1 Introduction

A closed quantum system is thought to be completely isolated from the surroundings and there is no effect of the environment on the system [92]. Whereas, we can not describe the dynamics of open quantum system by the unitary time evolution. In this chapter, we will discuss density matrix formalism to describe a system. We will derive the master equation. It is used to study the quantum dynamics of an open system. We will also study the case of a moving atomic system inside the field modes.

3.2 Quantum States and the Density Operator

In quantum mechanics, we describe the state of a system entirely by a state vector $|\Psi\rangle$. The state vector $|\Psi\rangle$ belongs to a Hilbert space $\mathcal{H}$. In general, a Hilbert space can have any number of dimensions. A pure state can be written by a state vector. However, for physical systems, the quantum state is not fully known. Let $|\psi_i\rangle$ is the state vector of the system, and p_i is the probability of the state $|\psi_i\rangle$, the density operator $\hat{\rho}$ describes the state of the system is defined as

$$\hat{\rho} = \sum_i p_i |\psi_i\rangle \langle\psi_i| \tag{3.1}$$

The state of the system described in equation (3.1) is called the mixed state. A mixed state is a mixture of two or more states. The following properties are obeyed by a density

operator:

- $\hat{\rho}$ has a trace equal to 1:

$$Tr[\hat{\rho}] = 1, \tag{3.2}$$

- $\hat{\rho}$ is a positive operator:

$$\langle \psi | \hat{\rho} | \psi \rangle \geq 1 \tag{3.3}$$

for any state vector $|\psi\rangle$.

- $\hat{\rho}$ is a Hermitian:

$$\hat{\rho}^\dagger = \hat{\rho} \tag{3.4}$$

The density operator formalism provides a convenient route for describing a quantum system whose state is not completely known. In this formalism, a quantum system is formed by an ensemble of pure states with some finite probability. We can formulate all the postulates of quantum mechanics by the density matrix formalism.

Mixed and Pure States

Consider a system is in a state $|\psi\rangle$. We suppose that this system could be expandable in some orthonormal basis, such as $|a_i\rangle$

$$|\psi\rangle = \alpha_1 |a_1\rangle + \alpha_2 |a_2\rangle + \cdots + \alpha_n |a_n\rangle \tag{3.5}$$

The $|\alpha_i|^2$ is the probability of finding the system in state $|a_i\rangle$. The system is said to be in a pure state if it is present in a definite state as given in Eq. (3.5). The density operator for this case is $\hat{\rho} = |\psi\rangle \langle\psi|$, then

$$\hat{\rho}^2 = (|\psi\rangle \langle\psi|)(|\psi\rangle \langle\psi|) = |\psi\rangle \langle\psi| = \hat{\rho} \tag{3.6}$$

The first property of density operator as described in Eq. (3.2), we have generalized that for the pure states only $Tr[\hat{\rho}^2] = 1$.

The density operator describes the way to deal with the states that appear in the statistical mixture. The mixed states have no coherence. Therefore, the off-diagonal elements of the density matrix are zero, i.e. $\hat{\rho}_{mn}$ when $m \neq n$.

Reduced Density Operator

Suppose a bipartite system which is composed of Alice (A) and Bob (B), the composite system has density operator $\hat{\rho}_{AB}$. If we are interested to study the behavior of one subsystem of this composite system, we can comprehend this situation by reducing the density matrix. If we want to analyze the subsystem A from this composite system, the reduced density operator is described by,

$$\hat{\rho}_A = \text{Tr}_B[\hat{\rho}_{AB}] \tag{3.7}$$

where Tr_B is referred to as the partial trace taken over the subsystem B. The partial trace is defied by

$$\text{Tr}_B[|a_1\rangle \langle a_2| \otimes |b_1\rangle \langle b_2|] = |a_1\rangle \langle a_2| \, \text{Tr}[|b_1\rangle \langle b_2|] \tag{3.8}$$

The vectors $|a_1\rangle$ and $|a_2\rangle$ belong to the Hilbert space $\mathcal{H}_A$ and vectors $|b_1\rangle$ and $|b_2\rangle$ belong to the in Hilbert space $\mathcal{H}_B$. The trace of Eq. (3.8) is the trace on the subsystem B. The partial trace is physically justified on the basis that by the implication of trace in this way in Eq. (3.8) provides correct results of measurement made on system A. In addition, Eq. (3.8) also requires that the partial trace has a linear implication. For example, for any two operators M^{AB} and N^{AB}, the trace $\text{Tr}_B[M^{AB} + N^{AB}] = \text{Tr}_B[M^{AB}] + \text{Tr}_B[N^{AB}]$.

3.3 The dynamics of a closed system

3.3.1 Liouville-von Neumann equation

The time evolution of a quantum state $|\psi(t)\rangle$ can be found by the Schrodinger equation, i.e.

$$i\hbar \frac{d}{dt} |\psi(t)\rangle = \hat{H} |\psi(t)\rangle . \tag{3.9}$$

Since $\hat{H}$ is a Hermitian operator, we can write

$$-i\hbar \frac{d}{dt} \langle \psi(t)| = \langle \psi(t)| \hat{H} \tag{3.10}$$

The dynamics of a closed system are described by Eq. (3.9) and the state of the system is pure. For a pure state $|\psi(t)\rangle$, $\hat{\rho}$ is

$$\hat{\rho}(t) = |\psi(t)\rangle \langle \psi(t)| . \tag{3.11}$$

By taking the time derivative of the density operator, we have

$$\frac{d\hat{\rho}(t)}{dt} = \frac{d}{dt}(|\psi(t)\rangle\langle\psi(t)|) \tag{3.12}$$

By using the product rule and using Eqs. (3.9) and (3.10), we can write

$$\frac{d\hat{\rho}(t)}{dt} = -\frac{i}{\hbar}\left[\hat{H}, \hat{\rho}(t)\right]. \tag{3.13}$$

This equation is called the Liouville-von Neumann equation and describes the time evolution of $\hat{\rho}(t)$ for a closed system [94].

3.4 Dynamics of Open Quantum System

In this section we derive the Master equation. This equation can be derived from intuition based on physical grounds. The derivation provides a clear idea of the physics behind the master equation.

3.4.1 The Master Equation

An open quantum system is the one that interacts with another external quantum system which is generally known as the environment. To study the dynamics, it is assumed that the system and environment belong to a bigger closed system [95]. We consider a situation that is described by a Hamiltonian $\hat{H}$ of the form

$$\hat{H} = \hat{H}_S + \hat{H}_E + \hat{H}_I \tag{3.14}$$

where the constituent Hamiltonians $\hat{H}_S$, $\hat{H}_E$ and $\hat{H}_I$ describe the system, the environment and the interaction, respectively. The density operator of the system and environment, given by $\hat{\rho}_{tot}(t)$, in the Schrodinger picture, satisfies,

$$\frac{d\hat{\rho}_{tot}}{dt} = -\frac{i}{\hbar}\left[\hat{H}_S + \hat{H}_E + \hat{H}_I, \hat{\rho}_{tot}\right] \tag{3.15}$$

The part of the system density operator is,

$$\hat{\rho}(t) = \text{Tr}_E\{\hat{\rho}_{tot}(t)\} \tag{3.16}$$

Transformation to the Interaction Picture

It is convenient to transform the equation of motion into the interaction picture, we can write

$$\hat{\rho}_I(t) = \exp\left(\frac{i(\hat{H}_S + \hat{H}_E)t}{\hbar}\right) \hat{\rho}_{tot}(t) \exp\left(-\frac{i(\hat{H}_S + \hat{H}_E)t}{\hbar}\right) \tag{3.17}$$

The density operator $\hat{\rho}_I(t)$ obeys the equation of motion,

$$\frac{d\hat{\rho}_I}{dt} = -\frac{i}{\hbar}\left[\hat{H}_I, \hat{\rho}_I(t)\right] \tag{3.18}$$

where

$$\hat{H}_I(t) = \exp\left(\frac{i(\hat{H}_S + \hat{H}_E)t}{\hbar}\right) \hat{H}_I \exp\left(-\frac{i(\hat{H}_S + \hat{H}_E)t}{\hbar}\right), \tag{3.19}$$

On the same arguments of Eq. (3.16), we can write,

$$\hat{\rho}(t) = \text{Tr}_E\left\{\exp\left(-\frac{i(\hat{H}_S + \hat{H}_E)t}{\hbar}\right) \hat{\rho}_I(t) \exp\left(\frac{i(\hat{H}_S + \hat{H}_E)t}{\hbar}\right)\right\} \tag{3.20}$$

Since $\hat{H}_E$ is a function of only the environment variable, we can use the cyclic property of the trace of Eq. (3.20), to cancel out the factors that involve $\hat{H}_E$, we get

$$\hat{\rho}(t) = \exp\left(-\frac{i\hat{H}_S t}{\hbar}\right) \hat{\rho}(t) \exp\left(\frac{i\hat{H}_S t}{\hbar}\right) \tag{3.21}$$

where

$$\hat{\rho}(t) \equiv \text{Tr}_E\{\hat{\rho}_I(t)\} \tag{3.22}$$

is the reduced density operator in the interaction picture.

Initial Conditions

We assume that the system and the environment are initially independent of each other. In this assumption, the total density operator can be written in a direct product,

$$\hat{\rho}_{tot}(t) = \hat{\rho}(0) \otimes \hat{\rho}_E \tag{3.23}$$

In addition, we assume that the environment is so large that the weak coupling of the system and the environment does not affect the statistical properties of the environment.

Integration of the Equation of Motion

We integrate Eq. (3.18) from time 0 to t and using the initial condition given in Eq. (3.23), after two iteration we have

$$\hat{\rho}_I(t) = \hat{\rho}_I(0) - \frac{i}{\hbar} \int_0^t \left[\hat{H}_I(t'), \hat{\rho}_I(0) \right] dt' - \frac{1}{\hbar^2} \int_0^t \int_0^{t'} \left[\hat{H}_I(t'), \left[\hat{H}_I(t''), \hat{\rho}_I(t'') \right] \right] dt' dt'' \tag{3.24}$$

If we differentiate Eq. (3.24) with respect to t we get

$$\dot{\rho}_I(t) = -\frac{i}{\hbar} \left[\hat{H}_I(t), \hat{\rho}_I(0) \right] - \frac{1}{\hbar^2} \int_0^t \left[\hat{H}_I(t), \left[\hat{H}_I(t'), \hat{\rho}_I(t') \right] \right] dt' \tag{3.25}$$

Trace Over the Environment Variables

If we take trace both sides of Eq. (3.25) over the environment variables and use Eq. (3.22), we obtain

$$\dot{\rho}_I(t) = -\frac{1}{\hbar^2} \int_0^t \left[\hat{H}_I(t), \left[\hat{H}_I(t'), \hat{\rho}_I(t') \right] \right] dt' \tag{3.26}$$

where we have used

$$\text{Tr}_E \left\{ \hat{H}_I(t) \hat{\rho}_I(0) \right\} = 0 \tag{3.27}$$

and

$$\hat{\rho}_I(0) = \hat{\rho}_{\text{tot}}(0) = \hat{\rho}(0) \otimes \hat{\rho}_E \tag{3.28}$$

as given in Eq. (3.23). This implies that we assume the interaction has no diagonal elements in the representation in which $\hat{H}_E$ is diagonal.

Weak Coupling Assumption

We assume that $\hat{H}_I$ is very less than either $\hat{H}_S$ or $\hat{H}_E$. And we assume that the environment density operator $\hat{\rho}_B$ is not significantly affected by the interaction. In these assumptions, we can replace $\hat{\rho}_I(t')$ in Eq. (3.26) by a factorized approximation

$$\hat{\rho}_I(t') \simeq \hat{\rho}(t') \otimes \hat{\rho}_E \tag{3.29}$$

In the above equation, we have made the following assumptions;

i) The environment density operator is not significantly affected by the interaction.

ii) The system density operator is allowed to change significantly. This assumption is made because the system is much smaller than the environment.

iii) We assume the density operator may be written approximately as a direct product. The approximations like,

$$\text{Tr}_E\big\{[A_E(t),[A_E(t'),\hat{\rho}_I(t')]]\big\} \simeq \hat{\rho}(t') \otimes \text{Tr}_E\big\{[A_E(t),[A_E(t'),\hat{\rho}_E]]\big\} \qquad (3.30)$$

are valid approximations. This means that the environment correlation functions are not significantly affected by the interactions.

Markov Approximation

By using the weak coupling assumption, we can write Eq. (3.26) as

$$\dot{\rho}_I(t) = -\frac{1}{\hbar^2} \int_0^t \left[\hat{H}_I(t), \left[\hat{H}_I(t'), \hat{\rho}(t') \otimes \hat{\rho}_E\right]\right] dt' \qquad (3.31)$$

The interaction is assumed weak, therefore, the rate of change of the system density operator in the interaction picture is quite slow compared to that of the environment operator. The environment correlation functions are generally determined by a thermal choice of ρ_E, which is much shorter than the time constant expected for $\hat{\rho}(t)$. Within these limits, the factor $\hat{\rho}(t')$ changes significantly over the time that is taken for the correlation function in Eq. (3.31) to vanish. In this case, we can take

i) $\hat{\rho}(t') \rightarrow \hat{\rho}(t)$

ii) For $t \gg \tau_T$ called thermal correlation time, which is defined by $\tau_T = \frac{\hbar}{2\pi kT}$ (k is Boltzmann constant and T is temperature), we can take the the lower limit of the integral of Eq. (3.31) go to $-\infty$

In this case, we write the master equation,

$$\dot{\rho}_I(t) = -\frac{1}{\hbar^2} \int_0^\infty \left[\hat{H}_I(t), \left[\hat{H}_I(t-\tau), \hat{\rho}(t) \otimes \hat{\rho}_E\right]\right] dt \qquad (3.32)$$

This is called the master equation. The approximation, $\hat{\rho}(t') \rightarrow \hat{\rho}(t)$ is known as the Markov approximation.

3.5 Intrinsic Decoherence

In time interval $(t + \tau)$, the dynamics of a system can be written as

$$\hat{\rho}(t + \tau) = \exp\left[-\frac{i\hat{H}\tau}{\hbar}\right] \hat{\rho}(t) \exp\left[\frac{i\hat{H}\tau}{\hbar}\right]. \qquad (3.33)$$

This relation is true for any size of time interval τ in standard quantum mechanics. If the time scale τ is sufficiently small, Milburn [96] postulated that the change in the phase of the state of the system is uncertain. The following properties hold for small τ: (i) $p(\tau)$ is the probability of the change of state of the system, (ii) the change in the state is given by

$$\hat{\rho}(t+\tau) = \exp\left[-\frac{i\varepsilon(\tau)\hat{H}}{\hbar}\right]\hat{\rho}(t)\exp\left[\frac{i\varepsilon(\tau)\hat{H}}{\hbar}\right]. \tag{3.34}$$

$$\hat{\rho}(t+\tau) \equiv F(\tau)\hat{\rho}(t) \tag{3.35}$$

(iii) even if the interval $\tau \to 0$, some minimum unitary phase change exists, mathematically

$$\lim_{\tau \to 0}\varepsilon(\tau) = \varepsilon_0, \tag{3.36}$$

For a sufficiently large time interval τ, in standard quantum mechanics $p(\tau) \longrightarrow 1$ and $\varepsilon(\tau) \longrightarrow \tau$. Thus one possible choice for $\varepsilon(\tau)$

$$\varepsilon(\tau) = \frac{\tau}{p(\tau)}. \tag{3.37}$$

We divide the interval $(0,\ t)$ into N intervals of size τ. Hence $t = N\tau$. We have

$$\begin{aligned}
\hat{\rho}(t) &= \sum_{n=0}^{N}\binom{N}{N}p(\tau)^n\left[1 - p(\tau)\right]^{N-n}F(\tau)^n\hat{\rho}(0) \\
&= \left[1 + p(\tau)S(\tau)\right]^N\hat{\rho}(0),
\end{aligned} \tag{3.38}$$

where $F(\tau)$ and $S(\tau)$ related through

$$S(\tau) = F(\tau) - 1. \tag{3.39}$$

A similar equation has been used to describe the sub-Poissonian pumped laser[97]. The rate of change of Eq. (3.38) is,

$$\frac{d\hat{\rho}(t)}{dt} = \frac{1}{\varepsilon(\tau)p(\tau)}\ln\left[1 + p(\tau)S(\tau)\right]\hat{\rho}(t). \tag{3.40}$$

For $\tau \longrightarrow 0$, Eq. (3.40) reduces to

$$\frac{d\hat{\rho}(t)}{dt} = \frac{1}{\varepsilon_0 p_0}\ln\left[1 + p_0 S_0\right]\hat{\rho}(t). \tag{3.41}$$

For stochastic time steps, a Poisson model can be defined by putting $p_0 \longrightarrow 0$ and $\gamma = \frac{1}{\varepsilon_0}$, we can write

$$\frac{d\hat{\rho}(t)}{dt} = \gamma\exp\left[\frac{-i}{\hbar\gamma}\hat{H}\right]\hat{\rho}\exp\left[\frac{i}{\hbar\gamma}\hat{H}\right] - \gamma\hat{\rho}. \tag{3.42}$$

For a sufficiently short time interval, we can show that the probability of the evolution of the state of the system is given by $\gamma\tau$. We expand Eq. (3.41) and neglect the higher-order terms [98], we have

$$\frac{d\hat{\rho}(t)}{dt} = \frac{-i}{\hbar}\left[\hat{H}, \hat{\rho}\right] - \frac{1}{2\hbar^2\gamma}\left[\hat{H}, \left[\hat{H}, \hat{\rho}\right]\right]. \tag{3.43}$$

For $\gamma \longrightarrow \infty$, we get back the Schrodinger equation. In the energy eigenbasis Eq. (3.42), we can write

$$
\begin{aligned}
\frac{\partial}{\partial t}\langle E'|\,\rho(\hat{t})\,|E\rangle &= -\frac{-i}{\hbar}\langle E'|\left[\hat{H}, \hat{\rho}\right]|E\rangle - \frac{1}{2\hbar^2\gamma}\langle E'|\left[\hat{H}, \left[\hat{H}, \hat{\rho}\right]\right]|E\rangle \\
&= -\frac{-i}{\hbar}(E' - E)\langle E'|\,\hat{\rho}\,|E\rangle - \frac{1}{2\hbar^2\gamma}(E' - E)^2\langle E'|\,\hat{\rho}\,|E\rangle .
\end{aligned}
$$

Eq. (3.43) shows that the rate of decoherence between the states of the system depends on the square of energy separations between the superposed states. Therefore, the first-order correction in Eq. (3.43) leads to the decoherence in the energy eigenstates.

3.6   Kerr Effect

The relationship between polarization vector **P** and the applied electric field **E** is given as,

$$\mathbf{P} = \chi\epsilon_0\mathbf{E} \tag{3.44}$$

where the factor χ is called susceptibility of the medium. When the electric field E is increased significantly, nonlinear effects appear within the medium. For this case, we generalize Eq. (3.44) as follows

$$\mathbf{P} = \epsilon_0(\chi^{(1)}E + \chi^{(2)}E^2 + \chi^{(3)}E^3 + \dots) \tag{3.45}$$

where $\chi^{(1)}$ is known as the linear susceptibility, and $\chi^{(2)}$ and $\chi^{(3)}$ are referred to as the second-and third-order non-linear optical susceptibilities. The even-order terms of Eq. (3.45) drop out due to the inversion symmetry of the Kerr medium. Kerr effect is a change in the refractive index of a medium in response to an applied electric field and it is a non-linear phenomenon [68–70]. The polarizability of a Kerr medium is related to third-order polarizability $\chi^{(3)}$. An intensity-dependent phase shift appears in the field in this process. The the intensity of the field is proportional to the refractive index of the Kerr medium. In the optical Kerr effect,

$$\mathbf{E} = E_\omega\cos(\omega t) \tag{3.46}$$

36

where ω is the frequency of the light waves. By using this equation in Eq. (3.45), and dropping out square terms, we have

$$\mathbf{P} \approx \epsilon_o(\chi^{(1)} + \frac{3}{4}\chi^{(3)}|\mathbf{E}_\omega|^2)E_\omega \cos(\omega t) = \epsilon_o \chi E_\omega \cos(\omega t) \qquad (3.47)$$

The factor $\frac{3}{4}$ is due to non-zero coefficients in $\chi^{(3)}$[99], where

$$\chi = (\chi^{(1)} + \frac{3}{4}\chi^{(3)}|\mathbf{E}_\omega|^2) \qquad (3.48)$$

and since the refractive n index is defined as

$$n = (1 + \chi)^{1/2} \qquad (3.49)$$

we can write

$$n \approx n_o + \frac{3}{8n_o}\chi^{(3)}|\mathbf{E}_\omega|^2 = n_0 + n_2 I^2 \qquad (3.50)$$

where $n_o = (1 + \chi^{(1)})^{1/2}$, $n_2 = \frac{3}{8n_o}\chi^{(3)}$ and $I = \mathbf{E}_\omega$. In quantum mechanics, we can model the Kerr-like medium as an anharmonic oscillator[100]. The effective Hamiltonian describes the Kerr effect is given by,

$$\hat{H}_{\text{Kerr}} = \frac{\hbar\chi}{2}(\hat{a}^\dagger\hat{a})^2 \qquad (3.51)$$

where $\hat{a}$ and $\hat{a}^\dagger$ are the field operators, and the parameter χ corresponds to the third-order non-linear susceptibility of the medium.

3.7 Stark Effect

In the presence of the external electric field $\mathbf{E}$, the energy levels of atoms and molecules split. We assume that $\mathbf{p}_{el}$ is the permanent dipole moment of the atomic energy levels. Let J represent the total angular momentum of the energy level. When the electric field is present, the energy levels split into $2J + 1$ lines. The effect of splitting of energy levels in the presence of the electric field is called the Stark effect[101]. In the absence of the external electric field, J has constant magnitude and direction. If the direction of the electric dipole moment $\mathbf{p}_{el}$ and the orientation of J are different, the time average component of $\mathbf{p}_{el}$

$$\langle \mathbf{p}_{el} \rangle = |p_{el}| \cdot \frac{K}{\sqrt{J^2 + J}}. \qquad (3.52)$$

K defines the projection of J in the $\mathbf{p}_{el}$ direction. In the presence $\mathbf{E}$, the $\mathbf{p}_{el}$ precesses around the field direction. The total angular momentum $\mathbf{J}$ precesses with constant projection M with the field orientation. We can compute the energy shift of an energy level using the relation

$$\Delta E = -\langle \mathbf{p}_{el} \rangle \cdot \mathbf{E} = |\mathbf{p}_{el}| \cdot \mathbf{E} \cdot \frac{K \cdot M}{J(J+1)}. \tag{3.53}$$

In this case, the splitting ΔE is proportional to $\mathbf{E}$, therefore it is called the linear Stark effect [102]. Even without a permanent electric dipole moment, the electric field can polarize the charge distribution in the molecule when it is placed in the electric field, which may cause an induced electric dipole moment

$$\mathbf{p}_{el}^{ind} = \bar{\alpha} \cdot \mathbf{E}, \tag{3.54}$$

where $\bar{\alpha}$ is a polarizability tensor of the molecule. $\bar{\alpha}$ is the function of the charge displacement from the equilibrium position. The energy shift due to induced dipole is

$$\Delta E = \mathbf{p}_{el}^{ind} \cdot \mathbf{E} = (\bar{\alpha} \cdot \mathbf{E}) \cdot \mathbf{E} = \sum_{i,j} \bar{\alpha}_{ij} \mathbf{E}_i \mathbf{E}_j. \tag{3.55}$$

Eq. (3.55) shows that the Stark shift caused by an induced dipole is proportional to the square of the electric field. This is called a non-linear Stark effect or a quadratic Stark-effect.

The influence of the Stark shift on a TLS is also an important topic of study[103]. The Stark shift caused by an electric field is proportional to the photon numbers $\hat{a}^\dagger \hat{a}$ inside the cavity. Furthermore, the Stark shift is also proportional to the polarizabilities of the two resonant states of a TLS. Therefore, we incorporate such shifts as intensity-dependent corrections $\hbar \beta_j \hat{a}^\dagger \hat{a}$ to the energy of the system, with β_j, is the Stark parameter corresponding to the state $|j\rangle$ of a TLS. The Stark Hamiltonian is, therefore, given as

$$\hat{H}_{\text{Stark}} = \hbar \sum_{j=0,1} \beta_j \hat{a}^\dagger \hat{a} \hat{R}_{jj} \tag{3.56}$$

where the atomic operator $\hat{R}_{jj}$ is defined as

$$\sum_{j=0,1} \hat{R}_{jj} = |j\rangle \langle j| \tag{3.57}$$

3.8 Atomic Motion inside the cavity

We consider a moving case of the atomic system. We consider that the atomic system is moving in one dimension inside the cavity. The atomic system is moving with constant

velocity v. We assume a beam of atoms is passing through the axis of a closed rectangular or a cylindrical cavity of length L. We also assume that the passage time of the beam through the finite cavity and the interaction time of the beam and field, is comparable. Experiments are performed to investigate the interaction of atoms with different shape functions of cavity field eigenmodes [104, 105]. A moving atom experiences a sinusoidal field mode and it enters at a node of the field mode, follows the spatial variation of the field mode inside the cavity, and leaves again at a node of the field mode. Therefore, a moving atom experiences $(\eta + 1)$ nodes, where η denotes the number of half wavelengths of the field modes.

The JC model describes the interaction of the field with an atom at rest. If an atom is moving inside the cavity field, the JC Hamiltonian as in Eq. (2.89) is given as [106],

$$\hat{H} = \frac{1}{2}\hbar\omega_0\hat{\sigma}_z + \hbar\omega\hat{a}^\dagger\hat{a} + \hbar f(z)(\hat{\sigma}_+\hat{a} + \hat{\sigma}_-\hat{a}^\dagger) \tag{3.58}$$

where $f(z)$ is the shape function of the field mode. The coupling constant λ is hidden in $f(z)$. We only consider the atomic motion along the z-axis. This helps us to restrict our discussion to the z-axis dependent on the field mode shape function. The atomic motion can be incorporated as,

$$f(z) \rightarrow f(vt) \tag{3.59}$$

where v stands for the atomic velocity. To study the dynamical aspects of the moving atomic system, we focus on a cavity field mode shape function,

$$f(vt) = \lambda \sin\left(\frac{\eta\pi vt}{L}\right) \tag{3.60}$$

where L is the length of the cavity along the z-axis direction.

If an atom enters inside the cavity at $z_1 = 0$ in time $t_1 = 0$ and leaves it at $z_2 = L$ in time $t_2 = t$, the atom experiences the field mode during this time t is given as,

$$f_1(vt) = \int_0^t f(vt)dt \tag{3.61}$$

which simplifies to,

$$f_1(vt) = \lambda\frac{L}{\eta\pi v}\left(1 - \cos\left(\frac{\eta\pi vt}{L}\right)\right) \tag{3.62}$$

If we take the constant velocity as $v = \frac{\lambda L}{\pi}$, under the assumption that the passage of an atom through a cavity is comparable with the interaction of it with an electromagnetic pulse. This leads us to,

$$f_1(vt) = \frac{1}{\eta}\left(1 - \cos\left(\frac{\eta\pi vt}{L}\right)\right) \tag{3.63}$$

39

Eq. (3.63) enables us to study the dynamics of a moving atomic system inside a cavity. We summarize the cases of static and moving atoms as,

$$
\begin{aligned}
f_1(vt) &= \frac{1}{\eta}\left(1 - \cos\left(\frac{\eta\pi vt}{L}\right)\right) \text{ for } \eta \neq 0, &\quad (3.64)\\
&= \lambda t \qquad\qquad\qquad \text{ for } \eta = 0. &\quad (3.65)
\end{aligned}
$$

3.9   Summary

We have studied the dynamics of open and closed system. We have briefly described some basic approximations, namely the Markov approximation, that is used to study the dynamics of an open system. We have also derived the Master equation and discussed the ID of an open system. We have briefly discussed the Kerr and Stark effect in this chapter. We have also studied the behavior of moving atomic system inside a cavity.

Chapter 4

Quantum Entanglement and Quantum Correlations

4.1 Introduction

In QIT, QE is considered to be a resource for information. In this chapter, we describe QE, the MPQC, and some different methods to compute the non-classical correlations of a system. We briefly describe VNE, quantum discord, and GQD.

4.2 Measurement and Operations in Quantum Mechanics

Measurements bear a main concept in the field of quantum mechanics and QIT. One of the established aspects of quantum measurement is the projective measurements that can be easily understood by the following example. For a spin-$\frac{1}{2}$ particle, let the particle reside in a superposition state

$$|\psi\rangle = \alpha |0\rangle + \beta |1\rangle \tag{4.1}$$

where the vectors $|0\rangle$ and $|1\rangle$ are the spin-up and spin-down states of a particle, respectively. The symbols α and β are the probability amplitudes related to the spin state. The probability of measuring the $|0\rangle$ state is $p(0) = |\alpha|^2$ and the probability of measuring the $|1\rangle$ state is $p(1) = |\beta|^2 = 1 - p(0)$. When the measurements are performed on this

spin system, the postulates of quantum mechanics are used to find the results. The state of the system collapses into either $|0\rangle$ or $|1\rangle$, which depends on the measurement results. We assign a classical register to store this information.

A collection of operators $\{\hat{E}_i\}$, described as the measurement operators are used as a general quantum measurement tool. These measurement operators must satisfy the completeness relation as given below

$$\sum_i \hat{E}_i^\dagger \hat{E}_i = \hat{I} \tag{4.2}$$

where $\hat{I}$ is the identity operator. Suppose a system is in state $|\psi\rangle$ and the density operator of this system is given by Eq. (3.1). Now the probability of finding the system in the ith outcome, with the application of the set of measurement operators $\{\hat{E}_i\}$ is

$$p_i = \text{Tr}[\hat{E}_i^\dagger \hat{E}_i \hat{\rho}] \tag{4.3}$$

After this measurement which results in the ith outcome, the system's state can be found by the density operator

$$\hat{\rho}_i = \frac{1}{p_i}(\hat{E}_i \hat{\rho} \hat{E}_i^\dagger) \tag{4.4}$$

The set of operators in Eq. (4.2)

$$\hat{M}_i = \hat{E}_i^\dagger \hat{E}_i \tag{4.5}$$

are also known as the positive operator-valued measure (POVM). Eq. (4.2) describes that the sum of each POVM operator $\hat{M}_i$ is equal to the identity operator, that is $\sum_i \hat{M}_i = \hat{I}$. Moreover, it is seen that according to Eq. (4.3), we can find the the probabilities p_i by using the set of operator elements of the POVM $\hat{M}_i$: $p_i = \text{Tr}[\hat{M}_i \hat{\rho}]$. The second property of the density operator, given by Eq. (3.3), suggests the positivity of the density operator $\hat{\rho}$ and this property implies that all the probabilities of events in the system are non-negative $p_i \geq 0$. If the Eq. (4.2) is used together with the Eq. (3.2), it is straight forward to find $\sum_i p_i = 1$.

The projective measurement operators, the operators $\hat{E}_i$ are orthogonal projectors, that is $\hat{E}_i \hat{E}_j = \delta_{ij} \hat{E}_i$. There are some special types of projective measurement operators, called von Neumann measurement $\hat{E}_i$ which are orthogonal projectors and have a rank of one. For a system described in Eq. (4.1) the projective measurement operators are

$\hat{E}_0 = |0\rangle \langle 0|$ and $\hat{E}_1 = |1\rangle \langle 1|$. For a general system, these measurement operators do not have to be orthogonal but for these operators, the completeness relation must be satisfied (Eq. (4.2)).

For a composite bipartite system, with subsystem Alice and Bob, we develop the local measurement operators for the subsystems of Alice and Bob. If we performed the local measurement on her subsystem of Alice, the subsystem belonging to Bob will be unaffected by this measurement. In this case, if the measurements are performed on Alice, the measurement operators can be described by the form $\hat{E}_i = \hat{E}_i^A \otimes \hat{I}^B$, where $\hat{I}^B$ is the identity operator that acts on the Hilbert space of the Bob. In the same manner, if the measurements are made on the Bob subsystem, the measurement operator has then the form $\hat{E}_i = \hat{I}^A \otimes \hat{E}_i^B$ and here the Alice subsystem remains unchanged.

4.3   Classical Information and Shannon Entropy

The fundamental entity to measure the information classically, is the "*bit*". A bit can have a value 0 or 1 and similar to an electronic switch. A combination of bits is used to transfer a message. Suppose that an event $\{x_i\}$ occurs in the random variables X with the probability $\{p_i\}$. The information content associated with this event is computed by the Shannon entropy given by,

$$H(X) = -\sum_i p_i \log_2 p_i \qquad (4.6)$$

Eq. (4.6) shows a measure of the uncertainty present in this event. The Shannon entropy satisfies basic axioms:

- $H(X)$ is a function of probability p: $H(X) = H(p_i)$;
- $H(X)$ is a smooth function of p;
- For two independent variables, suppose for variables X and Y, the information content present in the sum of the events is equal to the information content gained separately by these two events: $H(X, Y) = H(X) + H(Y)$.

Joint Entropy

We define the joint entropy $H(X, Y)$ associated with the joint distribution $p(x, y)$,

$$H(X, Y) = -\sum_{x \in X} \sum_{y \in Y} p(x, y) \log_2 p(x, y) \tag{4.7}$$

Relative Entropy

For two probability distributions p_i and q_i, relative entropy (RE) $H(p_i || q_j)$ is defined as,

$$H(p_i || q_j) = \sum p_i \log_2 \frac{p_i}{q_j} \tag{4.8}$$

We expand the Eq. (4.8) by using the logarithm property we have

$$H(p_i || q_j) = -H(X) - \sum p_i \log_2 q_j \tag{4.9}$$

We extract two important properties of the RE, that is $H(p_i || q_j) \geq 0$ and $H(p_i || q_j) = 0$ if and only if $p_i = q_j$.

Conditional Probability

Conditional probability $P(X|Y)$ for two events X and Y is defined as

$$P(X|Y) = \frac{P(X, Y)}{P(Y)} \tag{4.10}$$

where $P(X, Y)$ is the overlap or joint probability (or distribution) of two events X and Y.

Conditional Entropy

The conditional entropy between two random variables X and Y is denoted by $H(X|Y)$ and defined as

$$H(X|Y) = -\sum_{x,y} p(x, y) \log_2 \frac{p(x, y)}{p(x)} \tag{4.11}$$

where the elements $x \in X$ and $y \in Y$, and $p(x, y)$ is the joint probability of elements x and y and $p(x)$ is the probability of element x. Now if we use Eq. (4.10) into Eq. (4.11)

we have,

$$H(X|Y) = -\sum_{x,y} p(x,y) \log_2 p(y|x) \tag{4.12}$$

by taking into account

$$p(x,y) = p(y|x)p(x) \tag{4.13}$$

we have

$$H(X|Y) = -\sum_{x,y} p(y|x)p(x) \log_2 p(y|x) \tag{4.14}$$

If we separate the summation accordingly we have

$$H(X|Y) = -\sum_{x} p(x) \sum_{y} p(y|x) \log_2 p(y|x) \tag{4.15}$$

and we have conditional entropy at $X = x$ (conditional entropy y given x) that is

$$H(Y|X) = -\sum_{y} p(y|x) \log_2 p(y|x) \tag{4.16}$$

Finally, we have

$$H(X|Y) = \sum_{x} p(x)H(Y|X = x) \tag{4.17}$$

Joint and conditional entropy are related by

$$H(X|Y) = H(X,Y) - H(Y) \tag{4.18}$$

and likewise,

$$H(Y|X) = H(X,Y) - H(X) \tag{4.19}$$

Bayes' Theorem

For two events X and Y, the Bayes' theorem is defined as

$$P(X,Y) = P(X|Y)P(Y) = P(Y|X)P(X) \tag{4.20}$$

Mutual Information

Let random variables X and Y take the values $\{x_i\}$ and $\{y_i\}$ with the probabilities $\{p_i\}$ and $\{q_i\}$, respectively. Let these variables are correlated. The mutual information (MI) $I(X : Y)$, that is the information shared between these two random variables given by X

and Y, can be defined as

$$I(X:Y) = H(X) + H(Y) - H(X,Y) \tag{4.21}$$

If we recall the third axiom of the Shannon entropy, for any two independent variables we have,

$$I(X:Y) = 0. \tag{4.22}$$

By using the definitions of conditional entropy, given in Eqs. (4.18) and (4.19), and using in Eq. (4.21) we get an alternate form of the MI,

$$J(X:Y) = H(X) - H(X|Y) \tag{4.23}$$

and likewise,

$$J(Y:X) = H(Y) - H(Y|X) \tag{4.24}$$

4.4 Quantum Information and von Neumann Entropy

In QIT, we store the information in the states of quantum mechanical system. The variables to store the information in QIT are replaced by the observables. The values that are assigned to these observables are replaced by the eigenvalues of these observables. For example, we can designate a quantum system $|\psi\rangle$ with the values in the orthogonal quantum states $|0\rangle$, $|1\rangle$ and as quantum mechanics allows us that the quantum system $|\psi\rangle$ can also be in a coherent superposition of these orthogonal quantum states.
In QIT, the Shannon entropy is replaced by the VNE S.

von Neumann Entropy

The expression of VNE of a quantum mechanical state $|\psi\rangle$ can be defined with the help of $\hat{\rho}$. The VNE is defined as

$$S(\hat{\rho}) = -\text{Tr}[\hat{\rho} \log_2 \hat{\rho}] \tag{4.25}$$

The Eq. (4.25) shows the base-two logarithm of $\hat{\rho}$. This logarithm can be computed on the eigenvalues λ_i of the density operator, which can be obtained by diagonalizing the density operator $\hat{\rho}$ into its eigenstates $|i\rangle$. On the diagonalized density operator, the base-two logarithm can be computed by $\log_2 \hat{\rho} = \sum_i \log_2 \lambda_i |i\rangle \langle i|$. With the help of a

simplified definition, we can write the VNE of the system as

$$S(\hat{\rho}) = -\sum_i \lambda_i \log_2 \lambda_i \tag{4.26}$$

So far we have two types of entropies that measure the information contained in two different regimes. One is the Shannon entropy (Eq. (4.6)) which takes into account how much uncertainty is present in a classical random event. In quantum mechanics, the lack of certainty of a quantum mechanical state is measured by the VNE (Eq. (4.26)). For a pure quantum state, the full knowledge about the state is given, so the content of information and therefore the VNE yields nothing.

On the other hand, for a quantum system with a d-dimensional Hilbert space, the maximum uncertainty of the system is given by a completely mixed state and corresponding ρ with the VNE of the order of $\log_2 d$. The VNE (Eq. (4.25)) is a suitable parameter that quantifies the mixedness of a state.

Quantum Joint Entropy

Consider two subsystems A and B and the density operators of the composite system and its subsystems be given by $\hat{\rho}_{AB}$, $\hat{\rho}_A$, and $\hat{\rho}_B$, respectively. The related entropies $S(\hat{\rho}_A)$, $S(\hat{\rho}_B)$, and $S(\hat{\rho}_{AB})$ are then related by subadditivity inequality,

$$S(\hat{\rho}_{AB}) \leq S(\hat{\rho}_A) + S(\hat{\rho}_B) \tag{4.27}$$

The equality holds for $\hat{\rho}_{AB} = \hat{\rho}_A \otimes \hat{\rho}_B$, which corresponds to uncorrelated subsystems. Quantum joint entropy is the entropy of the composite system $\hat{\rho}_{AB}$. It is equal to or less than the subsystem entropies.

Quantum Conditional Entropy

For given subsystems A, B and its composite system AB, quantum conditional entropy $S(\hat{\rho}_A|\hat{\rho}_B)$ is

$$S(\hat{\rho}_A|\hat{\rho}_B) = S(\hat{\rho}_{AB}) - S(\hat{\rho}_B) \tag{4.28}$$

and likewise,

$$S(\hat{\rho}_B|\hat{\rho}_A) = S(\hat{\rho}_{AB}) - S(\hat{\rho}_A) \tag{4.29}$$

Quantum Mutual Information

For a system A and B, the VNE of the system can be used to define a quantum analog of the MI between the two parties. Let quantum joint entropy is given by $\hat{\rho}_{AB}$ and the reduced density operators $\hat{\rho}_A$ and $\hat{\rho}_B$ of the system A and B, respectively. The quantum analog of classical MI (Eq. (4.21)) is defined as

$$I(\hat{\rho}_{AB}) = S(\hat{\rho}_A) + S(\hat{\rho}_B) - S(\hat{\rho}_{AB}) \tag{4.30}$$

For completely uncorrelated quantum states A and B the MI is zero. For completely uncorrelated quantum states, the density state for a composite system has the form as $\hat{\rho}_{AB} = \hat{\rho}_A \bigotimes \hat{\rho}_B$. If we cannot write the state of the composite system this way, the MI is greater than zero. Generally, Eq. (4.30) finds the content of quantum correlations between two systems A and B.

If we use the definitions of quantum RE, given in Eqs. (4.28) and (4.29), quantum MI can be written as,

$$J(\hat{\rho}_{AB}) = S(\hat{\rho}_A) - S(\hat{\rho}_A|\hat{\rho}_B) \tag{4.31}$$

and likewise,

$$J(\hat{\rho}_{AB}) = S(\hat{\rho}_B) - S(\hat{\rho}_B|\hat{\rho}_A) \tag{4.32}$$

Quantum Relative Entropy

The idea of quantum RE is related closely to the VNE. For two different quantum systems with density matrices, $\hat{\rho}$ and $\hat{\sigma}$, the quantum RE for these two systems is defined as,

$$S(\hat{\rho}||\hat{\sigma}) = Tr[\hat{\rho}\log_2\hat{\rho}] - Tr[\hat{\rho}\log_2\hat{\sigma}] \tag{4.33}$$

The quantum RE is non-negative. It is zero if and only if $\hat{\sigma} = \hat{\rho}$. One can easily check that Eq. (4.30) can be modified as the quantum RE between the composite system $\hat{\rho}^{AB}$ and $\hat{\rho}^A \otimes \hat{\rho}^B$ [107].

$$I(\hat{\rho}^{AB}) = S(\hat{\rho}^{AB}||\hat{\rho}^A \otimes \hat{\rho}^B) \tag{4.34}$$

4.5 Quantum Entanglement

For a system with two subsystems A and B, we can write the total state as

$$|\Psi\rangle = |a\rangle \otimes |b\rangle \tag{4.35}$$

The vectors $|a\rangle$ and $|b\rangle$ belong to $\mathcal{H}_A$ and $\mathcal{H}_B$ respectively. That kind of states, given by this form same as in Eq. (4.35) are not the entangled states, and these states are called the separable states. However, in quantum mechanics, all quantum states are not separable states. The superposition principle in quantum mechanics permits the quantum states to superimpose, and these superimposed states are not always product state

$$|\Phi\rangle = \frac{1}{N}\big(|a_1\rangle |b_1\rangle + |a_2\rangle |b_2\rangle\big) \tag{4.36}$$

where N is the normalization constant such that $\langle\Phi|\Phi\rangle = 1$. If we cannot write $|\Phi\rangle$ in the product form, i.e., $|\Phi\rangle \neq |a\rangle \otimes |b\rangle$, we call the state an entangled state. The state $|\Phi\rangle = \frac{1}{\sqrt{2}}\big(|01\rangle - |10\rangle\big)$ is an entangled states because it cannot be written in the form as a product (4.35).

Another form of a quantum state is mixed states. A mixed state is a separable state if it is possible to write it as a combination of pure product states [108].

$$\hat{\rho}_{separ} = \sum_i p_i |a_i\rangle \langle a_i| \otimes |b_i\rangle \langle b_i| \tag{4.37}$$

where the pure state vectors $|a_i\rangle$ and $|b_i\rangle$ belongs to the Hilbert spaces $\mathcal{H}_A$ and $\mathcal{H}_B$. Here $p_i \geq 0$, and $\sum_i p_i = 1$. If we cannot write a state as Eq. (4.37), it is called entangled state.

Bell's State

An example of maximally entangled states is Bell's states. Bell's states are given below as

$$|\chi_{00}\rangle = \frac{1}{\sqrt{2}}(|00\rangle + |11\rangle), \tag{4.38}$$

$$|\chi_{01}\rangle = \frac{1}{\sqrt{2}}(|01\rangle - |10\rangle), \tag{4.39}$$

$$|\chi_{10}\rangle = \frac{1}{\sqrt{2}}(|00\rangle - |11\rangle), \tag{4.40}$$

$$|\chi_{11}\rangle = \frac{1}{\sqrt{2}}(|01\rangle + |10\rangle). \tag{4.41}$$

In a compact form, these four states can be written as

$$|\chi_{xy}\rangle = \frac{1}{\sqrt{2}}(|0y\rangle + (-1)^x |1\bar{y}\rangle), \tag{4.42}$$

where $x = 0, 1$ and $y = 0, 1$ and if $y = 0$, $\bar{y} = 1$ and vice versa.

4.6 Quantum Correlations

Suppose a bipartite system composed of Alice and Bob sharing a mixed state between them. We assume the orthogonal basis states belonging to Alice's subsystem $\mathcal{H}_A$ are $\{|i\rangle_A\}$. Also $\{|j\rangle_B\}$ represents the orthogonal basis states that belong to Bob's subsystem Hilbert space $\mathcal{H}_B$. The mixed state is said to be classically correlated if the system can be expressed in the following way [109]

$$\hat{\rho}_{cc} = \sum_{i,j} p_{i,j} |i\rangle \langle i|_A \otimes |j\rangle \langle j|_B , \tag{4.43}$$

where p_{ij} is the probability of the mixed state such that $\sum_{i,j} p_{ij} = 1$. If the state cannot be expressed as shown in Eq. (4.43), then the state is said to be quantum mechanically correlated. It is important to mention that every state that is correlated classically is also separable. On the other hand, the contrary statement is not necessarily true. That is, a separable state in the form $\hat{\rho}_s = \sum_i p_i |a_i\rangle \langle a_i| \otimes |b_i\rangle \langle b_i|$, it is not necessary for this state to be classically correlated because the states that belongs to Alice and Bob, that is $\{|i\rangle_A\}$ and $\{|i\rangle_B\}$ respectively, are not necessarily orthogonal. Moreover, a pure state has a different nature. Besides the mixed states, for a pure quantum state, entanglement provides the correlations nature in the state. A pure quantum state is an entangled state if and only if this pure state is quantum mechanically correlated. This means that the entanglement in pure states is equal to the non-locality and it carries the perception of quantumness of the system. The situation gets different for the mixed states. Thus non-local states must be entangled and the sets of these states are smaller than the set of entangled states, hence non-local states are a subset of entangled states. So for this reason the properties of the mixed states correlations are studied in the following passages.

We now discuss that mixed states, even mixed separable states show the MPQC and these states present no entanglement. The MPQC gives a more precise picture of the

system than the entanglement. By definition, the MPQC is the difference between the total correlation in the system and the classical correlation in the system.

So what are the classical correlations (CC)? Suppose some states are classically correlated. If we apply some quantum mechanical disturbance or operations to these CC states, these states do not show any reaction to this disturbance because of the nature of the states. So we assign a general intuition to the CC states that these states are not affected by certain quantum operations, that is the von Neumann measurement, on each party (Alice and Bob) subspaces. For the bipartite system that shares a mixed state, we can write the quantum measurement operators by $E_A^i = |i\rangle\langle i|_A$ and $E_B^j = |j\rangle\langle j|_B$. These von Neumann measurement operators do not disturb a mixed separable state. The corresponding set of quantum mixed states ρ_{cq} can also be defined which is not affected by the given von Neumann operations on any party subspace (for example Alice). For this case, the resulting stats are given by

$$\hat{\rho}_{cq} = \sum_i p_i |i\rangle\langle i|_A \otimes \rho_B^i \tag{4.44}$$

where ρ_B^i corresponds to the states of Bob's Hilbert space $\mathcal{H}_B$, also with $p_i \geq 0$ and $\sum_i p_i = 1$. The form of the states, that is represented in Eq. (4.44) are called classical-quantum states [110, 111]. For a mixed state, represented in Eq. (4.44), we can generate measurement operators for the state. The relevant von Neumann operator for measurement on Alice's subsystem is given by $\hat{E}_A^i = |i\rangle\langle i|_A$. We can check that this operator does not disturb the state:

$$\hat{E}_A^i \hat{\rho}_{cq} = |i\rangle\langle i|_A \sum_i p_i |i\rangle\langle i|_A \otimes \hat{\rho}_B^i = \sum_i p_i |i\rangle\langle i|_A |i\rangle\langle i|_A \otimes \hat{\rho}_B^i = \hat{\rho}_{cq}$$

We checked that the state is not disturbed by the action of the measurement operator. This state is a classical-quantum state for the local measurement operator $\hat{E}_A^i$. Similarly, for Bob's subsystem, the classical-quantum state has the form $\hat{\rho}_{cq} = \sum_i p_i \hat{\rho}_A^i \otimes |i\rangle\langle i|_B$ and the von Neumann operator for the measurement on the Bob's subsystem is $\hat{E}_B^i = |i\rangle\langle i|_B$. Hence, it is concluded that the disturbance-induced measurements of any state provide a good tool to sense the quantumness of the state.

4.7 Measures of Quantum Correlations

Several studies have been put forward to analyze the MPQC. Recently, many quantifier used to quantitatively and qualitatively evaluate the MPQC have been introduced in the literature [43, 44, 109, 112–121]. All the measures of the MPQC are grouped into two main classes:

1. Entropic Quantities Based Measurement

2. Geometric Measures of the Correlations

An entropic measurement-based way to find the correlations, which is the original quantum discord (QD), was used by Zurek [44], we use Shannon relation of entropy (Eq. (4.6)). In this measure, we require basic tools of information theory or simply a thermodynamic interpretation but it is very difficult to find a result explicitly by this way of measurement [122, 123]. On the other hand, a geometric measure of MPQC provides a different approach to finding the correlations. This measure is a comparison between two states. One state is the state in which we are interested to find the MPQC and the other state is a classical-quantum state which has zero MPQC. We measure some relative quantity (generally RE) between these two states and compute the MPQC of the given state. For example, it has been studied that the RE (Eq. (4.33)) of a state ρ [118], which is under observations are used to define the correlation as $Q^{A(B)}(\hat{\rho}) = \min_{\hat{\rho}_{CQ}} S(\hat{\rho}||\hat{\rho}_{CQ})$. This expression of correlations represents the distance between two states in terms of the RE of the state under observation. This is closest to classical-quantum state.

4.8 Quantum Discord (QD)

The foundations of QIT and quantum computation rely on the core quantum mechanical effect known as entanglement. The entanglement measures the correlations that are present between the parts of quantum systems. These correlations are a quantum mechanical effect and cannot be explained by classical laws. It is considered that the entanglement or non-locality is similar to the MPQC. This consideration is true for a pure quantum state, that is, if we are dealing with a pure quantum state, the entanglement and non-locality of the term are treated as a synonym. But for the mixed quantum

mechanical states, entanglement is no more similar to the MPQC and the situation becomes more complex as two core concepts in quantum theory separate their ways. In this regard, a new and more general tool to measure the MPQC in the mixed quantum states was presented [44] and named these correlations as QD. QD is defined as the difference between total correlations and CC in the system.

QD is historically the first the measurement of MPQC beyond entanglement [43, 44, 124]. Our point of interest is to analyze the MPQC between two-party systems. For this purpose quantum mechanical description of the MI is required. As measuring a quantum state, collapse the state, the results of I and J differ as we use the von Neumann definition of entropy (Eq. (4.25)) instead of Shannon entropy (Eq. (4.6)). It was shown by Zurek [44], under quantum operations and measurements Eq. (4.30) and Eq. (4.32) are no longer equal. This difference that occurs between two classically the same quantities has laid foundations of a quantity which is defined as QD. We use the disturbance-induced measurements approach to calculate an improved version of Eq. (4.32) and then find the QD.

4.9 Measurement-Induced Based Approach For Bipartite system

Suppose a bipartite system, constituting of A and B subsystems. Composite system density operator is $\hat{\rho}_{AB}$ and $\hat{\rho}_A$ and $\hat{\rho}_B$ for the subsystems A and B. The total correlation between subsystem A and B can be computed by the MI given in Eq. (4.32)

$$J(\hat{\rho}_{AB}) = S(\hat{\rho}_A) - S(\hat{\rho}_A|\hat{\rho}_B)$$

Now we introduce a measurement-based approach to solve the quantum conditional entropy. Now by using the measurement-based approach, we can derive another definition of quantum conditional entropy $S(\hat{\rho}_A|\hat{\rho}_B)$. We define local projectors $\{\hat{\Pi}_B^j\} = \{|b_j\rangle \langle b_j|\}$ on subsystem B. The post-measurement conditional operator after applying $\{\hat{\Pi}_B^j\}$ results in

$$\hat{\rho}_{AB|j} = \frac{1}{p_j}\left(\hat{\mathbf{1}}_A \otimes \hat{\Pi}_B^j\right)\rho_{AB}\left(\hat{\mathbf{1}}_A \otimes \hat{\Pi}_B^j\right) \tag{4.45}$$

where the probability of having the jth outcome after measurement is $p_J = \text{Tr}\left[(\hat{\mathbf{1}}_A \otimes \hat{\Pi}_B^j)\hat{\rho}_{AB}\right]$, $\hat{\mathbf{1}}_A$ represents the identity operator acting on the system A. We write the measurement-based quantum conditional entropy as,

$$S(\hat{\rho}_{AB}|\hat{\Pi}_B^j) = \sum_j p_j S(\hat{\rho}_{AB|j}) \tag{4.46}$$

That allows us to find the classical information [43]

$$J(\hat{\rho}_{AB}) = S(\hat{\rho}_A) - S(\hat{\rho}_{AB}|\hat{\Pi}_B^j) \tag{4.47}$$

The difference between quantum MI $I(\hat{\rho}_{AB})$ and CC $J(\hat{\rho}_{AB})$, minimized over the whole set of measurements $\hat{\Pi}_B^j$ performed on B, defines QD $D(\hat{\rho}_{AB})$ given as

$$D(\hat{\rho}_{AB}) = \min_{\{\hat{\Pi}_B^j\}}[I(\hat{\rho}_{AB}) - J(\hat{\rho}_{AB})] \tag{4.48}$$

By using the definition of quantum RE given in Eq. (4.33) and the MI in terms of the RE given in Eq. (4.34), Zurek [44] proposed the definition of QD, given as,

$$D_{AB}(\hat{\rho}_{AB}) = \min_{\{\hat{\Pi}_A^j \otimes \hat{\Pi}_B^k\}}[S(\hat{\rho}_{AB}||\hat{\Pi}\hat{\rho}_{AB}) - \sum_{j=A,B} S(\hat{\rho}_j||\hat{\Pi}_j\hat{\rho}_j)] \tag{4.49}$$

with $\hat{\Pi}(\hat{\rho}_{AB}) = \sum_{j,k}(\hat{\Pi}_A^j \otimes \hat{\Pi}_B^k)\hat{\rho}_{AB}(\hat{\Pi}_A^j \otimes \hat{\Pi}_B^k)$.

General Measures of Quantum Discord

There are some general postulates regarding the measurement of QD. These postulates have been proposed by K. Modi and his co-authors in the paper with the title "Criteria for the measure of Quantum correlations"[125]. The authors point out that every QD measure must satisfy these three necessary conditions. These conditions are:

i. QD is non-negative,

ii. Under the local unitary operations, QD is invariant

iii. QD is zero for classically correlated system states.

4.10 Global Quantum Discord

Starting with the definition of GQ given in Eq. (4.49), the GQD can be written as

$$\text{GD}(\hat{\rho}_T) = \min_{\{\hat{\Pi}_k\}}\left\{S(\hat{\rho}_T||\hat{\Pi}\hat{\rho}_T) - \sum_{j=1}^N S(\hat{\rho}_j||\hat{\Pi}_j\hat{\rho}_j)\right\} \tag{4.50}$$

which measure the global content of the MPQC in the total state $\hat{\rho}_T$ of a system with N subsystems. And $\hat{\rho}_j = \text{Tr}[\hat{\rho}_T]$ is the reduced state of subsystem j. The trace is taken over all the subsystems except subsystem j. The projectors in Eq. (4.50) are given as follows,

$$\hat{\Pi}_j(\hat{\rho}_j) = \sum_l \hat{\Pi}_j^l \hat{\rho}_j \hat{\Pi}_j^l \tag{4.51}$$

and

$$\hat{\Pi}(\hat{\rho}_T) = \sum_k \hat{\Pi}^k \hat{\rho}_T \hat{\Pi}^k \tag{4.52}$$

where $\hat{\Pi}^k = \otimes_{l=1}^{k_l} \hat{\Pi}_l^{k_l}$. The minimization in Eq. (4.50) is computed on all possible multi-local projectors $\hat{\Pi}^k$. By using the definition of quantum RE, we can expand Eq. (4.50) as,

$$\text{GD}(\hat{\rho}_T) = \min_{\{\hat{\Pi}_k\}} \left\{ -\text{Tr}(\hat{\rho}_T \log_2 \hat{\Pi}(\hat{\rho}_T)) + \sum_j \text{Tr}(\hat{\rho}_j \log_2 \hat{\Pi}_j(\hat{\rho}_j)) \right\} - S(\hat{\rho}_T) + \sum_j^N S(\hat{\rho}_j) \tag{4.53}$$

For the N-party system, the multi-local projectors can be written as

$$\hat{\Pi}^k = \hat{R} \left| k \right\rangle \left\langle k \right| \hat{R}^\dagger \tag{4.54}$$

where $\{|k\rangle\}$ are the separable, multi-local eigenstates of the multipartite Pauli operator $\bigotimes_{j=1}^N \hat{\sigma}_j^z$ and multi-qubit rotation operator is $\hat{R}$, operating on local jth subsystem, expressed as $\hat{R} = \bigotimes_{j=1}^N \hat{R}_j(\theta_j, \phi_j)$ with $\hat{R}_j(\theta_j, \phi_j) = \cos\theta_j \hat{1} + i\sin\theta_j \cos\phi_j \hat{\sigma}_y + i\sin\theta_j \sin\phi_j \hat{\sigma}_x$. With the help of the projector operators, we can expand a term in Eq. (4.50) as,

$$\text{Tr}[\hat{\rho}_T \log_2 \hat{\Pi}(\hat{\rho}_T)] = \text{Tr}\left[\hat{\rho}_T \log_2 \sum_k \hat{R} \left| k \right\rangle \left\langle k \right| \hat{R}^\dagger \hat{\rho}_T \hat{R} \left| k \right\rangle \left\langle k \right| \hat{R}^\dagger \right] \tag{4.55}$$

By using $\langle k| \hat{R}^\dagger \hat{\rho}_T \hat{R} |k\rangle = \tilde{\rho}_T^{kk}$ we get,

$$\text{Tr}[\hat{\rho}_T \log_2 \hat{\Pi}(\hat{\rho}_T)] = \text{Tr}\left[\hat{\rho}_T \log_2 \sum_k \hat{R} \left| k \right\rangle \tilde{\rho}_T^{kk} \left\langle k \right| \hat{R}^\dagger \right] \tag{4.56}$$

By using the property of trace and by opening the trace of the above equation, we get

$$\text{Tr}[\hat{\rho}_T \log_2 \hat{\Pi}(\hat{\rho}_T)] = \sum_k \tilde{\rho}_T^{kk} \log_2 \tilde{\rho}_T^{kk} \tag{4.57}$$

Similarly, the other term in Eq. (4.50) can be solved, we have

$$\text{Tr}[\hat{\rho}_j \log_2 \hat{\Pi}_j(\hat{\rho}_j)] = \sum_{l=0}^1 \tilde{\rho}_j^{ll} \log_2 \tilde{\rho}_j^{ll} \tag{4.58}$$

where $\tilde{\rho}_j^{ll} = \langle l| \hat{R}^\dagger \hat{\rho}_j \hat{R} |l\rangle$ and $|l\rangle$ being two eigenstate of of σ_j^z. By using Eqs. (4.57) and (4.58) into Eq. (4.53), we have

$$\text{GD}(\hat{\rho}_T) = \min_{\{\Pi^k\}} \left\{ \sum_{j=1}^{N} \sum_{l=0}^{1} \tilde{\rho}_j^{ll} \log_2 \tilde{\rho}_j^{ll} - \sum_{k=0}^{2^N-1} \tilde{\rho}_T^{kk} \log_2 \tilde{\rho}_T^{kk} \right\} - S(\hat{\rho}_T) + \sum_{j=1}^{N} S(\hat{\rho}_j) \quad (4.59)$$

The above equation decreases the computational power required to evaluate the GQD of the N-party system.

4.11   Summary

In this chapter, we have reviewed some basic definitions for classical information and QIT and discussed Shannon and VNE. We have also discussed QE and the MPQC for multipartite systems. We have also reviewed the QD and GQD of a system.

Chapter 5

Global quantum discord and von Neuman entropy in multipartite two-level atomic systems

5.1   Introduction

In this chapter, we present a study of the GQD and VNE in the N TLS coupled with the single-mode field in a Fock field. We investigate the effect of different parameters that are present in the model, such as ID, parameters in the initial state, and photon number in the system, on the GQD and VNE.

This chapter is arranged as follows; In Sec. (5.2) we briefly describe the model and the initial state of the system. In Sec. (5.3) we present MPQC and compute the GQD. In Sec. (5.4), we study the behavior of the GQD and VNE. The behavior of both the quantifiers is analyzed regarding the field and with various possible initial states. We also study the effect of ID on the system. The results are extrapolated for both the quantifiers and also studied for the higher TLS. In the last section, we conclude our findings.

5.2   The Model

We explore multipartite TLS interacing with the Fock field. The Hamiltonian of the system we study, given in Eq. (2.93),

$$\hat{H} = \frac{\omega_0}{2}\sum_{i=1}^{N}\hat{\sigma}_i^z + \omega\hat{a}^\dagger\hat{a} + \lambda\sum_{i=1}^{N}(\hat{a}\hat{\sigma}_i^+ + \hat{a}^\dagger\hat{\sigma}_i^-) \tag{5.1}$$

The system dynamics under the Markovian approximation is given by Eq. (3.43) [96], i.e.

$$\dot{\hat{\rho}}(t) = -i[\hat{H},\hat{\rho}(t)] - \frac{\gamma}{2}[\hat{H},[\hat{H},\hat{\rho}(t)]] \tag{5.2}$$

where γ is the coefficient of ID. For $\gamma \to 0$, Eq. (5.2) reduces to the Schrodinger equation. The formal solution of Eq. (5.2) is given by,

$$\hat{\rho}(t) = \sum_{k=0}^{\infty}\frac{(\gamma t)^k}{k!}\hat{M}^k(t)\hat{\rho}(0)\hat{M}^{k\dagger}(t), \tag{5.3}$$

with

$$\hat{M}^k(t) = \hat{H}^k\exp(-i\hat{H}t)\exp(-\gamma t\hat{H}^2/2), \tag{5.4}$$

where $\hat{\rho}(0)$ is the initial state of the system.

We assume atoms and field ae initially uncoupled, thus we prepare initial state of the system $\hat{\rho}_{AF}(0)$ as a product state

$$\hat{\rho}_{AF}(0) = [(1-p)\ket{\psi}\bra{\psi} + p\ket{g_1g_2...g_N}\bra{g_1g_2...g_N}] \otimes \ket{n}\bra{n}, \tag{5.5}$$

where $\ket{\psi} = \cos(\alpha)\ket{g_1g_2...g_N} + \sin(\alpha)\ket{e_1e_2...e_N}$, $\ket{g_i}$ and $\ket{e_i}$ are the ground and excited states of the TLS respectively. p corresponds to statistical probability, $0 \le p \le 1$, α is associated with super position of two level system, $0 \le \alpha \le \pi$ and $\ket{n}$ is the field state. In our model, the combined system i.e. the atoms and field form the set of allowable basis states $\{\ket{\psi_i}\}$ of the system given as,

$$\{\ket{\psi_i}\} = \ket{g_1, g_2, g_3, ...g_N, n+N}, \ket{e_1, g_2, g_3, ...g_N, n+N-1}, \ket{e_1, e_2, g_3, ...g_N, n+N-2}, ...$$
$$\ket{e_1, e_2, e_3, ...e_N, n}$$

$$\tag{5.6}$$

The ij^{th} matrix element of the Hamiltonian in the allowed basis is $\bra{\xi_i}\hat{H}\ket{\xi_j}$ with $\ket{\xi_i} = \bigotimes_{l=1}^{N}\ket{s}_l$ where s represents the ground and excited state of the lth TLS, the basis are $\ket{0} = \begin{bmatrix} 1 \\ 0 \end{bmatrix}$ and $\ket{1} = \begin{bmatrix} 0 \\ 1 \end{bmatrix}$. Now for the two TLS, the matrix elements of the Hamiltonian

in the allowable basis are,

$$
\begin{pmatrix}
0 & \lambda\sqrt{n+1} & \lambda\sqrt{n+1} & 0 \\
\lambda\sqrt{n+1} & 0 & 0 & \lambda\sqrt{n+2} \\
\lambda\sqrt{n+1} & 0 & 0 & \lambda\sqrt{n+2} \\
0 & \lambda\sqrt{n+2} & \lambda\sqrt{n+2} & 0
\end{pmatrix}.
\tag{5.7}
$$

The matrix elements for the large-N systems, more specifically for three, four and five TLS, are given as follows.

For three TLS, the matrix elements are (we take $\lambda = 1$)

$$a_{1,2} = a_{1,3} = a_{1,5} = a_{2,1} = a_{3,1} = a_{5,1} = \sqrt{1+n},$$

$$a_{4,2} = a_{2,4} = a_{3,4} = a_{4,3} = a_{2,6} = a_{6,2} = a_{3,7} = a_{7,3} = a_{5,6} = a_{6,5} = a_{5,7} = a_{7,5} = \sqrt{2+n}$$

$$a_{4,8} = a_{8,4} = a_{6,8} = a_{8,6} = a_{7,8} = a_{8,7} = \sqrt{3+n}$$

and the other elements are zero.

For four TLS, the matrix elements are

$$a_{1,2} = a_{1,3} = a_{1,5} = a_{2,1} = a_{3,1} = a_{5,1} = a_{1,9} = a_{9,1} == \sqrt{1+n},$$

$$a_{4,2} = a_{2,4} = a_{3,4} = a_{4,3} = a_{2,6} = a_{6,2} = a_{3,7} = a_{7,3} = a_{5,6} = a_{6,5} = a_{5,7} = a_{7,5} =$$

$$a_{2,10} = a_{10,2} = a_{3,11} = a_{11,3} = a_{5,13} = a_{13,5} = a_{9,10} = a_{10,9} = a_{9,11} = a_{11,9} = \sqrt{2+n}$$

$$a_{4,8} = a_{8,4} = a_{6,8} = a_{8,6} = a_{7,8} = a_{8,7} = a_{4,12} = a_{12,4} = a_{6,14} = a_{14,6} = a_{7,15} = a_{15,7} =$$

$$a_{12,10} = a_{10,12} = a_{12,11} = a_{11,12} = a_{14,10} = a_{10,14} = a_{15,11} = a_{11,15} = a_{14,13} =$$

$$a_{13,14} = a_{15,13} = a_{13,15} = \sqrt{3+n}$$

$$a_{8,16} = a_{16,8} = a_{16,12} = a_{12,16} = a_{12,14} = a_{14,12} = a_{12,15} = a_{15,12} = \sqrt{4+n}$$

and the other elements are zero.

For five TLS, the matrix elements are

$$a_{1,2} = a_{1,3} = a_{1,5} = a_{2,1} = a_{3,1} = a_{5,1} = a_{1,9} = a_{9,1} = a_{17,1} = a_{1,17} = \sqrt{1+n},$$

$$a_{4,2} = a_{2,4} = a_{3,4} = a_{4,3} = a_{2,6} = a_{6,2} = a_{3,7} = a_{7,3} = a_{5,6} = a_{6,5} = a_{5,7} = a_{7,5} =$$

$$a_{2,10} = a_{10,2} = a_{3,11} = a_{11,3} = a_{5,13} = a_{13,5} = a_{9,10} = a_{10,9} = a_{9,11} = a_{11,9} = a_{18,2} =$$

$$a_{2,18} = a_{19,3} = a_{3,19} = a_{21,5} = a_{5,21} = a_{25,9} = a_{9,25} = a_{25,17} = a_{17,25} = a_{17,18} =$$

$$a_{18,17} = a_{17,19} = a_{19,17} = a_{21,17} = a_{17,21} = \sqrt{2+n}$$

$$a_{4,8} = a_{8,4} = a_{6,8} = a_{8,6} = a_{7,8} = a_{8,7} = a_{4,12} = a_{12,4} = a_{6,14} = a_{14,6} = a_{7,15} = a_{15,7} =$$

$$a_{12,10} = a_{10,12} = a_{12,11} = a_{11,12} = a_{14,10} = a_{10,14} = a_{15,11} = a_{11,15} = a_{14,13} =$$

$$a_{13,14} = a_{15,13} = a_{13,15} = a_{4,20} = a_{20,4} = a_{6,22} = a_{22,6} = a_{7,23} = a_{23,7} =$$

$$a_{10,26} = a_{26,10} = a_{11,27} = a_{27,11} = a_{13,29} = a_{29,13} = a_{26,18} = a_{18,26} = a_{27,19} =$$

$$a_{19,27} = a_{29,12} = a_{12,29} = a_{20,18} = a_{18,20} = a_{20,19} = a_{19,20} = a_{22,18} = a_{18,22} = a_{23,19} =$$

$$a_{19,23} = a_{22,21} = a_{21,22} = a_{23,21} = a_{21,23} = a_{26,25} = a_{25,26} = a_{27,25} = a_{25,27} =$$

$$a_{29,25} = a_{25,29} = \sqrt{3+n}$$

$$a_{8,16} = a_{16,8} = a_{16,12} = a_{12,16} = a_{12,14} = a_{14,12} = a_{12,15} = a_{15,12} = a_{24,8} = a_{8,24} = a_{28,12} =$$

$$a_{12,28} = a_{30,14} = a_{14,30} = a_{31,15} = a_{15,31} = a_{28,20} = a_{20,28} = a_{22,30} = a_{30,22} = a_{31,23} =$$

$$a_{23,31} = a_{24,20} = a_{20,24} = a_{24,22} = a_{22,24} = a_{24,23} = a_{23,24} = a_{28,26} = a_{26,28} = a_{28,27} =$$

$$a_{27,28} = a_{30,26} = a_{26,30} = a_{31,27} = a_{27,31} = a_{30,29} = a_{29,30} = a_{31,29} = a_{29,31} = \sqrt{4+n}$$

$$a_{16,32} = a_{32,16} = a_{24,32} = a_{32,24} = a_{32,28} = a_{28,32} = a_{32,30} = a_{30,32} = a_{32,31} = a_{31,32} = \sqrt{5+n}$$

and the other elements are zero.

Eq. (5.5) in the allowable basis $\{|\psi_i\rangle\}$ is used to obtain the final state of the system at time t,

$$\hat{\rho}_{AF}(t) = \sum_{i,j;i\neq j}^{N} \exp[-\frac{\gamma t}{2}(E_i - E_j)^2 - i(E_i - E_j)t] \times \langle\psi_i| \hat{\rho}(0) |\psi_j\rangle |\psi_i\rangle \langle\psi_j| \qquad (5.8)$$

where E_i, E_j are the eigenvalues of the Hamiltonian in the states $\{|\psi_i\rangle\}$. The final state of the atomic system is obtained after taking the trace over the field i.e. $\hat{\rho}(t) = Tr_F[\hat{\rho}_{AF}(t)]$.

5.3 Multipartite Quantum Correlations

For a bipartite system with A and B subsystems QD $D^{A \to B}$, which is the difference between quantum MI $I(\rho)$ and CC $J(\rho)$, minimized over the measurements $\hat{\Pi}$ performed on the subsystem B, is given by Eq. (4.48) [22],

$$D^{A \to B}(\hat{\rho}_{AB}) = \min_{\{\hat{\Pi}^j_B\}} [I(\hat{\rho}_{AB}) - J(\hat{\rho}_{AB})_{\{\hat{\Pi}^j_B\}}] \tag{5.9}$$

where $\hat{\rho}_{AB}$ is the density matrix of composite system, and I and J are the expression of the MI given by Eqs. (4.30) and (4.32). Using the projective measurements on the system, the GQD for N-party system can be written by Eq. (4.59)

$$\text{GQD}(\hat{\rho}_T) = \min_{\{\Pi^k\}} \left\{ \sum_{j=1}^{N} \sum_{l=0}^{1} \tilde{\rho}_j^{ll} \log_2 \tilde{\rho}_j^{ll} - \sum_{k=0}^{2^N-1} \tilde{\rho}_T^{kk} \log_2 \tilde{\rho}_T^{kk} \right\} + \sum_{j=1}^{N} S(\rho_j) - S(\rho_T) \tag{5.10}$$

where $\hat{\rho}_T$ is the density matrix of total system and ρ_j is the density matrix of the jth subsystem. As given in Sec. (4.10), we know $\tilde{\rho}_T^{kk} = \langle k | \hat{R}^\dagger \rho_T \hat{R} | k \rangle$ and $\tilde{\rho}_j^{ll} = \langle l | \hat{R}^\dagger \rho_j \hat{R} | l \rangle$, and $\hat{\Pi}^k = \hat{R} | k \rangle \langle k | \hat{R}^\dagger$ are the multi-qubit projective operators. $S(\rho_j) = -Tr[\rho_j \log_2 \rho_j]$ and $S(\rho_T) = -Tr[\rho_T \log_2 \rho_T]$ are the VNE of the subsystem j and the total system respectively. Here $\{|k\rangle\}$ are the eigenstates of $\bigotimes_{j=1}^{N} \hat{\sigma}_j^z$ and $\hat{R}$ is a local multi-qubit rotation operator acting on the jth qubit, expressed as $\hat{R} = \bigotimes_{j=1}^{N} \hat{R}_j(\theta_j, \phi_j)$ with $\hat{R}_j(\theta_j, \phi_j) = \cos\theta_j \hat{1} + i\sin\theta_j \cos\phi_j \hat{\sigma}_y + i\sin\theta_j \sin\phi_j \hat{\sigma}_x$. Alongside the GQD, the VNE ($S(\rho) = -Tr[\rho \log_2 \rho]$) is also computed and compared with GQD.

5.4 Result and discussion

In this section, we explore the dynamics of the GQD and VNE of the system with an initially mixed state given by Eq. (5.5). The dynamical behavior of both quantifiers, the GQD and VNE are numerically evaluated for the different number of photons n, γ, and the mixing parameter α.

Fig. (5.1) shows the results for the time evolution of the GQD and VNE for the system with two ($N = 2$) and five ($N = 5$) TLS. In these plots, we have assumed that there is no ID. For $N = 2$ a periodicity in gradual increase and decrease of the GQD is seen in the system. It shows an interplay between the classical and MPQC. There is no abrupt vanishing of the MPQC in the system. Such behavior has also been seen by Fanchini

et. al. and Werlang et. al. [126, 127] for a two-qubit system where the sudden death of discord is not observed instead it remains periodic. Whereas, VNE attains three distinct phases corresponding to disorder in atomic states i.e. maximum, intermediate minima, and zero. The maximum value of VNE for $N = 2$ suggests a higher degree of accessible states in the system whereas zero value indicates that all the atoms are in only one atomic state. As the system's size increases with the addition of TLS in the system, the magnitudes of both the GQD and VNE show an increasing behavior. Extrema of both the GQD and VNE do not coincide especially for large-N systems where the atoms have more accessible atomic states. The intermediate phase in the VNE dynamics for $N = 2$ corresponds to non-zero entropy that hints at a phase with less quantum interference (Fig. (5.1)) and zero GQD. The dynamical behavior of these quantifiers suggests that the information can retain in such systems that can be useful in quantum processing. The behavior of the GQD and VNE for a non-zero n is also shown in Fig. (5.1). Rather periodic behavior of both quantifiers is present and that has not been seen in the zero photon case. This periodicity is due to the availability of the photons to cause atomic transitions in the system. We observe the effects of the field on the quantifiers, which is present even after tracing out the field from the final density matrix. Quantum systems are composed of TLS, and the environment with which they interact retains some information about the environment [128]. Therefore the effect of field resides in the time evolution of the density matrix that ensures both atom and field states have become a mixed state. This periodic behavior in both quantifiers is seen for the large-N system as well. The generalized dynamics of the system show long-lasting correlations because the revivals of both quantifiers are approximately doubled as compared with no photon case.
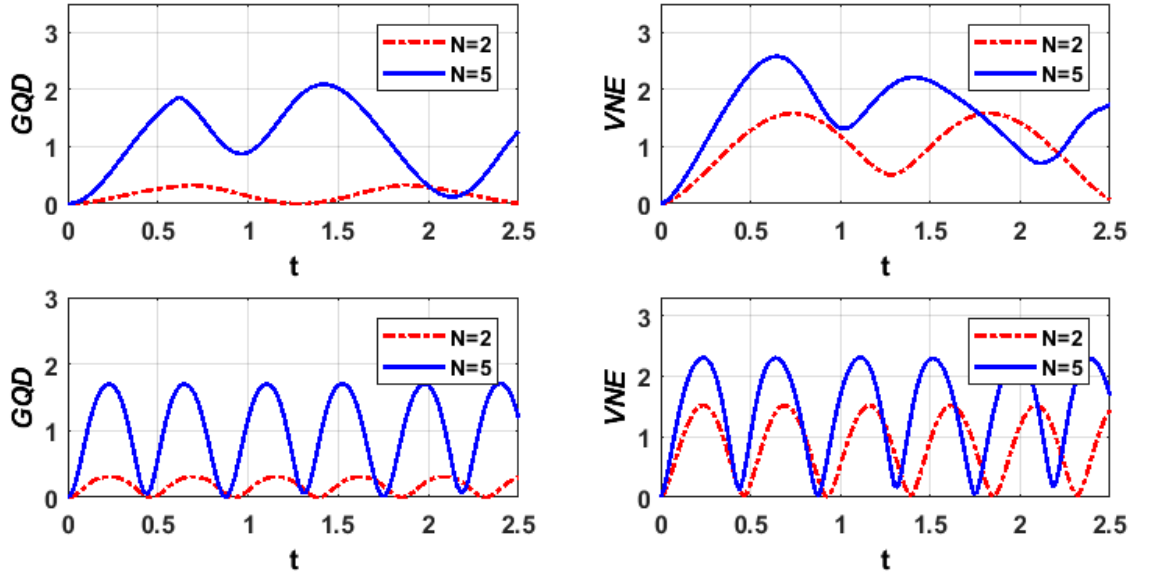
Figure 5.1: (color online) The GQD and VNE are plotted as a function of scaled time for $N = 2$ and $N = 5$ TLS. The plots in the upper panel are for $n = 0$ and in the lower panel are for $n = 10$. All data is for $\gamma = 0$, $p = 0$ and $\alpha = 0$.

The statistical mixture of the system as represented by $\hat{\rho}(t)$ can be quantified by measuring the purity, which is defined as $\text{Tr}\rho(t)^2$. For a pure quantum state, purity is 1 i.e. $\text{Tr}\rho(t)^2 = 1$ whereas for a mixed state $\text{Tr}\rho(t)^2 < 1$. For an entangled state, the purity level of the subsystems of the multipartite system is always less than the purity of the full system represented in Eq. (5.8). The dynamical variation between quantum purity and the quantifiers GQD and VNE for two and five TLS are shown in Fig. (5.2). The variations are plotted for two types of initial states, one is for $\alpha = 0$ and the other for $\alpha = \pi/4$. For $\alpha = 0$ when the system is allowed to evolve, both the GQD and VNE are non-zero for $\alpha = \pi/4$ state and zero for $\alpha = 0$ state. The purity satisfies $\frac{1}{d} \leq \text{Tr}\rho^2 \leq 1$, where d is the dimension of Hilbert space of multi TLS given as 2^d. For an initial state at $\alpha = \pi/4$, the GQD is zero while VNE is not.
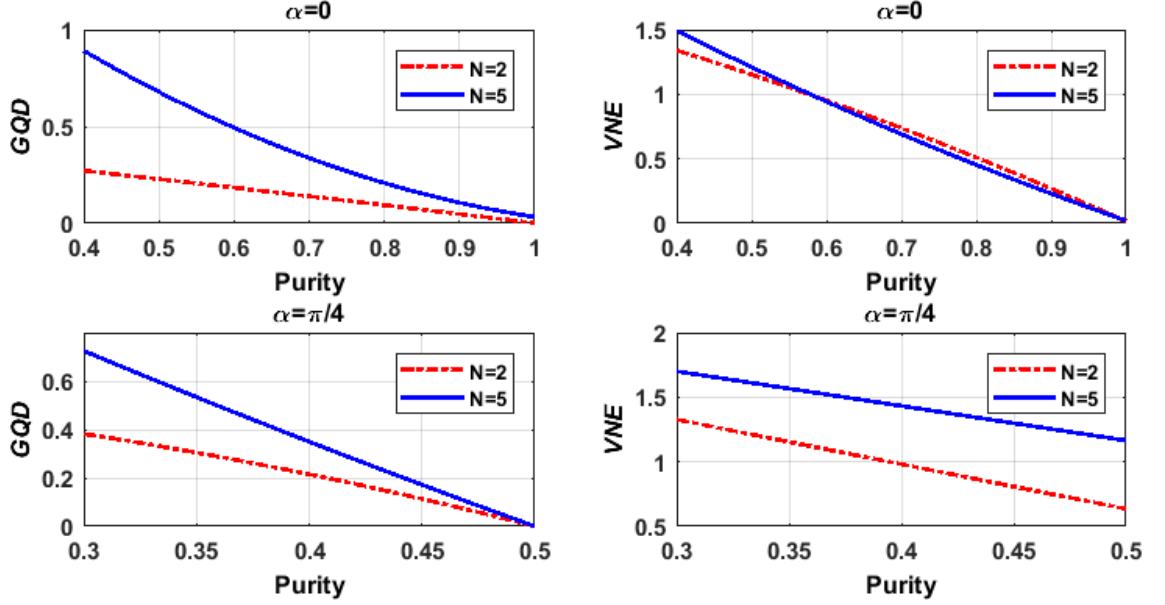
Figure 5.2: (color online) The variation in the correlations of the system is studied with respect to the purity of the system with two different initial states. All data is set for $\gamma = 0$, and $p = 0$.

Fig. (5.3) shows the effect of mixing parameter α on the dynamics of the GQD and VNE. It is observed that certain values of mixing parameters assist the dynamics of GQD. For $N = 2$, the system shows the maximum value of GQD around $\alpha = \pi/4$ that corresponds to the initially mixed state. For the large-N systems, the maximum value of GQD is observed at $\alpha = \pi/2$ represents an initially mixed state prepared in an equal statistical mixture of the ground states and excited states. This behavior points out that the large-N system favors the initial state prepared in $\alpha = \pi/2$. For the large-N systems, almost all states show non-zero MPQC. On the other hand, the dynamical behavior of VNE suggests that the initial state prepared in $\alpha = \pi/2$ shows the least quantum interference in the dynamics in atomic states.

64
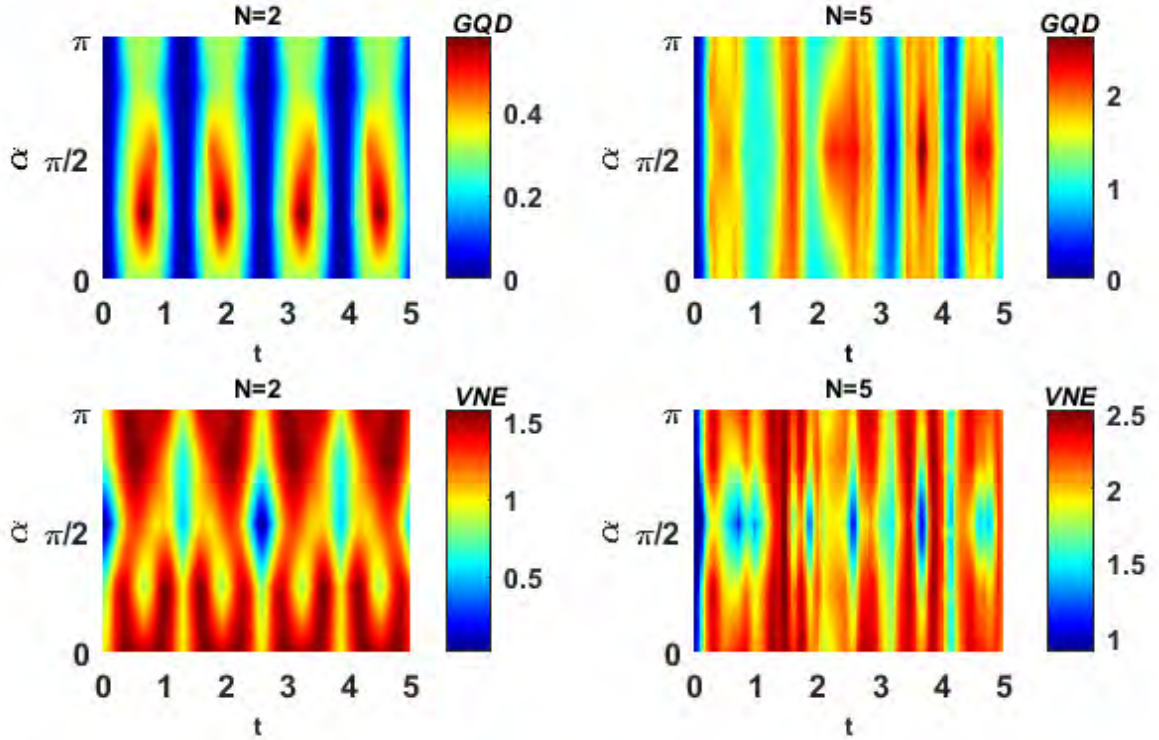
Figure 5.3: (color online) The density plots of the quantifiers as a function of α and scaled time t for $N = 2$ and $N = 5$ TLS. All data is set for $\gamma = 0$, $n = 0$ and $p = 0.5$.

Photons in the system play an important role to assist and boost the correlations. The effect of increasing the photons in the system has two important consequences: Firstly, increasing the photons support the MPQC in the system by reducing the revival time of the correlations, and secondly, the photons do not raise the maximum value of the MPQC in that system. Furthermore, the increase in the number of revivals in the unit time t, defined by t_R, as shown in Fig. (5.4) tends to increase non-linearly as the photons n in the system are increased. The maximum magnitude of the GQD which is defined by d_{max}, for a system is plotted against the photons n as shown in Fig. (5.5). The maximum value of correlations in the system does not change as the number of photons are increased in the system. It is also observed that the slope between the GQD and VNE remains nearly the same as the photons are increased inside the system, as shown in Fig. (5.6). Both the GQD and VNE are computed and plotted in Fig. (5.6). There is a slight increase in the slope as the photons are increased in the system. The effect of photon number n is nearly the same with a slight change in the slope. This behavior also shows that quantum interference supports the MPQC in the system. Furthermore, according to Fig. (5.1), the behavior of t_R to the change of the photons in the system is

not affected in the large-N systems and both the quantifies exhibits similar behavior.
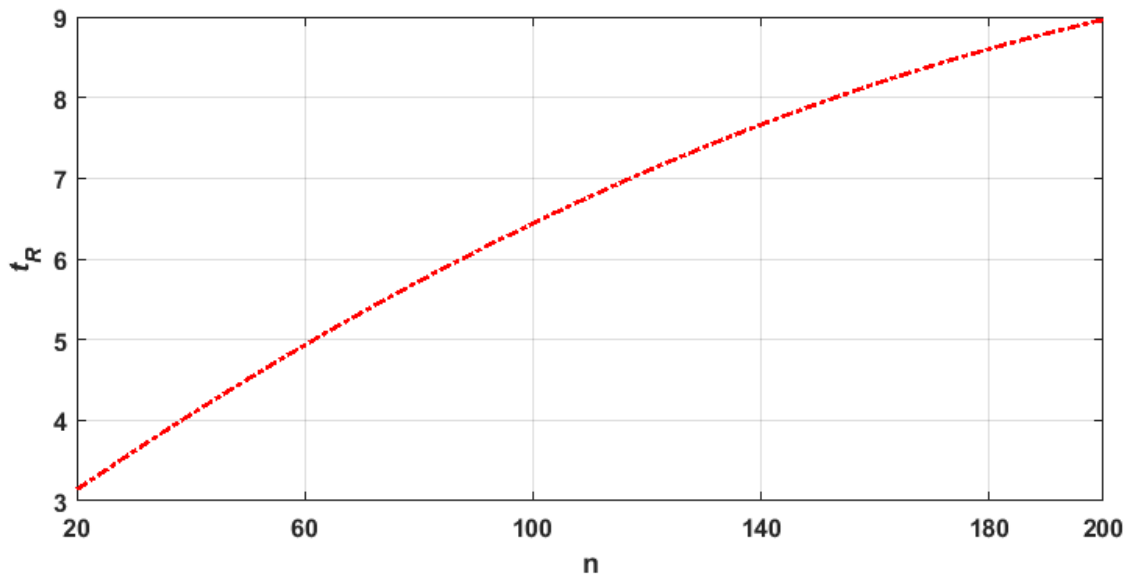
Figure 5.4: (color online) The GQD assisting curve of a system composed of two TLS. The number of revivals per unit time, t_R, is plotted against the number of photons. t_R increases in a non-linear fashion and increases if photons n are increased. All data is for $\gamma = 0$, $p = 0$ and $\alpha = 0$.
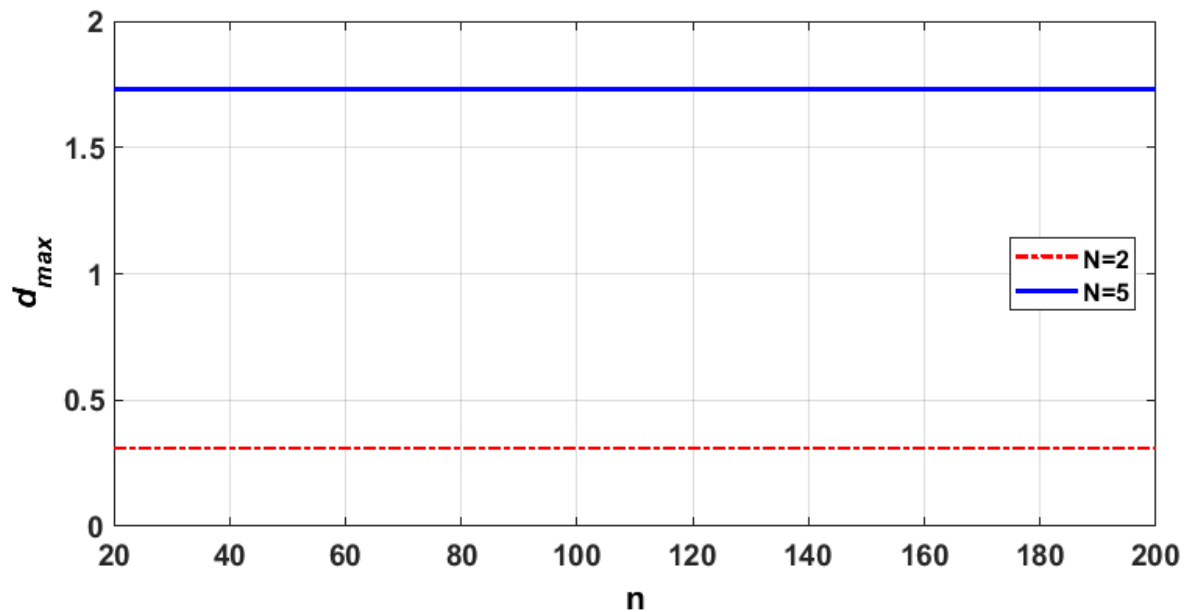
Figure 5.5: (color online) The maximum of the GQD of the system composed of two and five TLS is analyzed with the change in the photons n. There is no increase in the maximum value of the MPQC in the system with n. All data is for $\gamma = 0$, $p = 0$ and $\alpha = 0$.
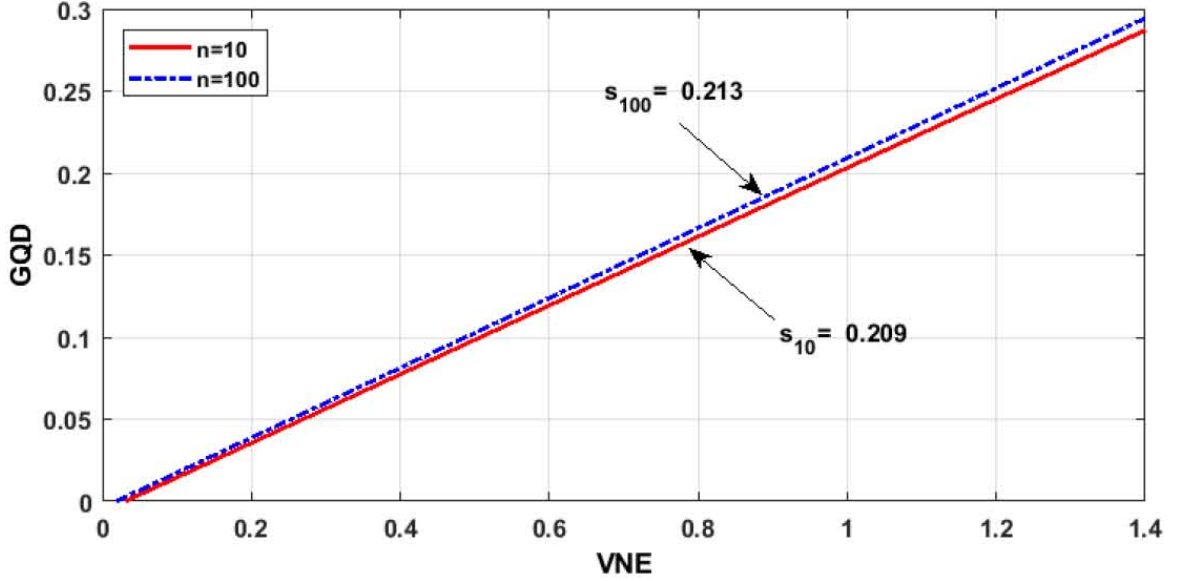
Figure 5.6: (color online) The slopes of the lines remain almost the same as the photons in the system are increased. Both quantifiers change with the almost same magnitude as the photons are changed in the system. All data is for $N = 2$, $\gamma = 0$, $p = 0$ and $\alpha = 0$.

The effect of ID upon the evolution of the quantifiers two and five TLS is shown in Fig. (5.7). For the zero photon case, the dynamics of the GQD and VNE have a maximum value of around $t \sim 0.5$. The maximum value of the GQD and VNE increases with the increase in the number of TLS N. The fluctuations of the GQD about maximum value, increase for larger N. The effects of the number of photons on the dynamics of the GQD and VNE are shown in Fig. (5.7) lower panel. In the multiphoton case, the system gets smoother dynamical behavior in both quantifiers, as compared to the zero photon case and this seize of fluctuations in dynamics hinders the system to process information. Fig. (5.8) shows the GQD and VNE dynamics in the system w.r.t. α. For $N = 2$, the MPQC are robust and vanishing for $\alpha = \pi/4$ and $\alpha = 3\pi/4$, respectively. It is observed that for a two TLS, the values of α have prominent effects on the dynamics of the GQD and VNE, whereas, for higher values of N, the system dynamics show less dependence on the mixing parameter α.
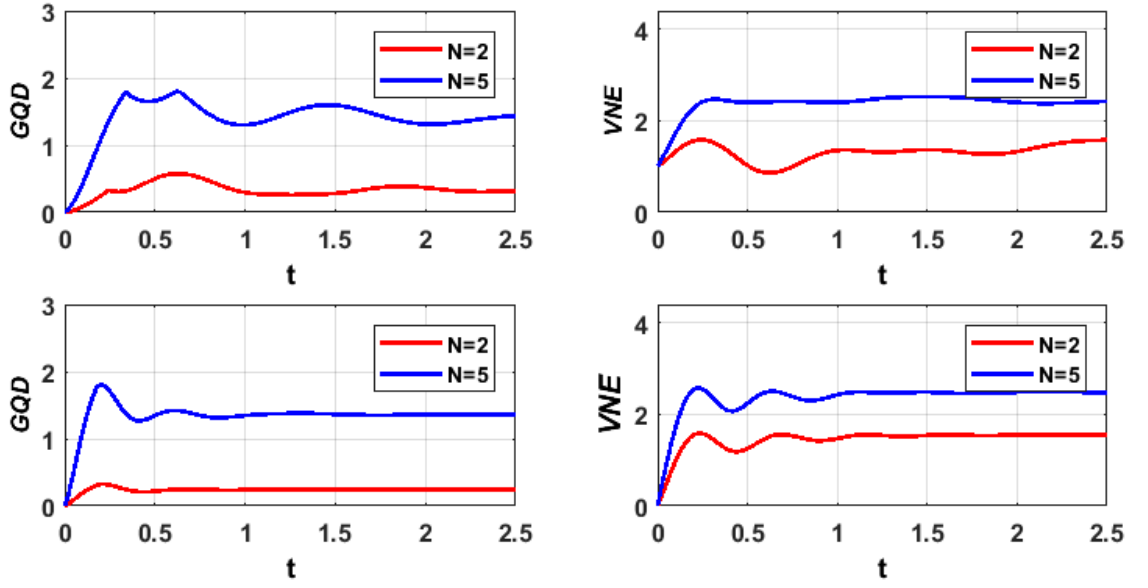
Figure 5.7: (color online) The quantifiers are plotted for $N = 2$ and $N = 5$ TLS with non-zero ID. The plots in the upper panel are for photon number $n = 0$ and in the lower panel are for $n = 10$. All data is for $\gamma = 0.05$, $\alpha = \pi/4$ and $p = 0$.
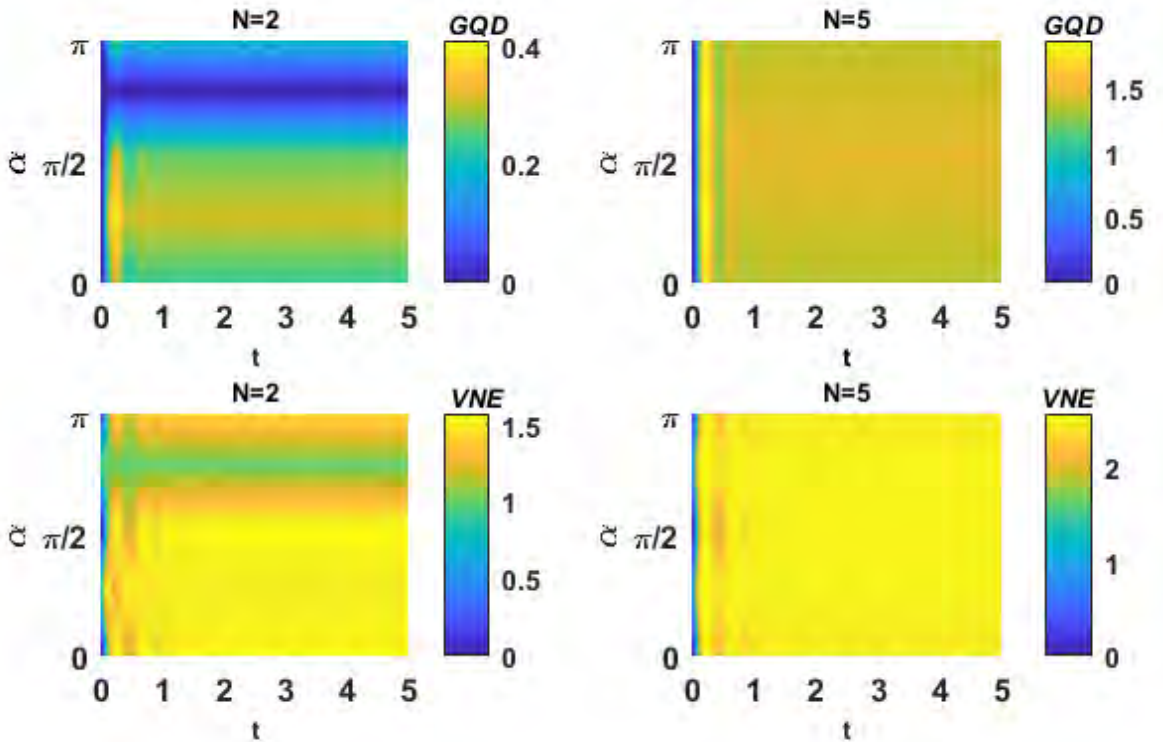
Figure 5.8: (color online) The density plots of the quantifiers as a function of α and scaled time t for $N = 2$ and $N = 5$ TLS. All data is set for $\gamma = 0.05$, $n = 10$ and $p = 0$.

The general behavior of the quantifier for a large-N system is studied. From Fig. (5.1),

it is seen that for the large-N system, the magnitude of the GQD and VNE is increased and the first maximum of each system is shifted towards the zero of the time scale. Fig. (5.9) shows the shift factor of revivals of the GQD, denoted by Δt_2 of three, four, and five TLS with the reference to the two TLS. It is seen that with the addition of each TLS in the system, the slope of the line is increased by 0.02 in a two TLS. The revival time of the GQD for the large-N system will become more and more shifted towards the origin of the time scale and the system has the MPQC early in the time evolution. The maximum value of the GQD and VNE of the system achieved in the time evolution, denoted by d_{max} and e_{max} respectively, are plotted in Fig. (5.10). Both d_{max} and e_{max} tend to increase with different non-linear fashion upon the increase in N. From Fig. (5.10), the GQD varies with the quadratic ($a_1 = 0.025$) and linear ($b_1 = 0.331$) coefficient both positive. On the other hand the VNE, the coefficient with quadratic ($a_2 = -0.037$) and linear ($b_2 = 0.955$) terms has opposite signs.
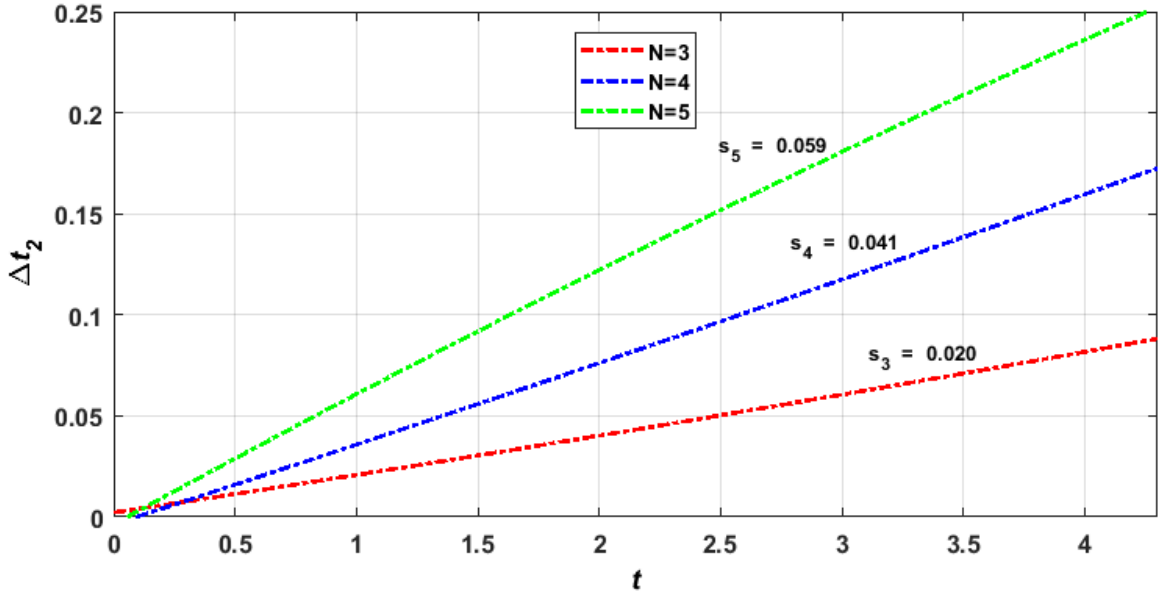
Figure 5.9: (color online) Shift in the compression time Δt_2 of the GQD is plotted for the three, four, and five TLS with reference to the two TLS. There is an increase in the value of the respective slope as the system gets more TLS. All data is for $n = 10$, $\gamma = 0$ and $\alpha = 0$.
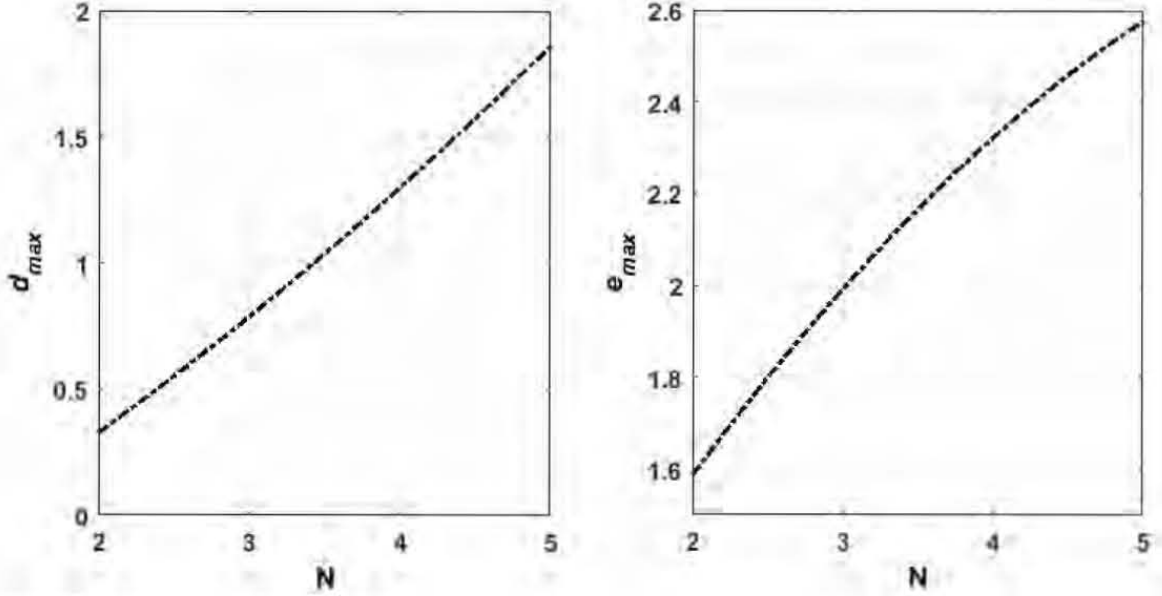
Figure 5.10: (color online) The change in the maximum value of the GQD, denoted by d_{max}, and VNE, denoted by e_{max}, with the increase of each TLS in the system is plotted. The d_{max} increases with the positive linear and quadratic curve fitting coefficients while e_{max} increases with negative quadratic and positive linear coefficients. All data is for $\gamma = 0$, $n = 10$ and $p = 0$.

5.5 Conclusions

In this paper we explored how GQD and VNE evolve with time for the multi TLS, that interacts with the single mode Fock field. We computed the GQD and VNE for two, three, four, and five TLS interacting with a single mode Fock field with and without ID. We found that with increasing the size of the system (number of atoms), the GQD and VNE are enhanced which can be regarded as a change in the content of information. The photons assisted the MPQC by reducing the revival time of the quantifiers. The revivals in unit time had a non-linear behavior with the number of photons in the system. It was also observed that the maximum value of the MPQC in the system did not change with the number of photons. The behavior of the quantifiers was also studied with different values of mixing parameters α with and without ID. The effect of the purity was analyzed and it showed an increase in the correlations that corresponded to less purity and a higher degree of mixing in the system. The effect of large-N on the quantifiers indicates that the GQD and VNE have different scaling behaviors.

Chapter 6

Multipartite quantum correlations and Entanglement in N two-level atoms interacting with the coherent field in the presence of the nonlinear Kerr medium

6.1 Introduction

In this chapter, we investigate the dynamics of QE of N moving TLS interacting with a coherent field in the presence of the non-linear Kerr medium (NLKM). The dynamics of the GQD and VNE under the influence of NLKM are studied for two, three, and four TLS. The NLKM has shown an important role in the evolution of the quantifiers of moving multi TLS.

This chapter is organized as follows. In Sec. (6.2), we present the model and the Hamiltonian of the system which interacts with the coherent field. The system is moving and influenced by the NLKM. In Sec. (6.3) we describe the GQD and VNE. In Sec. (6.4), we present the results and their discussion. In Sec. (6.5), we present a brief conclusion.

6.2 Hamiltonian model

The total Tavis-Cummings Hamiltonian given in Eq. (2.93), of the system composed of N TLS fixed system under the rotating wave approximation (RWA) and NLKM is,

$$\hat{H}_T = \frac{\omega_0}{2} \sum_{i=1}^{N} \hat{\sigma}_i^z + \omega \hat{a}^\dagger \hat{a} + \lambda \sum_{i=1}^{N} \left(\hat{a} \hat{\sigma}_i^+ + \hat{a}^\dagger \hat{\sigma}_i^- \right) + \chi \left(\hat{a}^\dagger \hat{a} \right)^2, \tag{6.1}$$

where χ is the Kerr parameter given by Eq. (3.51) and λ is atom-field coupling constant. We are considering the more general case of moving atoms with velocity v in the cavity of length L. We consider the one-dimensional case of the TLS moving along the cavity axis. In this case Eq. (6.1) will become

$$\hat{H}_T = \frac{\omega_0}{2} \sum_{i=1}^{N} \hat{\sigma}_i^z + \omega \hat{a}^\dagger \hat{a} + f(vt) \sum_{i=1}^{N} \left(\hat{a} \hat{\sigma}_i^+ + \hat{a}^\dagger \hat{\sigma}_i^- \right) + \chi \left(\hat{a}^\dagger \hat{a} \right)^2, \tag{6.2}$$

where $f(vt)$ is the shape function of the cavity field mode as given in Eq. (3.60). The general cases of atomic motion with velocity v, are given in Eqs. (3.63) and (3.65), we have

$$f(vt) = \lambda \sin\left(\frac{\eta \pi v t}{L} \right)$$

and

$$f_1(vt) = \int_0^t f(vt) dt = \lambda \frac{L}{\eta \pi v} \left(1 - \cos\left(\frac{\eta \pi v t}{L} \right) \right)$$

and we have,

$$\begin{aligned} f_1(vt) &= \frac{1}{\eta} \left(1 - \cos\left(\frac{\eta \pi v t}{L} \right) \right) \text{ for } \eta \neq 0, \\ &= \lambda t \qquad\qquad\qquad \text{ for } \eta = 0. \end{aligned}$$

where η represents the number of half wavelengths in the cavity of length L. We consider the total system prepared in the direct product of a mixed state of N TLS, that interacts with the coherent field. We are interested in studying the effects of both pure and mixed states of the atomic system on the quantifiers; hence, the initial state of the system can be written as

$$\hat{\rho}(0) = [(1-p)|\psi\rangle\langle\psi| + p|g_1 g_2 ..... g_N\rangle\langle g_1 g_2 ..... g_N|] \otimes \hat{\rho}_E, \tag{6.3}$$

with $|g_j\rangle$ and $|e_j\rangle$ being the ground and excited states of the atomic system, respectively and p is the statistical mixture parameter with $0 \leq p \leq 1$. The ket vector is given as

$|\psi\rangle = \cos(\theta) |g_1 g_2.....g_N\rangle + \sin(\theta) |e_1 e_2.....e_N\rangle$, where $0 \leq \theta \leq \pi$. The parameter θ in $|\psi\rangle$ allows us to study the effects of superposition of atomic states on the quantifiers. The particular choice of the initial state of the atomic system is important in the sense that for $p = 0$ and $\theta = \pi/4$, it reduces to a Greenberger-Horne-Zeilinger (GHZ) state which is maximally entangled. Moreover, it is mathematically convenient to handle such a state. $\hat{\rho}_E$ is the coherent field and it can be written as

$$\hat{\rho}_E = \sum_n p_n |n\rangle\langle n| \tag{6.4}$$

where the weight function p_n is

$$p_n = \frac{|\alpha|^{2n} e^{-|\alpha|^{2n}}}{n!} \tag{6.5}$$

and

$$\langle n \rangle = |\alpha|^2 \tag{6.6}$$

where n represents the photon number inside the cavity. The set of allowable basis states $\{|\psi_i\rangle\}$ can be written as

$$\{|\psi_i\rangle\} = |g_1 g_2.....g_N, n + N\rangle, |e_1 g_2.....g_N, n + N - 1\rangle, ..., |e_1 e_2.....e_N, n\rangle. \tag{6.7}$$

At later time t, the final state is

$$\hat{\rho}_{AF}(t) = \sum_{i,j}^N |\psi_i\rangle\langle\psi_i|\hat{\rho}(t)|\psi_j\rangle\langle\psi_j|, \tag{6.8}$$

where $\hat{\rho}(t)$ in terms of eigenvalues of the initial states can be written as

$$\hat{\rho}_{AF}(t) = \sum_{i,j}^N \exp\left(-i\left(E_i - E_j\right)t\right) \times \langle\psi_i|\hat{\rho}(0)|\psi_j\rangle|\psi_i\rangle\langle\psi_j|, \tag{6.9}$$

and E_i, E_j and $|\psi_i\rangle, |\psi_j\rangle$ are the eigenvalues and eigenvectors of $\hat{\rho}(0)$. The final state of TLS is obtained after taking the trace over the field i.e. $\hat{\rho}_T(t) = Tr_F\left[\hat{\rho}_{AF}(t)\right]$.

6.3 Multipartite Quantum Correlations and Entanglement

For a bipartite system, composed of two subsystems A and B, QD can be written [22], mathematically, as from Eq. (4.48)

$$\mathrm{D}^{A \to B}(\hat{\rho}_{AB}) = \min_{\{\hat{\Pi}_B^j\}}[I(\hat{\rho}_{AB}) - J(\hat{\rho}_{AB})_{\{\hat{\Pi}_B^j\}}] \tag{6.10}$$

where $\hat{\rho}_{AB}$ is the density operator of the composite system AB and I and J are the MI given by Eqs. (4.30) and (4.32). In order to calculate the multipartite the MPQC, the GQD given by Eq. (4.59),

$$\text{GQD}(\rho_T) = \min_{\{\Pi^k\}} \left\{ \sum_{j=1}^{N} \sum_{l=0}^{1} \tilde{\rho}_j^{ll} \log_2 \tilde{\rho}_j^{ll} - \sum_{k=0}^{2^N-1} \tilde{\rho}_T^{kk} \log_2 \tilde{\rho}_T^{kk} \right\} + \sum_{j=1}^{N} S(\rho_j) - S(\rho_T) \quad (6.11)$$

where $\hat{\rho}_T$ defines the density matrix of total system and ρ_j is the density matrix of the subsystem j. The other definitions, expressions of Eq. (6.11) can be found in Sec. (4.10). For a density operator $\hat{\rho}_T$, the VNE is defined as

$$S(\hat{\rho}_T) = -\text{Tr}(\hat{\rho}_T \log_2 \hat{\rho}_T) = -\sum_i r_i \ln r_i, \quad (6.12)$$

where r_i are the eigenvalues $\hat{\rho}_T$.

6.4   Results and discussions

We study the dynamical behavior of the GQD and VNE for N moving TLS (two, three, and four TLS). The system interacts with a single-mode coherent field in the NLKM. We have carried out numerical calculations to find the dynamics of the GQD and VNE and we have taken the time step-size of 0.1. The dynamical behavior of the GQD and VNE without the atomic motion ($\eta = 0$) for two TLS ($N = 2$) under the NLKM is shown in Fig. (6.1). The behavior is studied for initial pure ($p = 0$) and mixed ($p = 0.5$) atomic states with mixing parameter $\theta = 3\pi/4$. The GQD and VNE behavior is studied for different values of χ and $|\alpha|^2 = 36$. For initial pure and mixed states, repeated collapses and the revivals of the GQD and VNE are observed for different values of the NLKM parameter. It is seen that the revival time of the GQD and VNE is decreased when χ is increased. The GQD is found heavily suppressed at $\chi = 3$ as compared to $\chi=0.3$. According to Fig. (6.1), the decrease in the revival time of the GQD and VNE with the higher NLKM parameters values show that with the higher χ value, the MPQC arise in the system early in the time evolution. The amplitude of the VNE decreases slowly as compared to the amplitude of the GQD in the presence of the NLKM even at higher values of χ. It is also observed that the initial pure state has a slightly higher magnitude of GQD as compared to the mixed states with a small effect of the mixing parameter, p on the dynamics of these quantifiers. Furthermore, it has been observed that the revival

time of the quantifiers is almost the same for different initial states, and the NLKM parameter, χ values.

Figs. (6.2) and (6.3) show the behavior of the quantifiers in the presence of the NLKM for three ($N = 3$) and four ($N = 4$) TLS, respectively, with $\eta = 0$. It is observed that, in the case of $N = 3$ and $N = 4$, the collapses and revivals occur repeatedly for both VNE and GQD for different values of the NLKM parameter χ. In comparison with Fig. (6.1), the amplitude of the revivals of the GQD is increased for $N = 3$ and $N = 4$ for different χ. It is also observed that the time interval between two consecutive revivals is almost the same for $N = 3$ and $N = 4$. However, the effect of the NLKM parameter χ on the amplitude of the revivals has a promising effect for the $N = 4$ case. It is found that the VNE for $N = 3$ and $N = 4$ is increased as compared to $N = 2$ for $\chi = 0.3$, but no significant increase is observed for $\chi = 1$ and $\chi = 3$. This shows that the systems with large N values are more entangled at lower Kerr parameter values as compared to the higher values. Moreover, the revival time of the quantifiers decreases with the increase of χ for both the initial states in the case of the large N atomic systems.
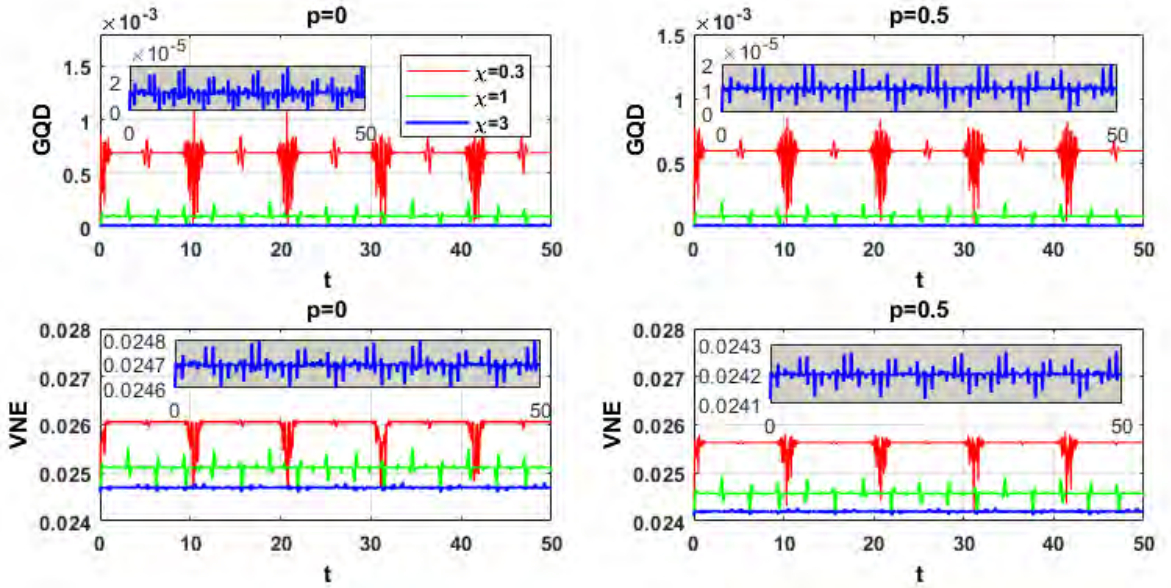
Figure 6.1: (color online) The dynamical behavior of the GQD and VNE for N=2 with $\chi = 0.3, 1$ and 3 at $\theta = 3\pi/4$, $|\alpha|^2 = 36$, $\eta = 0$. The insets show the magnified view of the quantifiers for $\chi = 3$.
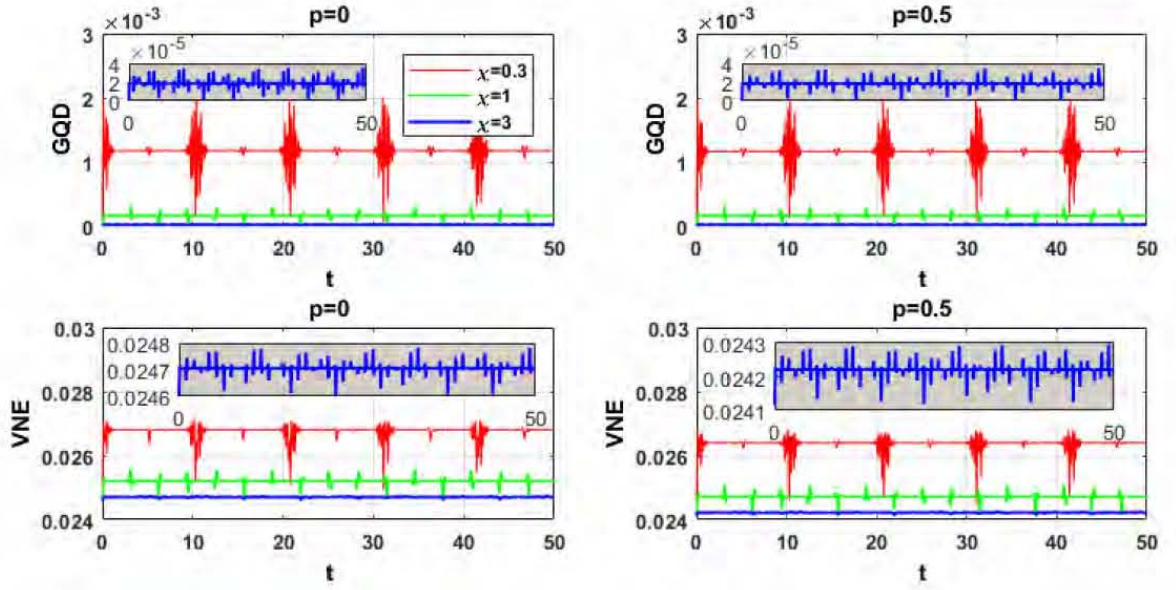
Figure 6.2: (color online) The dynamical behavior of the GQD and VNE for N=3 with $\chi = 0.3, 1$ and 3 at $\theta = 3\pi/4$, $|\alpha|^2 = 36$, $\eta = 0$. The insets show the magnified view of the quantifiers for $\chi = 3$.
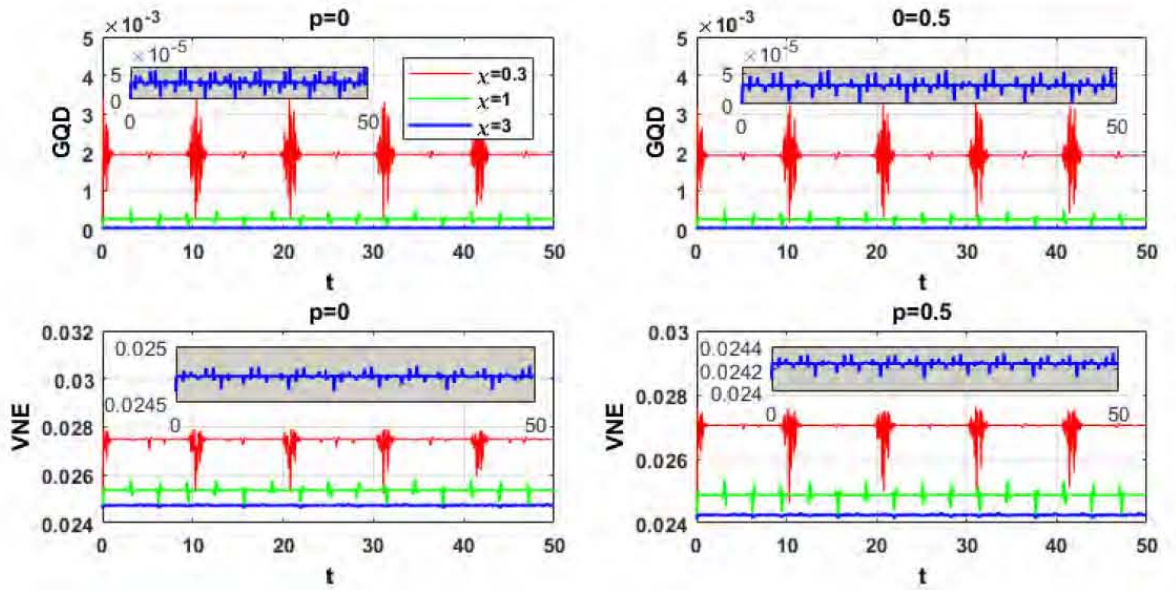
Figure 6.3: (color online) The dynamical behavior of the GQD and VNE for N=4 with $\chi = 0.3, 1$ and 3 at $\theta = 3\pi/4$, $|\alpha|^2 = 36$, $\eta = 0$. The insets show the magnified view of the quantifiers for $\chi = 3$.
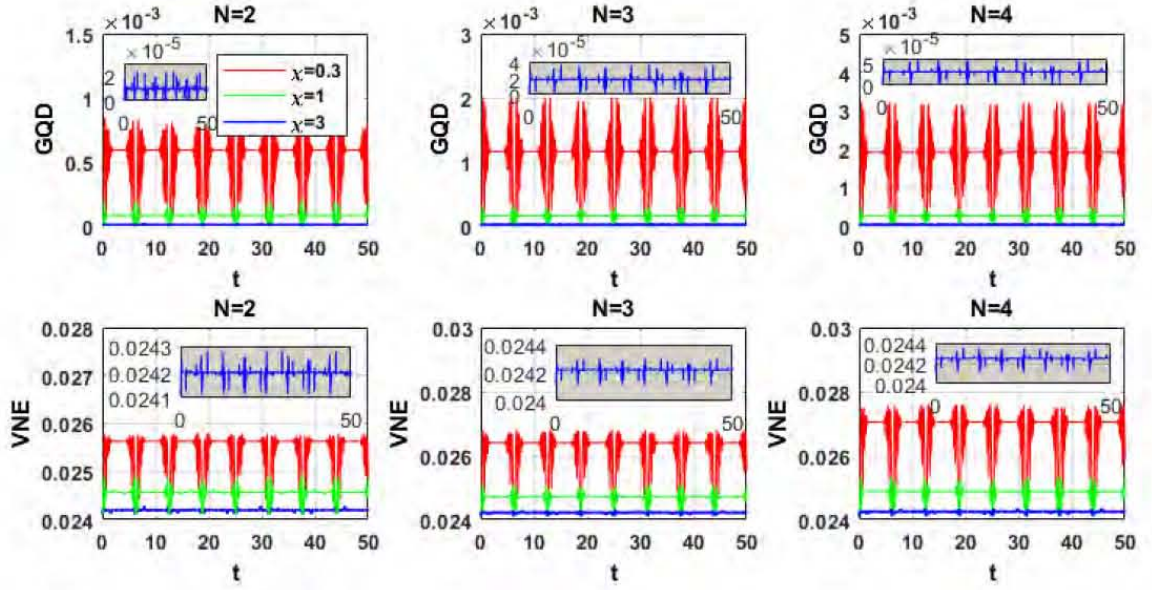
Figure 6.4: (color online) The dynamical behavior of the GQD and VNE for N=2,3 and 4 with $\chi = 0.3, 1$ and 3 at $p = 0.5$, $\theta = 3\pi/4$, $|\alpha|^2 = 36$, $\eta = 1$. The insets show the magnified view of the quantifiers for $\chi = 3$.
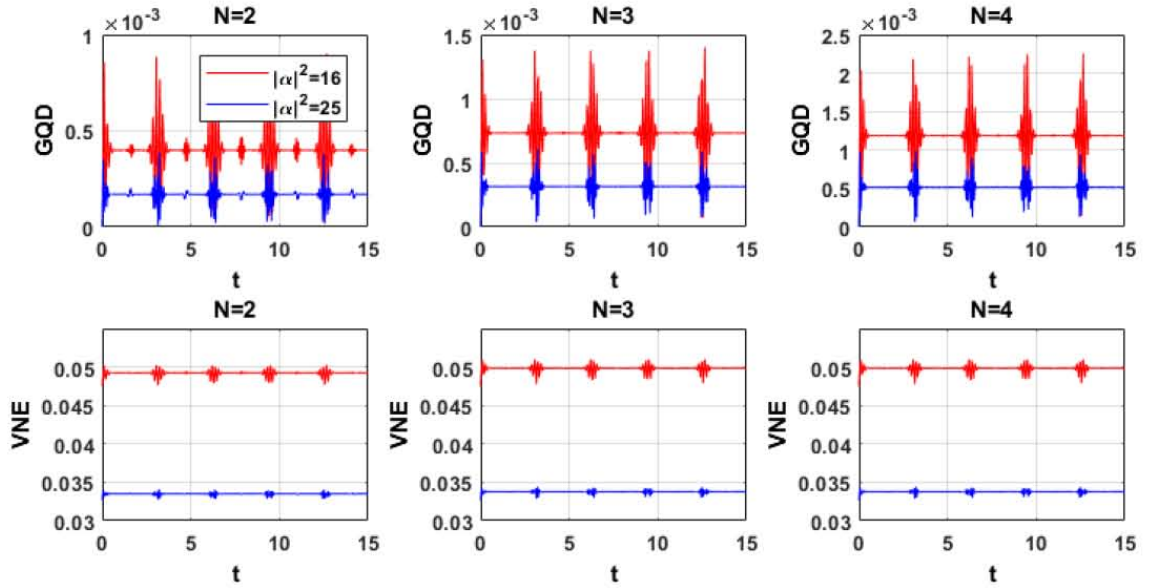
Figure 6.5: (color online) The dynamical behavior of the GQD and VNE of the system N=2,3 and 4 with $\chi = 1$ and $|\alpha|^2 = 16$ and 25. All data is for $p = 0.5$, $\theta = 3\pi/4$ and $\eta = 0$.

In Fig. (6.4), the dynamical evolution of the GQD and VNE is shown for two ($N = 2$), three ($N = 3$) and four ($N = 4$) moving TLS ($\eta = 1$) surrounded by the NLKM. As compared to Figs. (6.1-6.3), Fig. (6.4) shows that the number of revivals is increased for all the atomic systems which are almost doubled as compared to the atomic systems

with $\eta = 0$, in the NLKM. However, the amplitude of the revivals does not increase with the atomic motion. For $\eta = 1$, the amplitude of revivals only increases for higher N atomic systems and decreases by increasing χ. It is seen that the atomic motion assists the quantum system to sustain the revivals. Furthermore, the width of the revivals is increased as compared to $\eta = 0$. For $\chi = 0.3$ and $\chi = 1$, the number of revivals of the GQD and VNE is equal and the revivals occur at equal intervals of time. Comparing with the $\eta = 0$ case, the number of revivals per unit scaled time is decreased at $\chi = 3$ and by increasing the value of χ from 1 to 3, the dynamics of the GQD and VNE show a decrease in the revivals. Hence, the collapses and revivals describe the periodic nature of the GQD and VNE during the time evolution of the quantum system.

Fig. (6.5) shows the effect of the average number of photons on the dynamics of the GQD and VNE for different values of $|\alpha|^2$. It is seen that the change in the average number of photons in the system has a notable effect on the system dynamics. In the presence of the NLKM, at $\chi = 1$ and by increasing α, the GQD of the system is decreased. As we have seen in Figs. (6.1-6.3), the number of revivals increases with χ whereas the number of revivals remains the same with the increase of α and the dynamical behavior suggests that in the presence of the NLKM there is no change in the revivals with the increase of the number of average photons α. It is seen that under the influence of the NLKM with $|\alpha|^2 = 16$, and $|\alpha|^2 = 25$ rapid oscillations are observed in the revival of the GQD and VNE. However, the amplitude of the revival is decreased when the average number of photons is increased. Furthermore, no change in the VNE of the quantum systems is observed due to the variation of the average number of photons for the large N atomic systems.

6.5   Conclusion

We studied the dynamics of GQD and VNE for a system composed of N moving TLS that interact with a single-mode coherent field. The system is present in the NLKM. We considered the Tavis-Cumming model extended for N atoms. We explored the GQD and VNE under different scenarios, i.e. by changing the number of TLS in the system, the average photons $< n >$, and the NLKM parameter χ. Studies were made for both pure and mixed initial atomic states.

We observe the collapses and revivals in the quantifiers for different χ values. It was found that for higher Kerr parameter values, the magnitude of the revivals of QE is suppressed for the quantum system. It was shown that the periodic response of QE was sustained during the dynamics of a quantum system composed of relatively large N. It was also seen that mixed states have comparatively depressed oscillations of the GQD as compared to the pure states. However, the GQD and VNE were decreased by increasing the NLKM parameter and $< n >$. Moreover, the revivals increased with the increase of the Kerr parameter while remaining sustained when the average number of photons is increased. Furthermore, no change in the VNE of the quantum systems was observed due to the variation in the $< n >$ for the system composed of relatively larger N. Furthermore, the atomic systems with larger N were found more entangled at lower χ as compared to the higher values. Moreover, the revival time of both GQD and von Neumann entropy increased with the increase of χ for rather a large N in the system.

Chapter 7

Multipartite quantum correlations and entanglement in two, three and four two-level moving atoms interacting with Fock field in presence of nonlinear Kerr medium

7.1 Introduction

This chapter is focused to study the dynamics of moving N TLS interacting with the single-mode Fock field and are in the influence of the Non-Linear Kerr Medium (NLKM). The dynamics of the GQD and VNE in the presence of the NLKM for two, three, and four TLS are investigated.

This chapter is organized as follows; In Sec. (7.2), we present the model and the Hamiltonian. We also study the dynamics of the moving two, three, and four TLS. In Sec. (7.3), we present the discussion on the results. In Sec. (7.4), the results are concluded.

7.2 The Model

We consider a similar approach as introduced in the simplest Tavis-Cummings (TC) model [130]. We consider N moving TLS in the single mode Fock field. The cavity is

filled with the NLKM. The total Hamiltonian of the system, $\hat{H}_T$ under the RWA can be written as, also given in Eq. (2.93)

$$\hat{H}_T = \frac{\omega_0}{2} \sum_{i=1}^{N} \hat{\sigma}_i^z + \omega \hat{a}^\dagger \hat{a} + f(vt) \sum_{i=1}^{N} \left(\hat{a} \hat{\sigma}_i^+ + \hat{a}^\dagger \hat{\sigma}_i^- \right) + \chi \left(\hat{a}^\dagger \hat{a} \right)^2, \tag{7.1}$$

where $f(vt)$ is associated with the atomic motion and is defined in Eq. (3.60), and its conditions are also defined in Eqs. (3.63) and (3.65). The χ represents the Kerr nonlinearity as given by Eq. (3.51). The interaction part of the Hamiltonian is given by

$$\hat{H}_I = f(vt) \sum_{i=1}^{N} \left(\hat{a} \hat{\sigma}_i^+ + \hat{a}^\dagger \hat{\sigma}_i^- \right) + \chi \left(\hat{a}^\dagger \hat{a} \right)^2 \tag{7.2}$$

We take the initial state,

$$\hat{\rho}_{AF}(0) = \left[(1-p) |\psi\rangle\langle\psi| + p|g_1 g_2.....g_N\rangle\langle g_1 g_2.....g_N| \right] \otimes |n\rangle\langle n|, \tag{7.3}$$

where $|n\rangle$ represents the Fock field and n is the photons number inside the cavity. The state vector $|\psi\rangle$ can be written as

$$|\psi\rangle = \cos(\theta) |g_1 g_2.....g_N\rangle + \sin(\theta) |e_1 e_2.....e_N\rangle, \tag{7.4}$$

where p is the statistical mixture parameter that makes the initial atomic state pure or mixed with limits as given below

$$0 \leq p \leq 1 \text{ and } 0 \leq \theta \leq \pi. \tag{7.5}$$

The set of allowable basis states $\{|\psi_i\rangle\}$ can be written as

$$\{|\psi_i\rangle\} = |g_1 g_2.....g_N, n+N\rangle, |e_1 g_2.....g_N, n+N-1\rangle, ..., |e_1 e_2.....e_N, n\rangle. \tag{7.6}$$

At later time t, the final state is

$$\hat{\rho}_{AF}(t) = \sum_{i,j}^{N} |\Psi_i\rangle\langle\Psi_i|\hat{\rho}(t)|\Psi_j\rangle\langle\Psi_j|, \tag{7.7}$$

and $\hat{\rho}(t)$ in terms of eigenvalues can be written as

$$\hat{\rho}_{AF}(t) = \sum_{i,j}^{N} \exp\left(-i\left(E_i - E_j\right)t\right) \times \langle\Psi_i|\hat{\rho}(0)|\Psi_j\rangle|\Psi_i\rangle\langle\Psi_j|, \tag{7.8}$$

where E_i, E_j and $|\Psi_i\rangle, |\Psi_j\rangle$ are the eigenvalues and eigenvectors of the density matrix. In order to calculate total correlations in multipartite system, we use Eq. (4.59), given by

$$\text{GQD}(\rho_T) = \min_{\{\Pi^k\}} \left\{ \sum_{j=1}^{N} \sum_{l=0}^{1} \tilde{\rho}_j^{ll} \log_2 \tilde{\rho}_j^{ll} - \sum_{k=0}^{2^N-1} \tilde{\rho}_T^{kk} \log_2 \tilde{\rho}_T^{kk} \right\} + \sum_{j=1}^{N} S(\rho_j) - S(\rho_T), \tag{7.9}$$

where $\hat{\rho}_T$ defines the density matrix of total system and the density matrix of the subsystem j is $\hat{\rho}_j$. All other definitions and expressions of this equation can be found in Sec. (4.10). And VNE is

$$S(\hat{\rho}) = -\text{Tr}(\hat{\rho} \log_2 \rho) = -\sum_i r_i \ln r_i, \tag{7.10}$$

where r_i represents the eigenvalues belongs to the density matrix $\hat{\rho}$, and also

$$S(\hat{\rho}_j) = -\text{Tr}[\hat{\rho}_j \log_2 \hat{\rho}_j], \ S(\hat{\rho}_T) = -\text{Tr}[\hat{\rho}_T \log_2 \hat{\rho}_T], \tag{7.11}$$

are the VNE of the subsystem j and the total system respectively.

7.3 Results and discussion

The dynamical evolution is studied of the GQD and VNE of moving N TLS (two, three, and four TLS). The system interacts with a single-mode Fock field in the cavity filled with the Non-Linear Kerr Medium. In Fig. (7.1) and Fig. (7.2), the dynamical behavior of the quantifiers for the two TLS (i.e. $N = 2$), with the presence of a NLKM and with $\eta = 0$, is presented. The other parameters in Fig. (7.1) are $p = 0$, the initial pure atomic state is prepared with $\theta = 0$ and $\theta = 3\pi/4$ as the ground state and a superposition state, respectively. The behavior of both quantifiers is analyzed for different Kerr factor values. For an initial ground atomic state, the dynamics of the GQD under the Kerr Medium exhibit periodic behavior. It is shown that the amplitude of the GQD is decreased if the value of χ is increased. It is seen that the period of oscillations is reduced and its amplitude is suppressed for $\chi = 3$ as compared to $\chi = 0.3$. The dynamical behavior of the VNE for the initial ground state $(\theta = 0)$ also shows periodic oscillations. For initial superposition state, the dynamics show the revivals in both quantifiers at $\chi = 1$. These revivals are more prominent at $\chi = 1$ which means the system shares the MPQC and entanglement between two TLS. For the initial superposition state, slow periodic variations are seen in the GQD at $\chi = 3$ and for $\chi = 0.3$, the system shows varying amplitude between the maximum and minimum MPQC among the TLS. Therefore, the amplitude of periodic oscillations of the GQD is decreased for $\chi = 0.3$ to $\chi = 3$ in the two TLS. This dynamical behavior is also observed in the case of the VNE. However, the frequency of these oscillations shows different behavior in the system dynamics i.e. the frequency of oscillations increases by increasing χ. In Fig. (7.2), the behavior of the

GQD and VNE is plotted for the two different initial mixed states. Periodic oscillatory behavior is seen. The oscillations are comparatively suppressed for the GQD in the case of a mixed state.

Figure 7.1: (color online) The dynamics of the GQD and VNE for a two (N=2) TLS for $p = 0$, $n = 10$ and $\eta = 0$. The insets show the magnified view of the quantifiers for $\chi = 3$

Figure 7.2: (color online) The dynamics of the GQD and VNE for a two (N=2) TLS for $p = 0.5$, $n = 10$ and $\eta = 0$. The insets show the magnified view of the quantifiers for $\chi = 3$

Fig. (7.3) and Fig. (7.4) show the behavior of the GQD and VNE, for different Kerr parameter values for the three TLS (i.e. $N = 3$) for different initial pure and mixed

atomic states, respectively. We consider no atomic motion. The dynamics of the GQD and VNE have constant and periodic varying amplitude for $\chi = 0.3$ and $\theta = 0$. Both the GQD and VNE show constant oscillations at $\chi = 1$. If we further increase the value of the Non-Linear Kerr coefficient i.e. $\chi = 3$, rapid oscillations are observed in the dynamics of both quantifiers. For $\theta = 3\pi/4$, the three TLS has revivals in the GQD and VNE for the whole range of χ. The oscillations in these quantifiers reflect the sharing of quantum correlations among the atomic systems throughout the dynamics. Non-zero value of the VNE for this initial superposition of pure atomic states suggests that the atomic systems have non-vanishing quantum interference in the system due to the availability of photons and the accessible microstates of atomic states all the time. The dynamics are also computed with two different initial mixed states and both the quantifiers have shown periodic oscillations. The dynamics of VNE show non-vanishing quantum interference in the atomic system for both mixed states. The dynamical behavior of the GQD and VNE for $N = 4$ is shown in Fig. (7.5) and Fig. (7.6). No atomic motion is considered. From Fig. (7.5), the rapid oscillations can be observed in the GQD and VNE as χ is increased. However, the dynamics of the GQD and VNE are suppressed for higher values of χ. Furthermore, the dynamical behavior of both the quantifier is found highly prone to the NLKM.
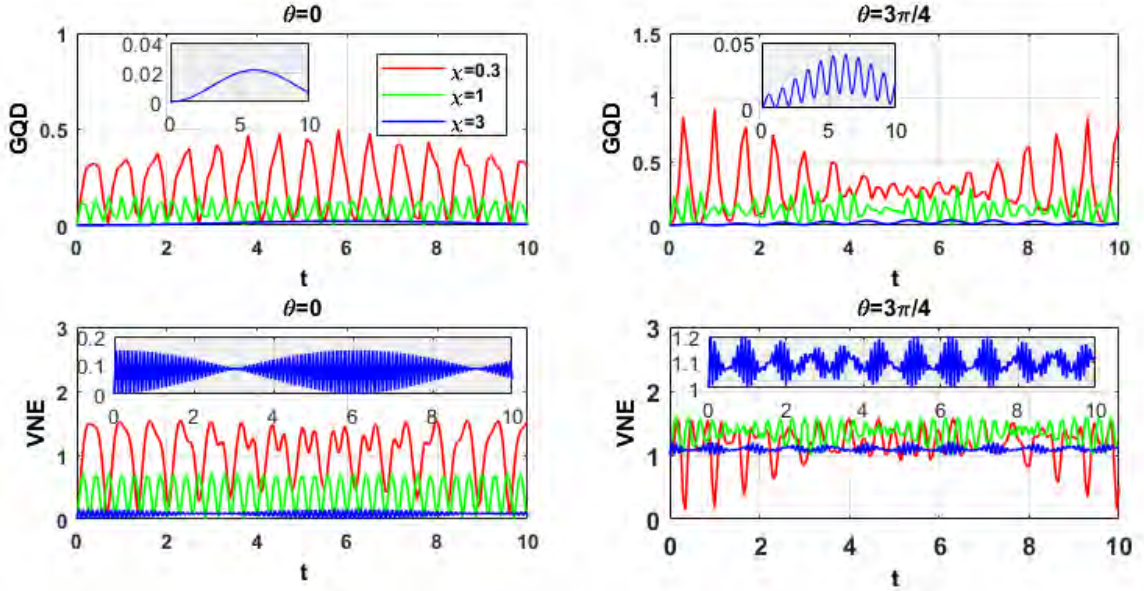

Figure 7.3: (color online) The dynamics of the GQD and VNE for a three (N=3) TLS for $p = 0$, $n = 10$ and $\eta = 0$. The insets show the magnified view of the quantifiers for $\chi = 3$
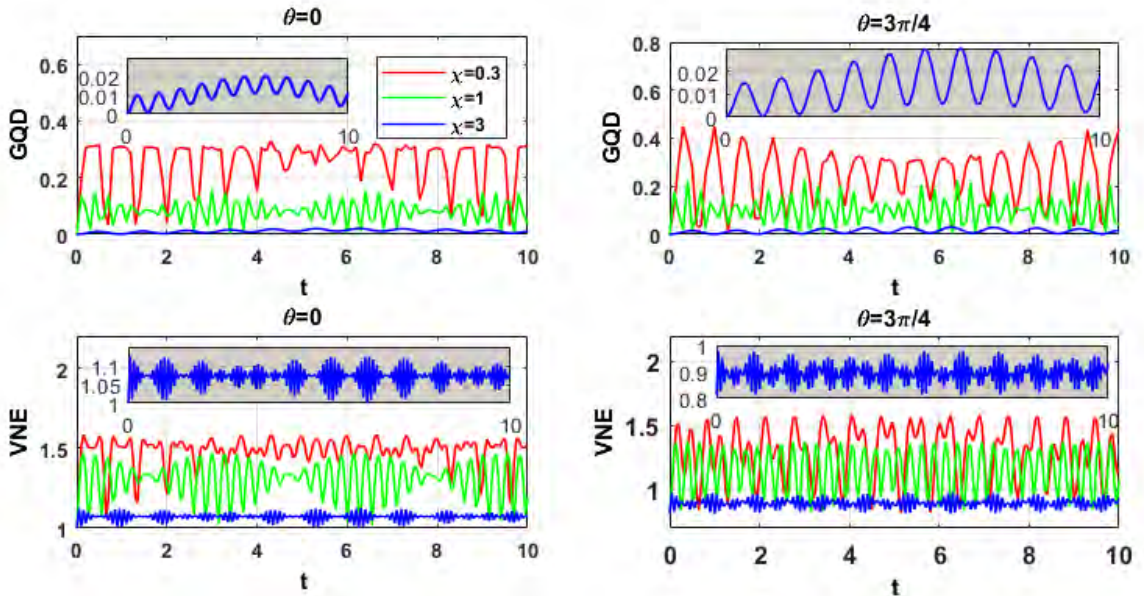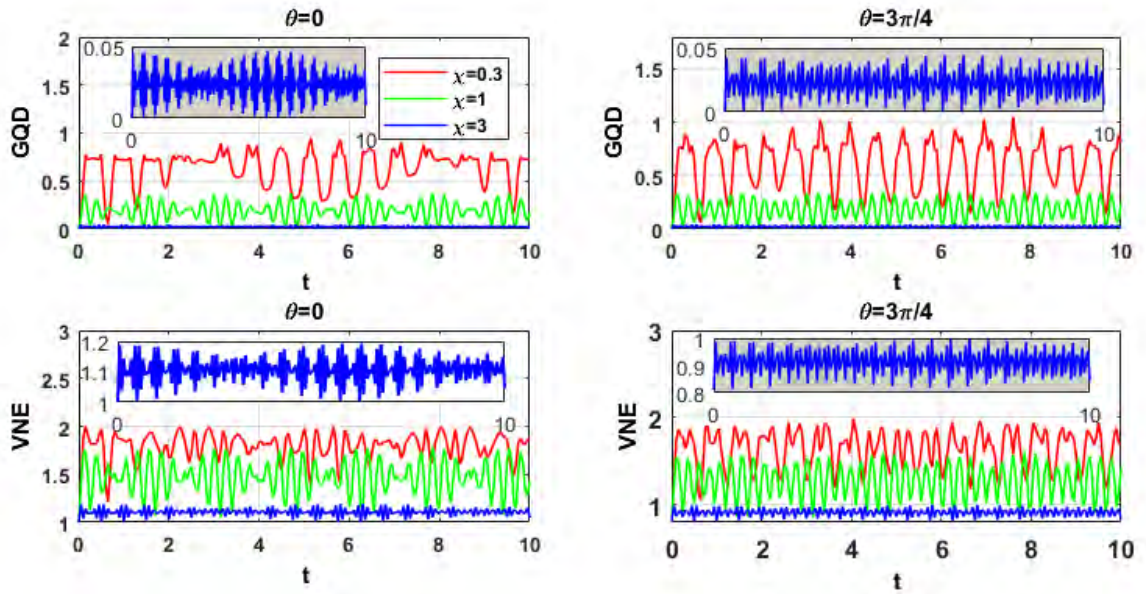
Figure 7.4: (color online) The dynamics of the GQD and VNE for a three (N=3) TLS for $p = 0.5$, $n = 10$ and $\eta = 0$. The insets show the magnified view of the quantifiers for $\chi = 3$

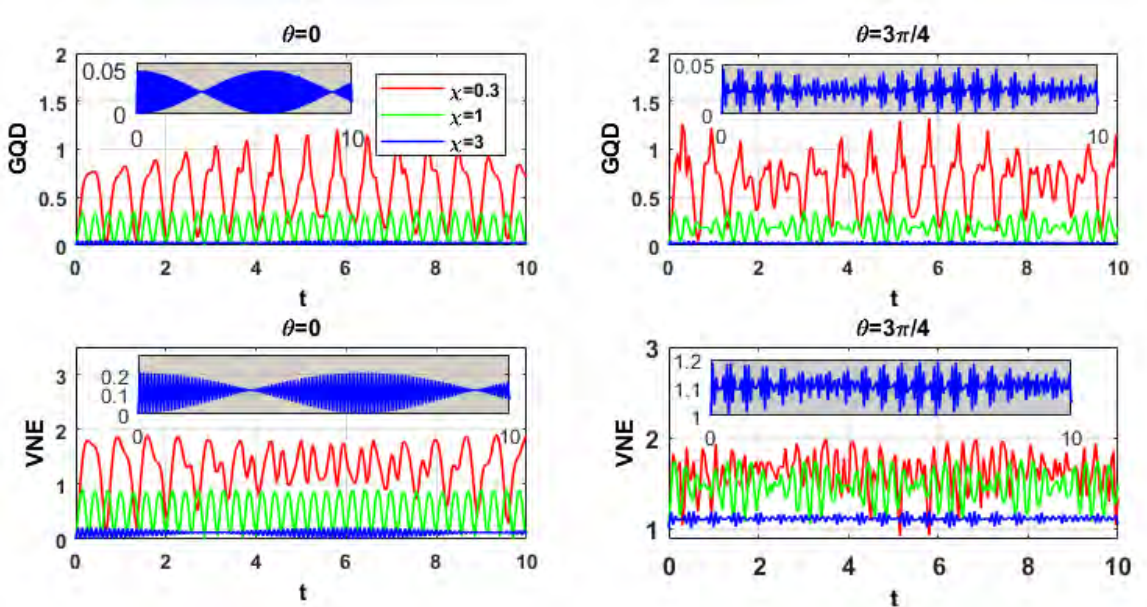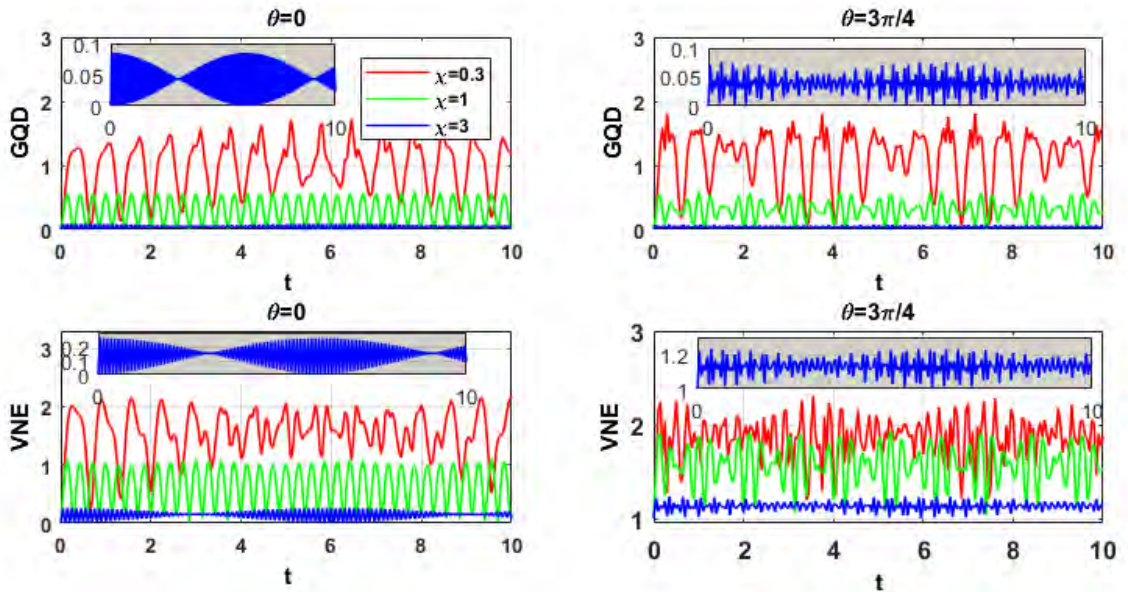
Figure 7.5: (color online) The dynamics of the GQD and VNE for a four (N=4) TLS for $p = 0$, $n = 10$ and $\eta = 0$. The insets show the magnified view of the quantifiers for $\chi = 3$
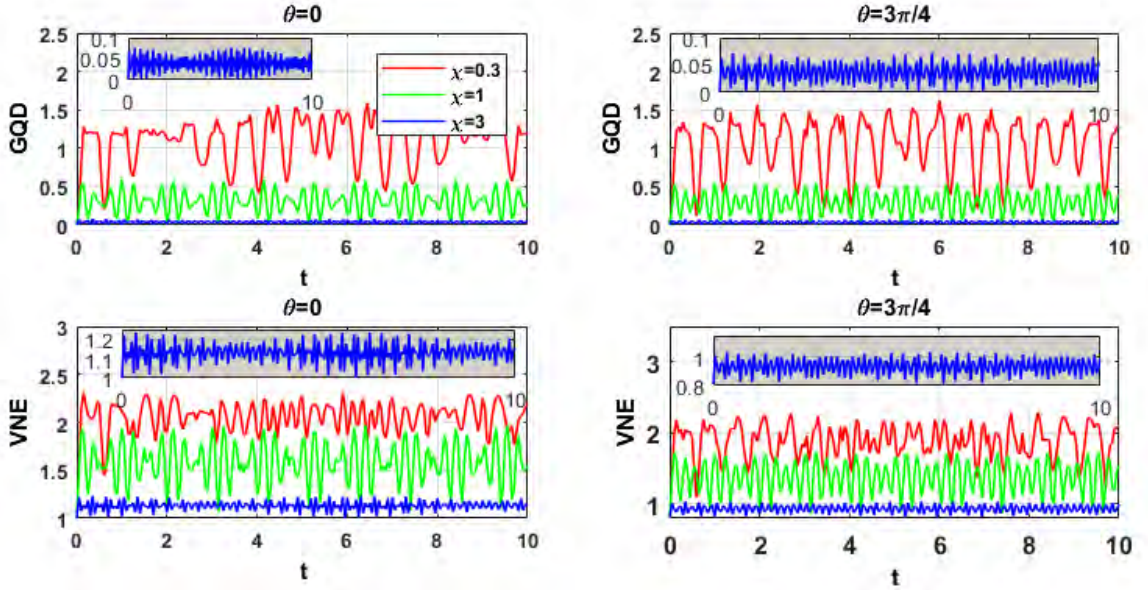
Figure 7.6: (color online) The dynamics of the GQD and VNE for a four (N=4) TLS for $p = 0.5$, $n = 10$ and $\eta = 0$. The insets show the magnified view of the quantifiers for $\chi = 3$

In Fig. (7.7), the effects of the Kerr parameter with zero photons case, and without the atomic motion, are studied in the dynamics of the GQD and VNE in the system for an initially mixed state and the results are plotted by taking $\theta = 3\pi/4$. When no photons are available in the system, the two, three, and four TLS have periodic behavior in both the quantifiers. Unlike the non-zero photon case, the GQD shows no rapid oscillations for all the range of Kerr parameter χ. Furthermore, without the presence of the photons in the system, the magnitude of the GQD and VNE in the dynamics is not suppressed in the same fashion as with the case of the non-zero photon (see Figs. (7.1)-(7.6)). The dynamics of the GQD suggest that for $N = 2$, the Kerr Medium does not have a prominent effect on the magnitude and behavior of the GQD. For $N = 3$ and $N = 4$, the Kerr parameter χ affects the dynamics of the GQD, and a prominent difference in the magnitude and behavior is observed for different χ values. For the zero photon case, the VNE dynamics show that the higher χ value decreases the VNE in the system. More periodic behavior in the VNE is observed for $\chi = 3$.
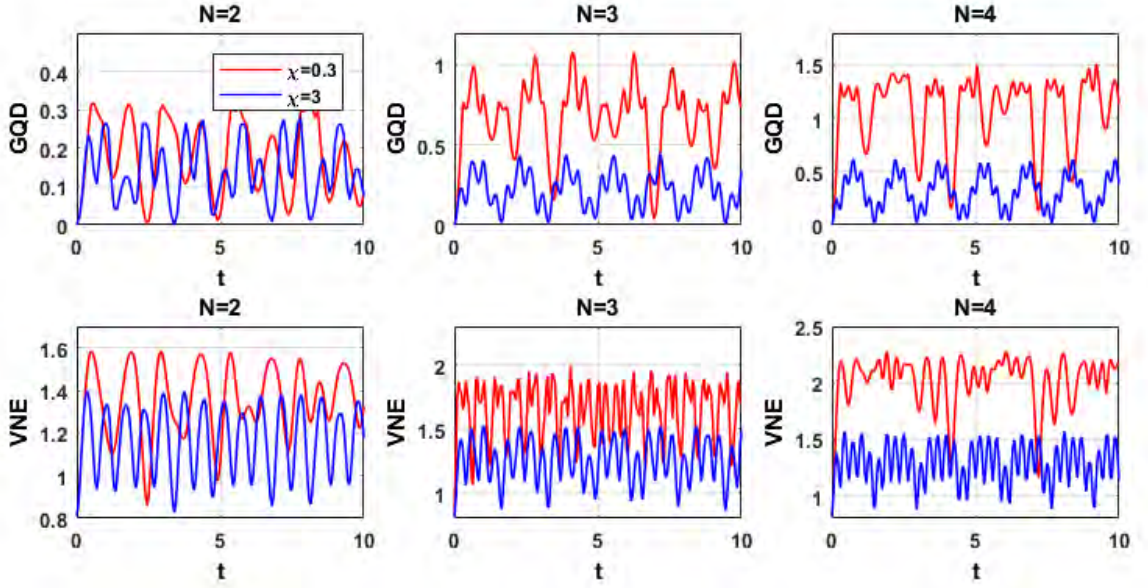
Figure 7.7: (color online) The dynamics of the quantifiers for a two, three and four TLS for $p = 0.5$, $\theta = 3\pi/4$, $n = 0$ and $\eta = 0$.

In Figs. (7.8) and (7.9) we have plotted the dynamics of the quantifiers for moving two, three, and four TLS in the presence of NLKM for an initial state corresponding to $p=0.5$. In Fig. (7.8), we take $\chi = 0.3$, $\theta = 0$, and $3\pi/4$, $\eta = 1$ and $n = 10$,. The dynamics of both GQD and VNE show periodic oscillations. In Fig. (7.9), Kerr parameter is taken as $\chi = 3$. For $\chi = 3$, a rapid oscillatory behavior of the GQD and VNE is observed. In the case of moving atoms, and for $\theta = 0$ and $\theta = 3\pi/4$, the behavior of the VNE shows the non-zero value for all the Kerr parameter values due to accessible states in the system. It is investigated that in the case of the moving atomic systems, increasing the Kerr parameter χ reduces the magnitude of the GQD and VNE causes rapid oscillations in these quantifiers. For $\chi = 3$, the GQD (see Fig. (7.9), three and four TLS have more rapid oscillations than two TLS, and this increase in oscillations is not observed for the case of $\chi = 0.3$ (Fig. (7.8)). We can conclude that the systems with more than two moving TLS are more prone to the Kerr parameter value χ. Therefore, the motion of atoms is favorable to sustain the QE in the atomic systems in the NLKM.
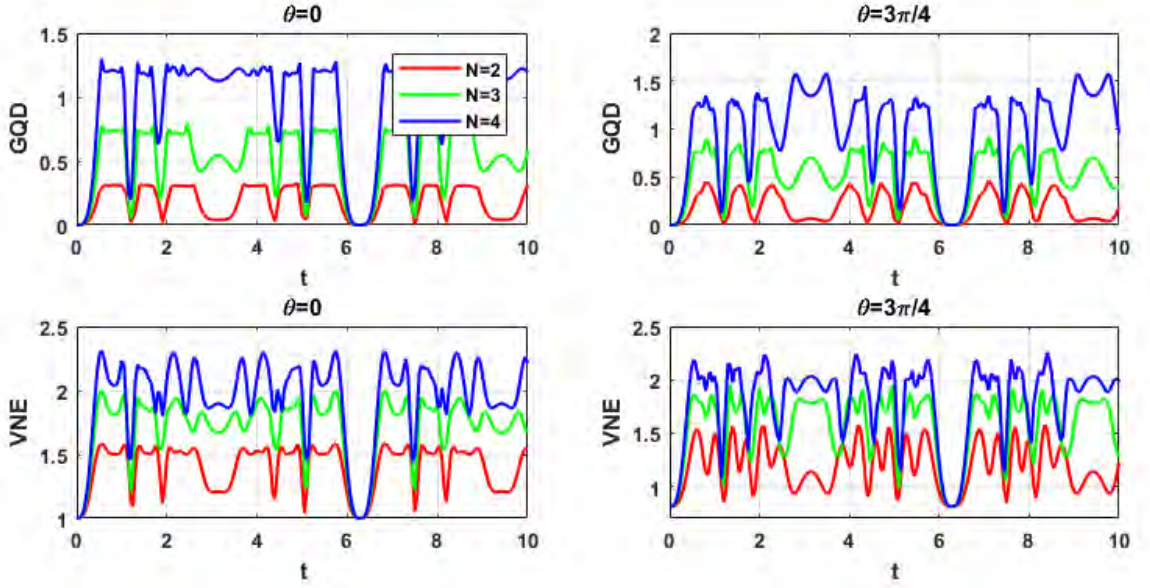
Figure 7.8: (color online) The dynamical behavior of the GQD and VNE of a moving two, three and four TLS for $\chi = 0.3$, $p = 0.5$, $n = 10$ and $\eta = 1$ at $\theta = 0$ and $\theta = 3\pi/4$.
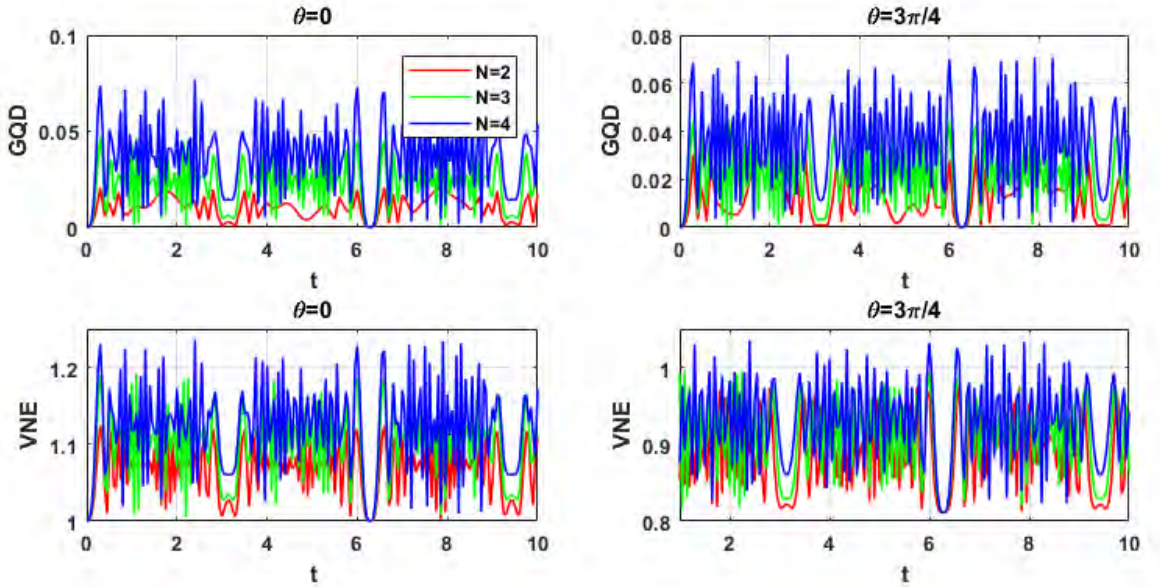
Figure 7.9: (color online) The dynamical behavior of the GQD and VNE of a moving two, three and four TLS for $\chi = 3$, $p = 0.5$, $n = 10$ and $\eta = 1$ at $\theta = 0$ and $\theta = 3\pi/4$.

7.4 Conclusions

We study the dynamics of the GQD and VNE for N TLS (two, three, and four TLS). The system is present in the Kerr medium and interacts with the single-mode Fock field. We observe that for higher Kerr parameter values, the GQD and VNE show periodic

behavior which leads to the collapses and revivals in the QE. The mixed states have comparatively suppressed oscillations of the GQD and the VNE has non-zero values of quantum interference throughout the dynamics for the mixed states which lead to the sustained response to the QE during the dynamics. The dynamical character of both quantifiers is found highly affected by the Kerr Medium. Moreover, the number of photons in the cavity affects the quantifiers for the entire range of Kerr values and photons are responsible for the rapid oscillations in the quantifiers. Furthermore, for moving TLS, the periodic behavior of the GQD and VNE is almost the same for initial pure and mixed atomic states. Hence the atomic motion is favorable to sustaining the QE in the systems in a Non-Linear Kerr Medium.

Chapter 8

Influence of the Stark shift on multipartite quantum correlations and entanglement of two, three and four two-level atomic systems

8.1   Introduction

The main focus of this chapter is to investigate the GQD and VNE dynamics of moving many TLS in the presence of Stark shift. We assume that the system is interacting with the Fock field and coherent field.

The structure of this chapter is as follows: in Sec. (8.2), we describe the model Hamiltonian. Furthermore, we review the GQD and VNE and the dynamics of the system. The findings and discussions are reported in Sec. (8.3). In Sec. (8.4), we conclude our results.

8.2   Hamiltonian model

The Tavis-Cummings model describing two identical TLS, A and B, coupled with the single-mode field C, given by Eq. (2.93). The total Hamiltonian of the system composed of N TLS $\hat{H}_T$ under the RWA can be written as

$$\hat{H}_T = \frac{\omega_0}{2} \sum_{i=1}^{N} \hat{\sigma}_i^z + \omega \hat{a}^\dagger \hat{a} + f(vt) \sum_{i=1}^{N} \left(\hat{a}\hat{\sigma}_i^+ + \hat{a}^\dagger \hat{\sigma}_i^- \right) + \sum_{i=1}^{N} \beta \hat{a}^\dagger \hat{a} |g_i\rangle \langle g_i|, \qquad (8.1)$$

The function $f(vt)$ is the cavity shape function for moving atomic system as we have described in Eq. (3.60). The conditions of moving and static atom cases are given in Eqs. (3.63) and (3.65). The parameter β is the Stark parameter as given in Eq. (3.56). Assuming that the atoms resonantly interact with the field, the interaction Hamiltonian of the system is

$$\hat{H}_I = f(vt) \sum_{i=1}^{N} \left(\hat{a}\hat{\sigma}_i^+ + \hat{a}^\dagger \hat{\sigma}_i^- \right) + \sum_{i=1}^{N} \beta \hat{a}^\dagger \hat{a} |g_i\rangle\langle g_i| \tag{8.2}$$

We consider the total system prepared in the direct product of a mixed state of N atoms with the field. The initial state of the atomic system and the field can be written as

$$\hat{\rho}(0) = [(1-p)\,|\psi\rangle\langle\psi| + \ p|g_1 g_2.....g_N\rangle\langle g_1 g_2.....g_N|] \otimes \hat{\rho}_E, \tag{8.3}$$

The ket vector is written as $|\psi\rangle = \cos(\theta)\,|g_1 g_2.....g_N\rangle + \sin(\theta)\,|e_1 e_2.....e_N\rangle$ where $0 \leq \theta \leq \pi$. p is the statistical mixture parameter with $0 \leq p \leq 1$, and $\hat{\rho}_E$ is the coherent field and it can be written as

$$\hat{\rho}_E = \sum_n p_n |n\rangle\langle n| \tag{8.4}$$

where the weight function p_n is

$$p_n = 1 \tag{8.5}$$

for the Fock field and

$$p_n = \frac{|\alpha|^{2n}\, e^{-|\alpha|^{2n}}}{n!}$$

for the Coherent field and

$$\langle n \rangle = |\alpha|^2 \tag{8.6}$$

where n represents the number of photons inside the cavity.

The set of allowable basis states $\{|\psi_i\rangle\}$ are

$$\{|\psi_i\rangle\} = |g_1 g_2.....g_N, n+N\rangle, |e_1 g_2.....g_N, n+N-1\rangle, ..., |e_1 e_2.....e_N, n\rangle. \tag{8.7}$$

where $|e_i\rangle$ is the excited state of the ith atom. At later time t, the final state is

$$\hat{\rho}_{AF}(t) = \sum_{i,j}^{N} |\psi_i\rangle\langle\psi_i|\hat{\rho}(t)|\psi_j\rangle\langle\psi_j|, \tag{8.8}$$

and $\hat{\rho}(t)$ in terms of eigenvalues of the initial states can be written as

$$\hat{\rho}_{AF}(t) = \sum_{i,j}^{N} \exp\left(-i\left(E_i - E_j\right)t\right) \times \langle\psi_i|\hat{\rho}(0)|\psi_j\rangle |\psi_i\rangle\langle\psi_j|, \tag{8.9}$$

91

where E_i, E_j and $|\psi_i\rangle, |\psi_j\rangle$ are the eigenvalues and eigenvectors of the density matrix $\hat{\rho}(0)$. The final state of the atomic system is obtained after taking the trace over the field i.e. $\hat{\rho}_T(t) = Tr_F[\hat{\rho}_{AF}(t)]$. To calculate the MPQC in our multipartite system we can use Eq. (4.59) of the GQD [22] given below

$$\text{GQD}(\rho_T) = \min_{\{\Pi^k\}} \left\{ \sum_{j=1}^{N} \sum_{l=0}^{1} \tilde{\rho}_j^{ll} \log_2 \tilde{\rho}_j^{ll} - \sum_{k=0}^{2^N-1} \tilde{\rho}_T^{kk} \log_2 \tilde{\rho}_T^{kk} \right\} + \sum_{j=1}^{N} S(\hat{\rho}_j) - S(\hat{\rho}_T), \quad (8.10)$$

Furthermore,where $\hat{\rho}_T$ defines the density matrix of total system and the density matrix of the subsystem j is $\hat{\rho}_j$. All other definitions and expressions of Eq. (8.10) can be found in Sec. (4.10). We define VNE as [132]

$$S(\hat{\rho}) = -\text{Tr}(\hat{\rho} \log_2 \hat{\rho}) = -\sum_i r_i \ln r_i, \quad (8.11)$$

where r_i are the eigenvalues ρ_T.

8.3   Results and discussions

Fig. (8.1) shows the effects of two different fields on the GQD and VNE for a two TLS (N=2) without the atomic motion with different values of the Stark shift parameters. A comparison is presented between the Fock field and coherent field with the same number and an average number of photons. We have considered the initial mixed atomic state with $p = 0.5$ and $\theta = 3\pi/4$. In the case of the Fock field, the Stark shift parameter has shown prominent and significant effects on the GQD and VNE. It is observed that by increasing the Stark shift parameter β, both GQD and VNE decrease with time evolution. Furthermore, the rapid oscillations of the GQD and VNE increase, and the time period of oscillations decrease with the increasing value of β. In the case of the coherent field, we have observed the collapses and revivals of GQD and VNE. The number of revivals increases by increasing the value of β, and on the other hand, the amplitude of revival and magnitude of the GQD and VNE decrease with β. When we compare both fields, it is observed that fields have different effects on GQD and VNE. For the Fock field, we observe that the maximum values of the magnitude of the GQD have decreased by an order of magnitude for $\beta = 3$ as compared to $\beta = 0.3$ with time evolution. The same is the case in the coherent field, the decrease of GQD is of the same order of magnitude. There is a sharp decrease in the maximum value of the GQD, however, the dynamics of

the VNE remain unchanged with the change of β. It is found that for the Fock field, the maximum value of VNE decreases by a factor of 2 for $\beta = 3$ as compared to $\beta = 0.3$, and for the coherent field, there is a slight decrease of VNE. This change in the magnitude of the GQD and VNE in the presence of the Stark shift suggests that the MPQC decrease with the increase of β for both Fock field and coherent field. The system loses quantum correlations more rapidly in the presence of the coherent field as compared to the Fock field with an increasing value of β. On the other hand, the QE remains almost the same value in the coherent field when β is increased and drops by a factor of 2 for the case of the Fock field. Hence, it is seen that due to the Stark effect, the GQD is decreased more for the coherent field as compared to the Fock field, and the increase of the Stark shift parameter β suppresses the GQD more in the presence of the coherent field as compared to the Fock field, and we observed that the Fock field sustains the MPQC in the system. The maximum value of the QE is decreased more rapidly for the Fock field with an increase of β as compared to the coherent field.

In Figs. (8.2) and (8.3), the effect of β on the dynamical behavior of the GQD and VNE is presented for the Fock field and coherent field for three (N=3) and four (N=4) TLS, respectively. We have taken the initial mixed atomic state with $p = 0.5$ and $\theta = 3\pi/4$. We observe that the values of the quantifiers are increased as the system gets more TLS. Furthermore, in the case of the Fock field, we have seen rapid oscillations for all the values of β. The period of these rapid oscillations is also decreased for the large N atomic system and the higher values of β. In the case of a coherent field, the GQD and VNE increase for large N systems. However, in the case of the coherent field, the number of revivals for N=3 and N=4 remain the same as for N=2. When we increase the value of β from 0.3 to 3 under the influence of the Fock field for $N = 3$, we observed an order of magnitude decrease in the value of GQD and the same is true for the coherent field. On the other hand, for the Fock field, the magnitude of VNE is decreased by half and for the coherent field, there is a slight decrease. When $N = 4$ and for the Fock field or coherent field, the decrease in the maximum values of GQD at $\beta = 0.3$ to $\beta = 3$ is n order of magnitude. The dynamics of VNE for $N = 4$ show that the maximum values of VNE decrease by half for the case of the Fock field and no change for coherent field with the increase in β from 0.3 to 3. For our system composed of N TLS, we have seen that for the higher N systems, the GQD, and VNE are increased in the presence of the

Stark shifted medium. Nonclassical fields have different trends in the quantifiers on the increase of the GQD and VNE. In the case of the Fock field, the increase of GQD and VNE is not linear, and the higher N systems have a non-linear increase of the GQD and VNE for different β values. Moreover, the values of GQD and VNE decrease with the increase of β for the system. For the coherent field, with the increase in N, the GQD increases non-linearly for the different β values. For the coherent field, the VNE increases linearly with the increase in N for $\beta = 0.3$ and remains the same with the increase in N for $\beta = 3$. It is important to mention that varying the β affects the correlations of the N TLS. The higher N systems are more prone to the increasing β and the magnitude of the GQD is more suppressed as compared to the case of $N = 2$. In comparison, the system has increased GQD for the Fock field as compared to the coherent field and the GQD is slightly more suppressed with the increase of β for the coherent field as compared to the Fock field. The dynamics of the VNE show that QE decreases with the increase of β and QE and non-classical correlations are affected in a different way for the Fock field and coherent field. The GQD increases with the N for both the Fock field and coherent field while the VNE increases only for the Fock field. In the case of the coherent field, larger β do not favor the system to enhance the QE with the N.

Fig. (8.4) shows the behavior of the quantifiers for a two TLS (N=2) with $\eta = 1$. The dynamical behavior is studied with the different β values. In this case of a two TLS (N=2), we have taken $n = 49$ for the Fock field and $|\alpha|^2 = 49$ for the coherent field. The dynamical behavior is studied with the initial mixed atomic state for $p = 0.5$, $\theta = 3\pi/4$ and taken $\eta = 1$. In the case of the Fock field, we observe periodic oscillations for the GQD and VNE for all the values of β. The period of oscillations remains the same for all the values of β but the oscillations get more rapid as β is increased. The magnitude of the oscillation decreases with the increase of β. For the coherent field, the magnitude of the GQD and VNE decrease with β. Furthermore, the collapses and revivals are observed for each value of the β. The magnitude of the revivals decreases with the increase of β but the number of main revivals per unit scaled time remains the same for the whole range of β. For $\beta = 1$, the collapses are more sustained as compared to $\beta = 0.3$ and $\beta = 3$. For $\beta = 3$, we observe further revivals along with the main revivals. These revivals occur in the middle of the main revivals and have a smaller amplitude as compared to the main revivals that correspond to $\beta = 3$. These results suggest that the QE is sustained and

maintained for the system with the atomic motion, for both the Fock field and coherent field in the Stark shift.

Figs. (8.5) and (8.6) shows the behavior of the quantifiers for three (N=3) and four (N=4) TLS for the Fock field and coherent field with $\eta = 1$. For the case of the moving atomic system, it is observed that both GQD and VNE show periodic oscillations for the Fock field. In the case of the coherent field, both GQD and VNE show collapses and revivals for all the values of the β. For N=3 and N=4, we observe the magnitude of the quantifiers is suppressed by the increase of β and the rapid oscillations increase with its increase. For the case of moving atoms, the number of periodic oscillations and revivals for the GQD and VNE, per unit scaled time, remain the same for both Fock field and coherent field. The magnitude of the GQD and VNE increase with the increase in the dimension of the system for the Fock field, while for the coherent field this increase is only prominent for $\beta = 0.3$ and $\beta = 1$. It is observed that for the large N atomic systems, the atomic motion does not affect the period of oscillations as the number of atoms N is increased. In the case of the Fock field, the period of oscillation remains the same with the increase of the β. Furthermore, for the Fock field, with the increase of β, rapid oscillations of the system increase, and it remain the same for the different number of the atoms N. For the coherent field, the atomic motion affects the system to have revivals that occur at the same scaled time for all the values of β. The increase in the system size N increases the GQD and VNE in the system. With the atomic motion, the coherent field has decreased GQD and VNE as compared to the Fock field. In comparison for both cases of with and without atomic motion, the nonclassical fields and Stark shift parameter β have some interesting effects on the dynamical behavior of the GQD and VNE of the system. For the case of the Fock field, atomic motion does not affect the magnitude of the GQD with β values and different N. In this case, the atomic motion changes the shape of the oscillations of the GQD and VNE and changes the period of these oscillations as compared to no atomic motion. This change in the period of oscillations is different for the different values of β. In the case of the coherent field, the atomic motion does not change the magnitude of the GQD with β. It is seen that the number of revivals per unit scaled time of the GQD and VNE change as compared to the case without the atomic motion and this change is different for the different values of β. In the case of $\beta = 0.3$, the number of revivals per unit scaled time increases as compared to the case when there is no atomic motion

present. For the case of $\beta = 1$, the number of revivals per unit scaled time remains the same and decreases for the case of $\beta = 3$. Therefore, the oscillations of the GQD and VNE show the sustained behavior of the QE with atomic motion in the presence of the Stark effect.

Figure 8.1: (color online) The dynamics of the GQD and VNE of a two TLS ($N = 2$) are plotted with different β values for two different field states with $n = 49$ and $|\alpha|^2 = 49$. All data is for $p = 0.5$, $\theta = 3\pi/4$, $\eta = 0$. The insets show the magnified view of the quantifiers for $\beta = 3$.

Figure 8.2: (color online) The dynamics of the GQD and VNE of a three TLS ($N = 3$) are plotted with different β values for two different field states with $n = 49$ and $|\alpha|^2 = 49$. All data is for $p = 0.5$, $\theta = 3\pi/4$, $\eta = 0$. The insets show the magnified view of the quantifiers for $\beta = 3$.

Figure 8.3: (color online) The dynamics of the GQD and VNE of a four TLS ($N = 4$) are plotted with different β values for two different field states with $n = 49$ and $|\alpha|^2 = 49$. All data is for $p = 0.5$, $\theta = 3\pi/4$, $\eta = 0$. The insets show the magnified view of the quantifiers for $\beta = 3$.
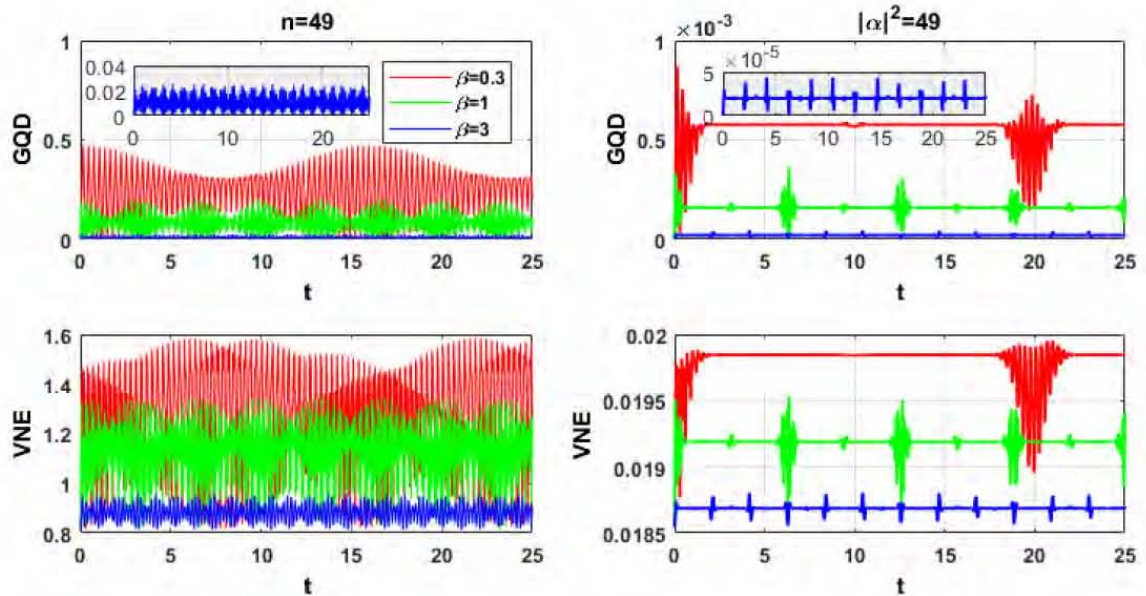
Figure 8.4: (color online) The dynamics of the GQD and VNE of a two TLS ($N = 2$) are plotted with different β values for two different field states with $n = 49$ and $|\alpha|^2 = 49$. All data is for $p = 0.5$, $\theta = 3\pi/4$, $\eta = 1$. The insets show the magnified view of the quantifiers for $\beta = 3$.

Figure 8.5: (color online) The dynamics of the GQD and VNE of a three TLS ($N = 3$) are plotted with different β values for two different field states with $n = 49$ and $|\alpha|^2 = 49$. All data is for $p = 0.5$, $\theta = 3\pi/4$, $\eta = 1$. The insets show the magnified view of the quantifiers for $\beta = 3$.
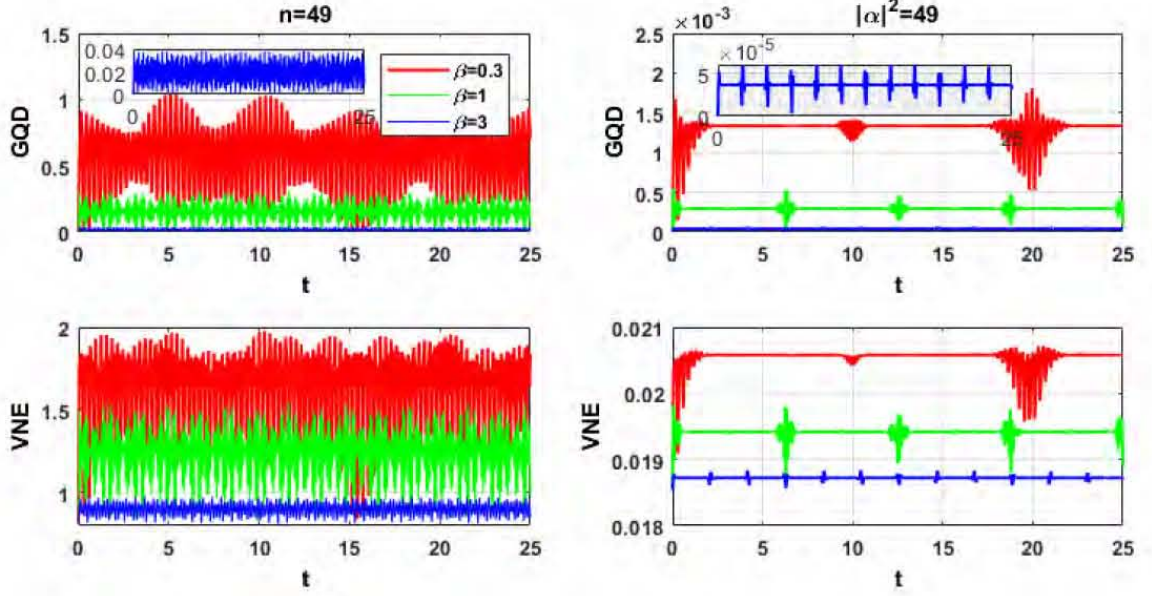
Figure 8.6: (color online) The dynamics of the GQD and VNE of a four TLS ($N = 4$) are plotted with different β values for two different field states with $n = 49$ and $|\alpha|^2 = 49$. All data is for $p = 0.5$, $\theta = 3\pi/4$, $\eta = 1$. The insets show the magnified view of the quantifiers for $\beta = 3$.
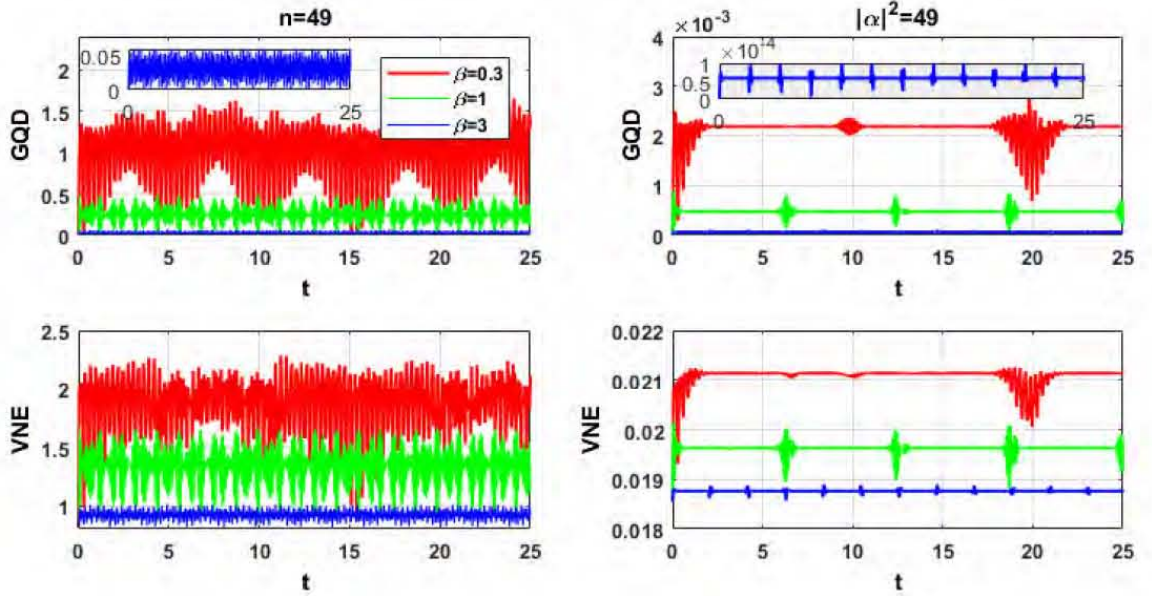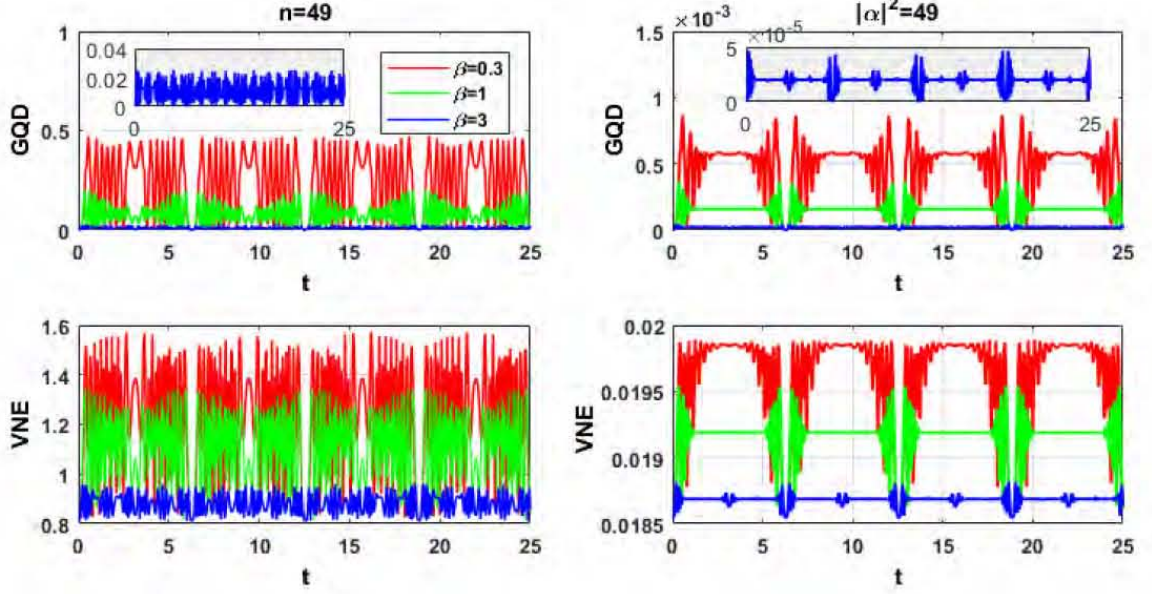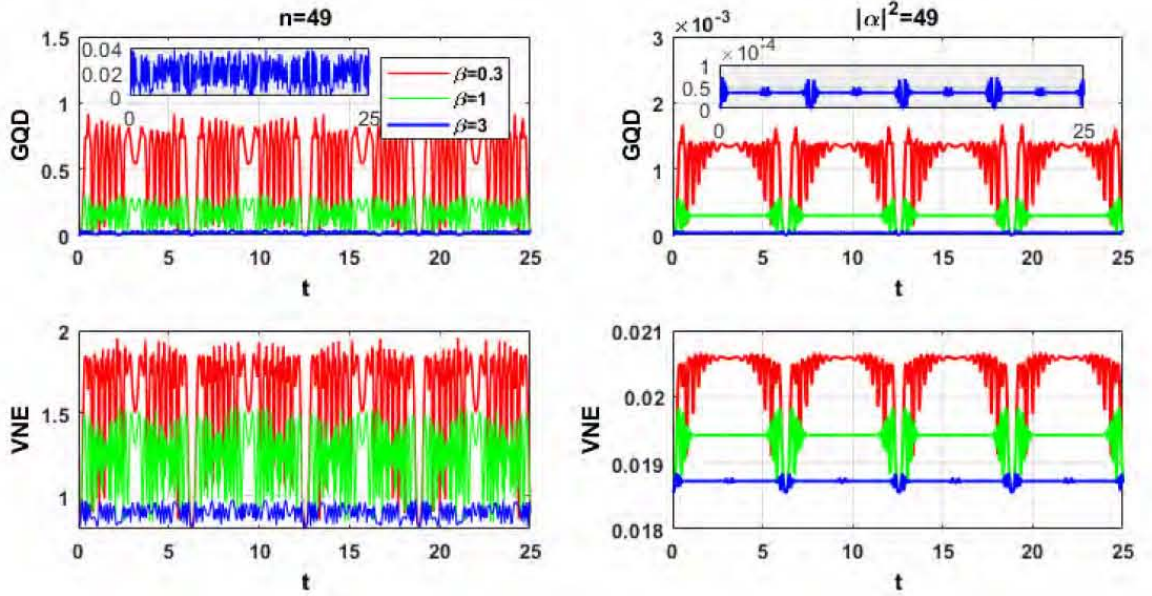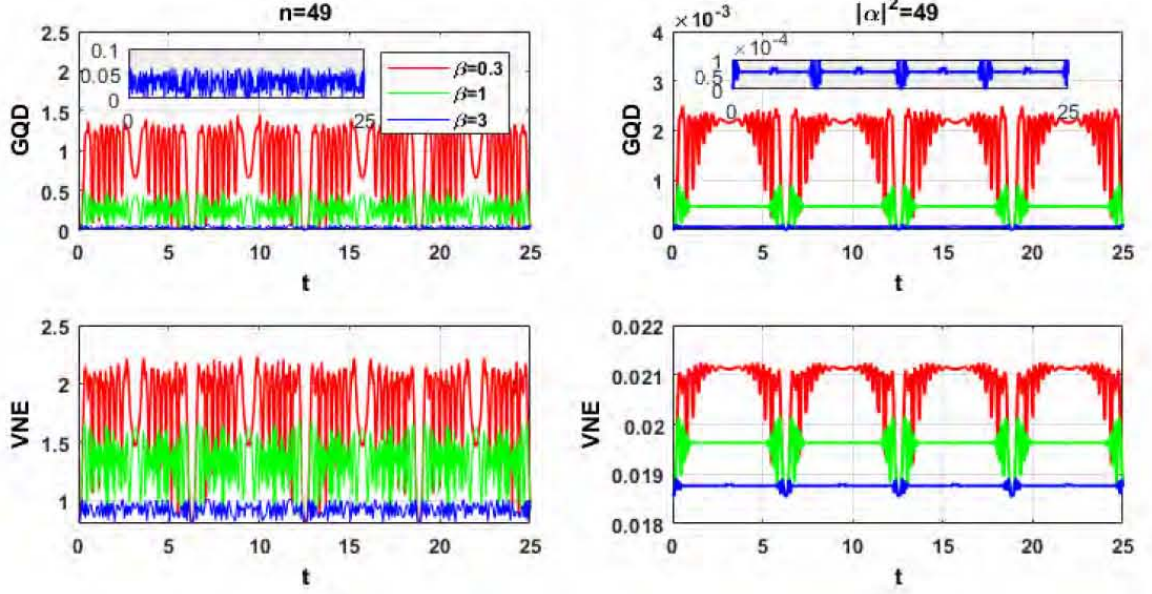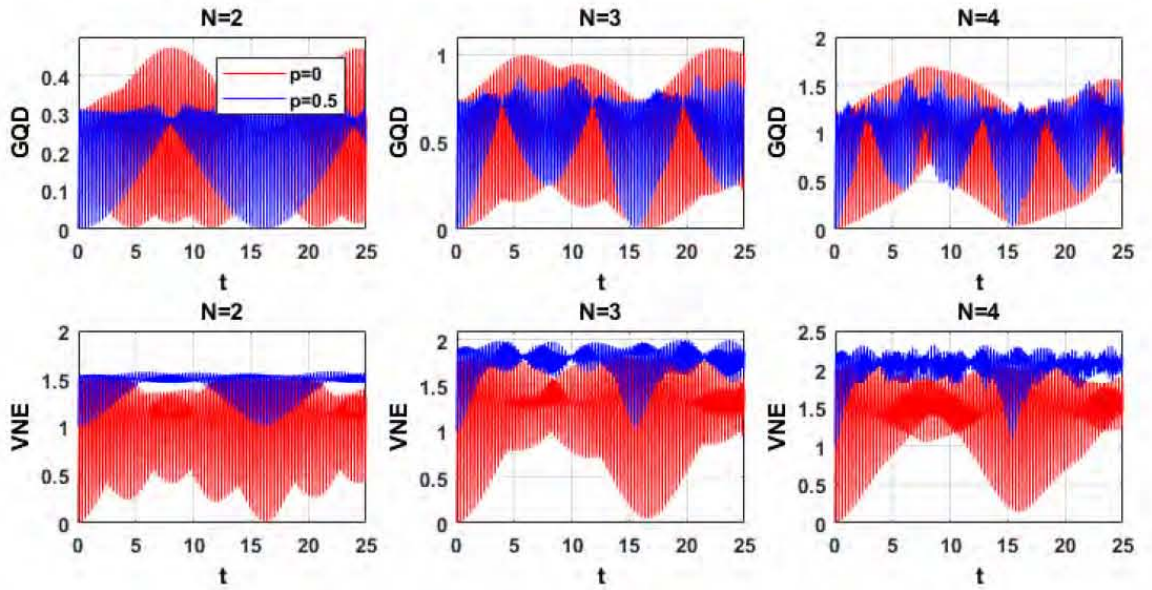

Figure 8.7: (color online) The dynamics of the GQD and VNE of the system composed of N TLS are plotted for the initial pure and mixed atomic state for the Fock field with $n = 49$, $\beta = 0.3$, $\theta = 0$, $\eta = 0$.
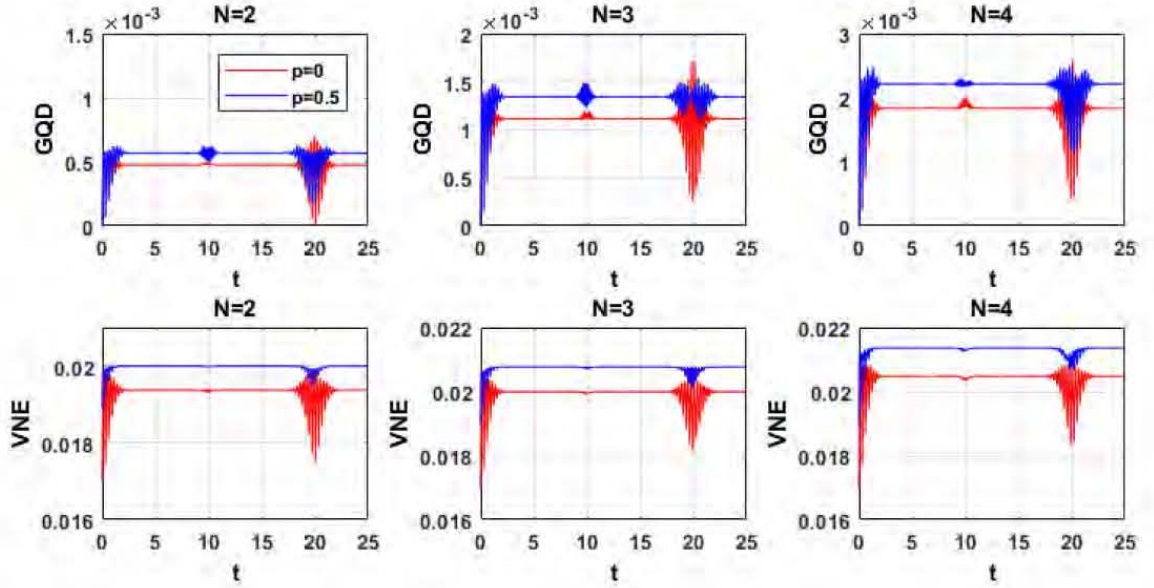
Figure 8.8: (color online) The dynamics of the GQD and VNE of the system composed of N TLS are plotted for the initial pure and mixed atomic state for the coherent field with $|\alpha|^2 = 49$, $\beta = 0.3$, $\theta = 0$, $\eta = 0$.

The effects of the initial atomic state on the dynamics of the GQD and VNE for the Fock field and coherent field is shown in Figs. (8.7) and (8.8). The dynamics of GQD and VNE are studied with the two different initial atomic states corresponding to pure ($p = 0$) and mixed ($p = 0.5$) and with $\theta = 0$. The Stark shift parameter is fixed at $\beta = 0.3$ for both the Fock and Coherent field. In the case of the Fock field, as shown in Fig. (7), it is seen that the pure state has slightly increased GQD as compared to the mixed state. But for the higher N systems, this difference is reduced and both initial pure and mixed states have almost equal GQD. Furthermore, for N=2, the GQD has an almost equal number of periodic oscillations with the time evolution. For the higher N values, it is observed that the mixed state shows more periodic oscillations as compared to the pure state. On the other hand, the initially mixed state shows slightly more VNE as compared to the pure state for all values of N (number of atoms). The initially mixed state has a non-zero VNE value showing that the system has sustained the QE. Fig. (8) represents the effect of initial atomic states on the GQD and VNE for the system in the case of the coherent field. For initial mixed and pure states, collapses and revivals are observed for QGD and VNE. The mixed state has slightly more GQD and VNE with time evolution as compared to the initial pure state. Both states have non-zero VNE values describing that the QE is present for all values of N (number of atoms) for both

100

pure and mixed states.

8.4 Conclusions

We studied the dynamics of the GQD and VNE of moving two, three, and four TLS interacting with the Fock field and coherent field in the presence of the Stark shift. The dynamics of the GQD and VNE for two, three, and four TLS affected by the Stark effect was examined. It was seen that the Stark effect has a prominent role on the GQD and VNE during the dynamics of the systems. The change in the magnitude of the GQD and VNE in the presence of the Stark shift suggested that the MPQC were decreased with the increase of β for both Fock field and coherent field. The system lost the MPQC more rapidly in the presence of the coherent field as compared to the Fock field with increasing β values. It was found that in the presence of the Stark shift, the GQD was decreased more for the coherent field as compared to the Fock field due to the increase of β values, and we observed that the Fock field sustains the MPQC in the system. The maximum value of the QE was decreased more rapidly for the Fock field with the increase of β as compared to the coherent field. The GQD and VNE were increased in the presence of the Stark shift for large N systems. It is important to mention that varying β affected the MPQC of the N TLS. The higher N systems were more prone to increasing values of β and the magnitude of the GQD was more suppressed as compared to the case of $N = 2$. In comparison, the system had increased GQD for the Fock field as compared to the coherent field and the GQD was rather more suppressed with the increase of β for the coherent field as compared to the Fock field. The dynamics of the VNE show that the QE decreased with the increase of β and the QE and non-classical correlations were affected in a different way for the Fock and the Coherent field. The GQD increased with the number of atoms N for both the Fock field and coherent field while the VNE increased only for the Fock field. For the coherent field, larger values of β did not favor the system to increase the QE with the number of atoms N. The QE was sustained and maintained for the system for both the Fock field and coherent field in the presence of the Stark shift. For the higher N atomic systems, the atomic motion did not affect the period of oscillations of the system. The oscillations of the GQD and VNE showed the sustained behavior of the QE with atomic motion in the presence of the Stark effect. For

initial mixed and pure states, collapses and revivals were observed for the GQD and VNE in the presence of the Stark shift for both the Fock field and coherent field. The mixed state had slightly more GQD and VNE with time evolution as compared to the initial pure state. Both states had non-zero VNE values describing that QE was present for all values of N (number of atoms).

Chapter 9

Summary and Conclusions

The MPQC and entanglement play a pivotal role in quantum computing and QIT. QE is thought to be a resource of information. In recent years, researchers have given much attention to exploring how MPQC and entanglement evolve with time in open quantum systems interacting with different environments. Motivations to study the MPQC and entanglement of many TLS comes from the possibility that quantum computers may be built on using such TLS. In chapters, one to four, a brief review of quantum optics, open quantum systems and the MPQC and QE is presented. Chapters five to eight are mainly based on the computational work we have done and the results obtained are presented and discussed.

In chapter five, we have investigated the GQD and VNE of multipartite TLS interacting with the single mode Fock field. We used Tavis-Cummings model. We explored how the MPQC and QE evolve with time. We computed the GQD and VNE for two, three, four, and five TLS. The dynamical character of the GQD and VNE show an interplay between the CC and MPQC. We found that with increasing the number of atoms in the system, the numeric values of GQD and VNE are enhanced. The photons assisted the MPQC. Number of revivals in unit time had a non-linear behavior with the number of photons in the system. It was also observed that the maximum value of GQD in the system does not change with the number of photons. The effect of an increasing number of TLS on the quantifiers indicates that the GQD and VNE have different scaling behaviors.

In chapter six, we have studied the dynamics of GQD and VNE for quantum systems composed of two, three and four TLS interacting with the single mode coherent field under the influence of the NLKM. The collapses and revivals of the GQD and VNE are

seen for different values of the NLKM parameter for both pure and mixed initial states. It is observed that at higher values of the NLKM parameter, the magnitude of revivals of the GQD and VNE is suppressed. It is also observed that for initial mixed states the GQD shows comparatively damped oscillation as compared to initial pure states. The interval between the revivals of both the GQD and VNE increases with the increase of the NLKM parameter in systems with a relatively large number of atoms.

In chapter seven we explored the dynamics of two, three and four TLS interacting with a single mode Fock field in presence of the NLKM. We computed the GQD and VNE for initially mixed and pure states. The effect of the NLKM is pronounced on both the entanglement and MPQC. It is seen that the mixed states have comparatively suppressed oscillations in the case of the GQD. We also consider the case of moving atoms. For the case of moving atoms, the periodic behavior of the GQD and VNE are rather similar for the initially pure and mixed atomics states. It seems that the presence of atomic motion in the cavity is favorable to sustaining the MPQC and entanglement in the many TLS in presence of the NLKM.

Finally, in chapter eight we consider the influence of the Stark effect on two, three and four TLS interacting with a single mode Fock field and coherent field. We investigated the evolution of GQD and VNE, We consider both, the cases of stationary and moving atoms initially in mixed or pure states. We observed that the MPQC and entanglement decrease with the increase of Stark shift parameter. The MPQC and QE deplete more rapidly in the case of the coherent field as compared to the Fock field with increasing values of the Stark effect parameter. Moreover, we have seen that the magnitude of GQD and VNE increases more rapidly with the increase in the number of photons in the system. For both the initial pure and mixed states, rather periodic behavior is observed for the GQD and VNE in the presence of the Stark shift for the Fock field and coherent field.

Quantum entanglement has been experimentally realized in several experiments. It is worth mentioning that Wang et al. have reported the experimental demonstration of quantum entanglement among ten single photons that were spatially separated [133]. This work established a cutting-edge platform for conducting multiphoton experiments and facilitated the development of advanced technologies for complex optical quantum information tasks. Cervera-Lierta et al. experimentally demonstrated a certification of

a high-dimensional multipartite entangled state using a superconducting quantum processor [134]. By designing specific pulses for high-dimensional quantum operations, they successfully created a three-qutrit Greenberger-Horne-Zeilinger state. Furthermore, Li et al. reported the creation of multipartite entanglement involving billions of motional atoms in a quantum memory at room temperature [135]. The researchers found a strong correlation between the information contained in a single photon and the shared excitation among the motional atoms, effectively driving the multipartite entanglement. The experimental setup allowed for direct observation of the dynamic evolution of entanglement depth and the effects of decoherence. These significant findings validate the presence of genuine multipartite entanglement among billions of motional atoms under ambient conditions, pushing the boundaries of accessible entanglement scales. Notably, entanglement generation through optical channels between individually controlled qubits has been demonstrated in various systems, such as trapped ions and atoms [136–138], diamond nitrogen vacancy centers [139, 140], and quantum dots [141, 142]. Furthermore, Pompili et al. have reported the successful realization of a three-node entanglement-based quantum network [143].

Our work provides a comparison between the MPQC and QE for many TLS interacting with a single mode Fock field and coherent field in presence of ID, nonlinear Kerr medium and Stark shift.

Bibliography

[1] C. H. Bennett and D. P. DiVincenzo, Quantum information and computation, Nature **404**, 247 (2000).

[2] L. Amico, R. Fazio, A. Osterloh, and V. Vedral, Entanglement in many-body systems, Rev. Mod. Phys. **80**, 517 (2008).

[3] T. J. Osborne and M. A. Nielsen, Entanglement in a simple quantum phase transition, Phys. Rev. A **66**, 032110 (2002).

[4] G. Vidal, J. I. Latorre, E. Rico, and A. Kitaev, Entanglement in Quantum Critical Phenomena, Phys. Rev. Lett. **90**, 227902 (2003).

[5] A. Osterloh, L. Amico, G. Falci, and R. Fazio, Scaling of entanglement close to a quantum phase transition, Nature **416**, 608 (2002).

[6] Y. Yang, J. Jing, and Z. Zhao, Enhancing estimation precision of parameter for a two-level atom with circular motion, Quantum Inf. Process. **18**, 120 (2019).

[7] C. C. Rulli and M. S. Sarandy, Global quantum discord in multipartite systems, Phys. Rev. A **84**, 042109 (2011).

[8] E. T. Jaynes and F. W. Cummings, Comparison of quantum and semiclassical radiation theories with application to the beam maser, Proc. IEEE **51**, 89 (1963).

[9] A. M. Abdel-Hafez, Degenerate and nondegenerate two-mode normal squeezing in a two-level atom and two-mode system, Phys. Rev. A **45**, 6610 (1992).

[10] M. Abdel-Aty, General formalism of interaction of a two-level atom with cavity field in arbitrary forms of nonlinearities, Phys. A Stat. Mech. Appl. **313**, 471 (2002).

[11] M. Abdel-Aty, An investigation of entanglement and quasiprobability distribution in a generalized Jaynes-Cummings model, J. Math. Phys. **44**, 1457 (2003).

[12] T. M. El-Shahat, S. Abdel-Khalek, M. Abdel-Aty and A.-S. F. Obada, Aspects on entropy squeezing of a two-level atom in a squeezed vacuum, Chaos Solitons Fractals **18**, 289 (2003).

[13] M. Abdel-Aty, M. S. Abdalla and A.-S. F. Obada, Entropy and phase properties of isotropic coupled oscillators interacting with a single atom: one-and two-photon processes, J. Opt. B, Quantum Semiclassical Opt. **4**, S133 (2002).

[14] I. Jex, Emission spectra of a two-level atom under the presence of another two-level atom, J. Mod. Opt **39**, 835 (1991).

[15] S. Bougouffa, Entanglement dynamics of two-bipartite system under the influence of dissipative environments, Opt. Commun. **283**, 2989 (2010).

[16] M. M. Ashraf, Effects of a phase shift on two-photon process, Opt. Commun. **166**, 49 (1999).

[17] H. Hekmatara and M. K. Tavassoly, Sub-Poissonian statistics, population inversion and entropy squeezing of two two-level atoms interacting with a single-mode binomial field: intensity-dependent coupling regime, Opt. Commun. **319,** 121 (2014).

[18] G. M. Nikolopoulos and P. Lambropoulos, Collective behaviour in a system of two two-level atoms at the edge of a photonic band-gap, J. Mod. Opt. **49**, 6 (2002).

[19] N. H. Abdel-Wahab and M. F. Mourad, On the interaction between two two-level atoms and a two mode cavity field in the presence of detuning and cross-Kerr nonlinearity, Phys. Scr. **84**, 015401 (2011).

[20] H. R. Baghshahi and M. K. Tavassoly, Dynamics of different entanglement measures of two three-level atoms interacting nonlinearly with a single-mode field, Eur. Phys. J. Plus, **130**, 37 (2015).

[21] A. Nourmandipour and M. K. Tavassoly, A novel approach to entanglement dynamics of two two-level atoms interacting with dissipative cavities, Eur. Phys. J. Plus, **130**, 148 (2015).

[22] S. Campbell, L. Mazzola, G. D. Chiara, T. J. G. Apollaro, F. Plastina, T. Busch, and M. Paternostro, Global quantum correlations in finite-size spin chains, New J. Phys. **15**, 043033 (2013).

[23] W. K. Wootters, Entanglement of formation of an arbitrary state of two qubits, Phys. Rev. Lett. **80**, 2245 (1998).

[24] S. P. Walborn et al., Experimental determination of entanglement with a single measurement, Nature **440**, 1022 (2006).

[25] A. Peres, Separability criterion for density matrices, Phys. Rev. Lett. **77**, 1413 (1996).

[26] G. Vidal, R. F. Werner, Computable measure of entanglement, Phys. Rev. A **65**, 032314 (2002).

[27] P. S. Y. Poon, C. K. Law, Negativity of asymmetric two-mode Gaussian states: An explicit analytic formula and physical interpretation, Phys. Rev. A **76**, 054305 (2007).

[28] S. Ryu, W. Cai, A. Caro, Quantum entanglement of formation between qudits, Phys. Rev. A **77**, 052312 (2008).

[29] C. S. Yu, K. H. Ma, H. S. Song, Observable estimation of bipartite mixed-state entanglement, Eur. Phys. J. D **56**, 431 (2010).

[30] A. Miranowicz, S. Ishizaka, Closed formula for the relative entropy of entanglement, Phys. Rev. A **78**, 032310 (2008).

[31] M. Hayashi et al., Bounds on multipartite entangled orthogonal state discrimination using local operations and classical communication, Phys. Rev. Lett. **96**, 040501 (2006).

[32] C. W. Zhang, C. F. Li, Z. Y. Wang, G. C. Guo, Probabilistic quantum cloning via Greenberger-Horne-Zeilinger states, Phys. Rev. A **62**, 042302 (2000).

[33] S. Groblacher et al., Experimental quantum cryptography with qutrits, New J. Phys. **8**, 75 (2006).

[34] J. Leon, C. Sabin, Photon exchange and correlation transfer in atom-atom entanglement dynamics, Phys. Rev. A **79**, 012301 (2009).

[35] F. Casagrande, A. Lulli, and M.G.A. Paris, Tripartite entanglement transfer from flying modes to localized qubits, Phys. Rev. A **79**, 022307 (2009).

[36] J. H. Huang, L. G. Wang, S. Y. Zhu, Disentanglement of three-qubit states in a noisy environment, Phys. Rev. A **81**, 064304 (2010).

[37] B. Militello, A. Messina, Genuine tripartite entanglement in a spin-star network at thermal equilibrium, Phys. Rev. A **83**, 042305 (2011).

[38] S. L. Braunstein and C. M. Caves, Information-Theoretic Bell inequalities, Phys. Rev. Lett. **61**, 662 (1988).

[39] C. H. Bennett, H. Bernstein, S. Popescu, and B. Schumacher, Concentrating partial entanglement by local operations, Phys. Rev. A **53**, 2046 (1996).

[40] C. H. Bennett, G. Brassard, S. Popescu, B. Schumacher, J. A. Smolin, and W. K. Wootters, Purification of Noisy Entanglement and Faithful Teleportation via Noisy Channels, Phys. Rev. Lett. **76**, 722 (1996).

[41] V. Vedral, M. B. Plenio, M. A. Rippin, and P. L. Knight, Quantifying Entanglement, Phys. Rev. Lett. **78**, 2275 (1997).

[42] V. Vedral and M. B. Plenio, Entanglement measures and purification procedures, Phys. Rev. A **57**, 1619 (1998).

[43] L. Henderson and V. Vedral, Classical, quantum and total correlations, J. Phys. A, Math. Gen. **34**, 6899 (2001).

[44] H. Ollivier and W. H. Zurek, Quantum discord: A measure of the quantumness of correlations, Phys. Rev. Lett. **88**, 017901 (2001).

[45] R. Dillenschneider, Quantum discord and quantum phase transition in spin chains, Phys. Rev. B **78**, 224413 (2008).

[46] T. Werlang, C. Trippe, G. A. P. Ribeiro, and G. Rigolin, Quantum Correlations in Spin Chains at Finite Temperatures and Quantum Phase Transitions, Phys. Rev. Lett. **105**, 095702 (2010).

[47] J. Maziero, L. C. Céleri, R. M. Serra, and M. S. Sarandy, Long-range quantum discord in critical spin systems, Phys. Lett. A **376**, 1540 (2012).

[48] D. Z. Rossatto, T. Werlang, E. I. Duzzioni, and C. J. Villas-Boas, Nonclassical behavior of an intense cavity field revealed by quantum discord, Phys. Rev. Lett. **107**, 153601 (2011).

[49] K. Berrada, Classical and quantum correlations for two-mode coherent-state super-position, Opt. Commun., **285**, 2227 (2012).

[50] Q. L. He, J. B. Xu, D. X. Yao, and Y. Q, Zhang, Sudden transition between classical and quantum decoherence in dissipative cavity QED and stationary quantum discord, Phys. Rev. A **84**, 022312 (2011).

[51] Y. X. Chen, S. W. Li, and Z. Yin, Quantum correlations in a clusterlike system, Phys. Rev. A **82**, 052320 (2010).

[52] S. Campbell, T. J. G. Apollaro, C. D. Franco, L. Banchi, A. Cuccoli, R. Vaia, F. Plastina, and M. M. Paternostro, Propagation of nonclassical correlations across a quantum spin chain, Phys. Rev. A **84**, 052316 (2011).

[53] H. Dai, S. Fu and S. Luo, Spin nonclassicality and quantum phase transition in the XY spin model, Phys. Scr. **95**, 105107 (2020).

[54] J. Bao, B. Guo, Y.-H. Liu, L.-H. Shen and Z.-Y. Sun, Multipartite nonlocality and GQD in the antiferromagnetic LipkinMeshkovGlick model, Physica B: Condensed Matter **593**, 412297 (2020).

[55] F. Benabdallah, A. Slaoui and M. Daoud, Quantum discord based on linear entropy and thermal negativity of qutritqubit mixed spin chain under the influence of external magnetic field, Quantum Inf. Process. **19**, 252 (2020).

[56] J. Maziero, L. C. Celeri, R. M. Serra, and V. Vedral, Classical and quantum correlations under decoherence, Phys. Rev. A **80**, 044102 (2009).

[57] J. Maziero, T. Werlang, F. F. Fanchini, L. C. Celeri, and R. M. Serra, System-reservoir dynamics of quantum and classical correlations, Phys. Rev. A **81**, 022116 (2010).

110

[58] A. Datta, A. Shaji, and C. M. Caves, Quantum discord and the power of one qubit, Phys. Rev. Lett. **100**, 050502 (2008).

[59] A. Ferraro, L. Aolita, D. Cavalcanti, F. M. Cucchietti, and A. Acin, Almost all quantum states have nonclassical correlations, Phys. Rev. A **81**, 052318 (2010).

[60] L. Mazzola, J. Piilo, and S. Maniscalco, Sudden Transition between Classical and Quantum Decoherence, Phys. Rev. Lett. **104**, 200401 (2010).

[61] P. Huang, J. Zhu, X. Qi, G. He, and G. Zeng, Different dynamics of classical and quantum correlations under decoherence, Quantum Inf. Process. **11**, 1845 (2012).

[62] A. Saguia, C. C. Rulli, T. R. de Oliveira, and M. S. Sarandy, Witnessing nonclassical multipartite states, Phys. Rev. A **84**, 042123 (2011).

[63] M. Abdel-Aty, A. M. Sebawe, and A. S. F. Obada, Uncertainty relation and information entropy of a time-dependent bimodal two-level system, J. Phys. B **35**, 4773 (2002).

[64] S. Abdel-Khalek, A.-S. F. Obada, The atomic Wehrl entropy of a V-type three-level atom interacting with two-mode squeezed vacuum state, J. Russ. Laser Res. **30**, 146 (2009).

[65] H. Eleuch, S. Guerin, and H. R. Jauslin, Effects of an environment on a cavity-quantum-electrodynamics system controlled by bichromatic adiabatic passage, Phys. Rev. A **85**, 013830 (2012).

[66] S. Abdel-Khalek, T.A. Nofal, Correlation and entanglement of a three-level atom inside a dissipative cavity, Physica A **390**, 2626 (2011).

[67] D. F. Walls, G. J. Milburn, Quantum Optics. 2nd Edition. Springer-Verlag Berlin Heidelberg (2008).

[68] P. Weinberger, John Kerr and his Effects Found in 1877 and 1878, Philosophical Magazine Letters **88**, 897 (2008).

[69] J. Kerr, A new relation between electricity and light: Dielectrified media birefringent, Philosophical Magazine **50**, 337 (1875).

[70] J. Kerr, A new relation between electricity and light: Dielectrified media birefringent (Second paper), Philosophical Magazine **50**, 446 (1875).

[71] R. A. Zait and N. H. Abdel-Wahab, A moving rubidium atom interacting with a single mode cavity field in the presence of Kerr medium, Mod. Phys. Lett. B **18**, 1087 (2004).

[72] N. Zidan, H. F. Abdel-Hameed, and N. Metwally, Quantum Fisher information of atomic system interacting with a single cavity mode in the presence of Kerr medium, Sci. Rep. **9**, 2699 (2019).

[73] A. Joshi and S. V. Lawande, Effect of atomic motion on Rydberg atoms undergoing two-photon transitions in a lossless cavity, Phys. Rev. A **42**, 1752 (1990).

[74] A. Joshi, Two-mode two-photon Jaynes–Cummings model with atomic motion, Phys. Rev. A **58**, 4662 (1998).

[75] A. Biswas, and G. S. Agarwal, Quantum logic gates using Stark-shifted Raman transitions in a cavity, Phys. Rev. A **69**, 062306 (2004).

[76] X. -B. Zou, Y. -F. Xiao, S. -B. Li, and G.-C. Guo, Quantum phase gate through a dispersive atom-field interaction, Phys. Rev. A **75**, 064301 (2007).

[77] M. J. Fernee, H. R. -Dunlop, and G. J. Milburn, Improving single-photon sources with Stark tuning, Phys. Rev. A **75**, 043815 (2007).

[78] S. J. Anwar, M. Ramzan, M. Usman, and M. K. Khan, Quantum Fisher Information of Two-Level Atomic System under the Influence of Thermal Field, Intrinsic Decoherence, Stark Effect and Kerr-Like Medium, JQIS **11,** 24 (2021).

[79] S. J. Anwar, M. Ramzan, and M. K. Khan, Effect of Stark- and Kerr-like medium on the entanglement dynamics of two three-level atomic systems, Quantum Inf. Process. **18**, 192 (2019).

[80] E. Schrdinger, Der stetige bergang von der Mikro- zur Makromechanik, Naturwissenschaften **14**, 664 (1926).

[81] E. H. Kennard, Zur Quantenmechanik einfacher Bewegungstypen, Zeitschrift für Physik **44**, 326 (1927).

[82] R. J. Glauber, The Quantum Theory of Optical Coherence, Phys. Rev. **130**, 2529 (1963).

[83] D. Stoler, Equivalence Classes of Minimum Uncertainty Packets, Phys. Rev. D **1**, 3217 (1970).

[84] E. Y. C. Lu, Quantum Correlations in Two-photon Amplification, Lettere al Nuovo Cimento **3**, 585 (1972).

[85] H. P. Yuen, Two-photon Coherent States of the Radiation Field, Phys. Rev. A **13**, 2226, (1976).

[86] N. J. Hollenhorst, Quantum Limits on Resonant-mass Gravitational-radiation Detectors, Phys. Rev. D **19**, 1669 (1979).

[87] W. Schleich, and J. A. Wheeler, Oscillations in Photon Distribution of Squeezed States and Interference in Phase Space, Nature **326**, 574 (1987).

[88] W. Schleich and J. A. Wheeler, Oscillations in Photon Distribution of Squeezed States, J. Opt. Soc. Am. B **4**, 1715 (1987).

[89] C. Gerry, and P. Knight, Introductory Quantum Optics, Cambridge University Press (2012).

[90] I. I. Rabi, Space Quantization in a Gyrating Magnetic Field, Phys. Rev. **51**, 652 (1937).

[91] M. Tavis, and F. W. Cummings, Approximate Solutions for an N-Molecule-Radiation-Field Hamiltonian, Phys. Rev., **188**, 692 (1969).

[92] Heinz-Peter Breuer, and F. Petruccione, The Theory of Open Quantum Systems, Oxford University Press (2007).

[93] M. A. Nielsen, and I. Chuang, Quantum computation and quantum information, Cambridge University Press (2002).

[94] M. Berman, R. Kosloff, and H. Tal-Ezer, Solution of the time-dependent Liouville-von Neumann equation: dissipative evolution, J. Phys. A: Math. Gen. **25**, 1283 (1992).

[95] C. Gardiner, and P. Zoller, Quantum Noise, Springer Series in Synergetics (2000).

[96] G. J. Milburn, Intrinsic decoherence in quantum mechanics, Phys. Rev. A **44**, 5401(1991).

[97] F. Haake, S. M. Tan, and D. F. Wall, Photon noise reduction in lasers, Phys. Rev. A **40**, 7121(1989).

[98] G. J. Milburn, Kicked quantized cavity mode: an open-systems-theory approach, Phys. Rev. A **36**, 744 (1987).

[99] G. New, Introduction to Nonlinear Optics, Cambridge University Press.

[100] B. Yurke, and D. Stoler, Generating quantum mechanical superpositions of macroscopically distinguishable states via amplitude dispersion, Phys. Rev. Lett. **57**, 13 (1986).

[101] Demtröder and Wolfgang, An Introduction to Atomic-, Molecular- and Quantum Physics, 2nd Edition. Springer-Verlag Berlin Heidelberg (2010).

[102] E. U. Condon, and G. H. Shortley, The Theory of Atomic Spectra, Cambridge University Press (1935).

[103] H. Moya-Cessa, V. Buek, and P. L. Knight, Power Broadening and Shifts of Micromaser Lineshapes, Optics Commun., **85**, 267 (1991).

[104] D. Meschede, H. Walther, and G. Mller, One-Atom Maser, Phys. Rev. Lett., **54**, 551 (1985).

[105] J. D. Jorgensen, et. al., Lattice instability and high-Tc superconductivity in $La_{2x}Ba_xCuO_4$, Phys. Rev. Lett., **58**, 1024 (1987).

[106] R. R. Schlicher, Jaynes-Cummings Model in Atomic Motion, Optics Commun., **70**, 97 (1989).

[107] V. Vedral, The Role of Relative Entropy in Quantum Information Theory, Rev. Mod. Phys. **74**, 197 (2002).

[108] R. F. Werner, Quantum states with Einstein-Podolsky-Rosen Correlations Admitting a Hidden-variable Model, Phys. Rev. A **40**, 4277, (1989).

[109] J. Oppenheim, M. Horodecki, P. Horodecki, and R. Horodecki, Thermodynamical Approach to Quantifying Quantum Correlations, Phys. Rev. Lett. **89**, 180402 (2002).

[110] M. Horodecki, et. al., Local Versus Nonlocal Information in Quantum-information Theory: Formalism and Phenomena, Phys. Rev. A **71**, 062307 (2005).

[111] M. Piani, P. Horodecki, and R. Horodecki, No-local-broadcasting Theorem for Multipartite Quantum Correlations, Phys. Rev. Lett. **100**, 090502 (2008).

[112] B. M. Terhal, M. Horodecki, D. W. Leung, and D. P. DiVincenzo, The Entanglement of Purification, Journal of Mathematical Physics **43**, 4286 (2002).

[113] D. P. DiVincenzo, M. Horodecki, D. W. Leung, J. A. Smolin, and B. M. Terhal, Locking Classical Correlations in Quantum States, Phys. Rev. Lett. **92**, 067902 (2004).

[114] A. K. Rajagopal, and R. W. Rendell, Separability and Correlations in Composite States Based on Entropy Methods, Phys. Rev. A **66**, 022104 (2002).

[115] S. Wu et. al., Correlations in Local Measurements on a Quantum State, and Complementarity as an Explanation of Nonclassicality, Phys. Rev. A **80**, 032319 (2009).

[116] R. Rossignoli, N. Canosa, and L. Ciliberti, Generalized Entropic Measures of Quantum Correlations, Phys. Rev. A **82**, 052342 (2010).

[117] B. Dakić, V. Vedral, and C. Brukner, Necessary and Sufficient Condition for Nonzero Quantum Discord, Phys. Rev. Lett. **105**, 190502 (2010).

[118] K. Modi, T. Paterek, W. Son, V. Vedral, and M. Williamson, Unified View of Quantum and Classical Correlations, Phys. Rev. Lett. **104**, 080501 (2010).

[119] D. Girolami, M. Paternostro, and G. Adesso, Faithful Nonclassicality Indicators and Extremal Quantum Correlations in Two-qubit States, J. Phys. A Math. Theor. **44**, 352002 (2011).

[120] D. Girolami, T. Tufarelli, and G. Adesso, Characterizing Nonclassical Correlations Via Local Quantum Uncertainty, Phys. Rev. Lett. **110**, 240402 (2013).

[121] A. Streltsov, H. Kampermann, and D. Bruß, Behavior of Quantum Correlations Under Local Noise, Phys. Rev. Lett. **107**, 170502 (2011).

[122] V. Madhok, and A. Datta, Interpreting Quantum Discord Through Quantum State Merging, Phys. Rev. A **83**, 032323, (2011).

[123] K. Modi, A. Brodutch, H. Cable, T. Paterek, and V. Vedral, The Classical-quantum Boundary for Correlations: Discord and Related Measures, Rev. Mod. Phys. **84**, 1655, (2012).

[124] W. H. Zurek, Einselection and Decoherence from an Information Theory Perspective, Annalen der Physik **9**, 855 (2000).

[125] B. Aharon, and M. Kavan, Criteria for Measures of Quantum Correlations, Quantum Inf. Comput. **12**, 0721 (2011).

[126] F. F. Fanchini, T. Werlang, C. A. Brasil, L. G. E. Arruda, and A. O. Caldeira, Non-Markovian dynamics of quantum discord, Phys. Rev. A **81**, 052107 (2010).

[127] T. Werlang, S. Souza, F. F. Fanchini, and C. J. Villas Boas, Robustness of quantum discord to sudden death, Phys. Rev. A **80**, 024103 (2009).

[128] M. S. Kim, J. Lee, D. Ahn and P. L. Knight, Entanglement induced by a single-mode heat environment, Phys. Rev. A **65**, 040101 (2002).

[129] M. Tavis, and F. W. Cummings, Exact Solution for an N-Molecule—Radiation-Field Hamiltonian, Phys. Rev. **170**, 379 (1968).

[130] R. R. Schlicher, Jaynes-Cummings model with atomic motion, Opt. Commun. **70**, 97 (1989).

[131] J. Machta, Entropy, information, and computation, Am. J. Phys. **67**, 1074 (1999).

[132] J. von Neumann, Mathematische Grundlagen der Quantenmechanik. 2nd Edition. Berlin: Springer (1996).

[133] Xi-Lin Wang et al., Experimental Ten-photon entanglement, Phys. Rev. Lett. **117**, 210502 (2016).

[134] A. Cervera-Lierta et al., Experimental high-dimensional Greenberger-Horne-Zeilinger entanglement with superconducting transmon qutrits, Phys. Rev. Applied **17**, 024062 (2022).

[135] H. Li et al., Multipartite entanglement of billions of motional atoms heralded by single photon, npj Quantum Information **7**, 146 (2021).

[136] S. Ritter et al., An elementary quantum network of single atoms in optical cavities, Nature **484**, 195 (2012).

[137] J. Hofmann et al., Heralded entanglement between widely separated atoms, Science **337**, 72 (2012).

[138] L. J. Stephenson et al., High-Rate, High-Fidelity entanglement of qubits across an elementary quantum network, Phys. Rev. Lett. **124**, 110501 (2020).

[139] H. Bernien et al., Heralded entanglement between solid-state qubits separated by three meters, Nature **497**, 86 (2013).

[140] P. C. Humphreys et al., Deterministic delivery of remote entanglement on a quantum network, Nature **558**, 268 (2018).

[141] A. Delteil et al., Generation of heralded entanglement between distant hole spins, Nat. Phys. **12**, 218 (2016).

[142] R. Stockill et al., Phase-Tuned entangled state generation between distant spin qubits, Phys. Rev. Lett. **119**, 010503 (2017).

[143] M. Pompili et al. Realization of a multinode quantum network of remote solid-state qubits, Science **372**, 259 (2021).

Turnitin Originality Report

Quantum correlations in multipartite quantum systems   by Muhammad Ibrahim .

From CL QAU (DRSML)

- Processed on 07-Nov-2022 10:10 PKT
- ID: 1946762811
- Word Count: 26724

Similarity Index
15%
Similarity by Source

Internet Sources:
9%
Publications:
11%
Student Papers:
3%

sources:

1 < 1% match (Internet from 11-May-2022)
https://www.researchgate.net/profile/Khalid-Khan-7

2 < 1% match (David McMahon. "Quantum Computing Explained", Wiley, 2007)
David McMahon. "Quantum Computing Explained", Wiley, 2007

3 < 1% match ()
Campbell, Steve, Mazzola, L., De Chiara, G., Apollaro, T. J. G., Plastina, F., Busch, Th., Paternostro, M.. "Global quantum correlations in finite-size spin chains", 'IOP Publishing', 2013

4 < 1% match ()
Campbell, Steve, Mazzola, Laura, Paternostro, Mauro. "Global Quantum Correlation in the Ising model", 'World Scientific Pub Co Pte Lt', 2011

5 < 1% match (Internet from 25-Oct-2022)
http://nozdr.ru/data/media/biblio/kolxoz/Cs/CsQc/Schumacher%20B.,%20Westmoreland%20M.D.%20Quantum%20Processes,%20Systems,%20and%20Information%20%28CUP,%202010%29%28ISBN%20052187534X%29%28O%29%28483s%29_CsQc_.pdf

6 < 1% match (Internet from 25-Oct-2022)
http://nozdr.ru/data/media/biblio/kolxoz/Cs/CsLn/Probabilistic%20Inductive%20Logic%20Programming%20-%20Theory%20and%20Applications%28LNCS4911,%20Springer,%202008%29%28ISBN%209783540786511%29%28347s%29.pdf

7 < 1% match (Internet from 25-Oct-2022)
http://nozdr.ru/data/media/biblio/kolxoz/Cs/CsQc/Desurvire%20E.%20Classical%20and%20Quantum%20Information%20Theory..%20An%20Introduction%20for%20the%20Telecom%20Scientist%20%28CUP,%202009%29%28ISBN%200521881714%29%28O%29%28715s%29_CsQc_.pdf

8 < 1% match (Internet from 23-Oct-2022)
http://nozdr.ru/data/media/biblio/kolxoz/Cs/CsAi/Barber%20D.%20Bayesian%20reasoning%20and%20machine%20learning%20%28CUP,%202011,%20draft%202010%29%28ISBN%200521518148%29%28O%29%28646s%29_CsAi_.pdf

9 < 1% match (Internet from 01-Nov-2022)
http://nozdr.ru/data/media/biblio/kolxoz/P/PT/PTin/Mezard%20M.,%20Montanari%20A.%20Information,%20Physics,%20and%20Computation%20%28OUP,%202009%29%28ISBN%20019857083X%29%28O%29%28584s%29_PTin_.pdf

10 < 1% match (Internet from 26-Oct-2022)
http://nozdr.ru/data/media/biblio/kolxoz/M/MA/MAr/Goodman%20R.,%20Wallach%20N.%20Symmetry,%20representations,%20and%20invariants%20%28Springer,%202009%29%28ISBN%20038779851X%29%28730s%29_MAr_.pdf

11 < 1% match ()
Bahari, Iskandar. "Collapse, Revival and Decoherence of Entanglement in Two Qubits Systems", Physics (York), 2018

12 < 1% match ()
Hosler, Dominic. "Relativistic Quantum Communication", 'University of Sheffield Conference Proceedings', 2013

13 < 1% match (student papers from 29-Jul-2017)
Submitted to Higher Education Commission Pakistan on 2017-07-29

14 < 1% match (student papers from 26-Sep-2017)
Submitted to Higher Education Commission Pakistan on 2017-09-26

15 < 1% match (student papers from 08-Aug-2017)
Submitted to Higher Education Commission Pakistan on 2017-08-08

16 < 1% match (Internet from 19-Oct-2022)
https://dokumen.pub/essentials-of-mathematical-methods-in-science-and-engineering-2nbsped-9781119580232.html

17 < 1% match (Internet from 09-May-2021)
https://dokumen.pub/digital-communication-933921952x-9789339219529.html

18 < 1% match (Internet from 21-May-2021)
https://dokumen.pub/thermodynamics-in-the-quantum-regime-recent-progress-and-outlook-9783319990453-3319990454.html